THE OPTICAL DISPLAY OF

ULTRASONIC WAVES IN LIQUIDS

By

DAVID ARTHUR HUTCHINS BSc (HONS)

A thesis submitted for the degree of

DOCTOR OF PHILOSOPHY

SEPTEMBER 1978

The University of Aston in Birmingham

SUMMARY

THE OPTICAL DISPLAY OF ULTRASONIC WAVES IN LIQUIDS

By

DAVID ARTHUR HUTCHINS, BSc(Hons)

A Thesis submitted for the Degree of

DOCTOR OF PHILOSOPHY

September 1978

The distribution and diffraction patterns of propagating
ultrasonic waves have been studied previously, both experimentally
and theoretically. The work to be described furthers this
study in two main areas.

The main bulk of experimental work, and its associated theory,
concerns a technique for the optical display of ultrasonic
waves in liquids. This is achieved by a system which combines
optical anisotropy, produced within a thin layer of suitable
material, with stroboscopic illumination. The result is a display,
providing information across a complete plane of section, with
negligible disturbance to the ultrasonic field.

The remaining work concerns a theoretical investigation into the
radiated pressure distributions of ultrasonic transducers. The
approach involves expressing the solution to the appropriate wave
equation as a limited series. This method makes it possible to
apply mixed boundary conditions, and allows a study to be made
of variations in baffle size. The principle is inherently
simple and permits a wide range of application. The results have
been correlated with existing surface integral techniques.

ultrasonic / photoelastic / optical / display / transducer

ACKNOWLEDGEMENTS

CONTENTS

CHAPTER ONE

INTRODUCTION

In recent years, ultrasonics has enjoyed wide application in many different fields, ranging from medical diagnosis at low acoustic powers to industrial applications requiring extremely high powers; it is thus important that the precise behaviour of ultrasonics be known.

A case in point is the behaviour of ultrasonic waves as a result of reflection or diffraction at various discontinuities in their path. This sort of problem is not restricted to simple boundary conditions, and theoretical approaches can only be applied in a limited number of simple cases; potentially the most effective method of establishing the resultant ultrasonic distribution is by experimental determination, especially in complex situations.

In most cases, the ultrasonic field under study will be produced by some sort of transducer. However, the ultrasonic pressure variations, produced in the irradiated medium by such a transducer, will be complex; this arises from diffraction and interference of the emanating waves. The resulting radiation patterns have been the subject of many investigations, both theoretical and experimental.

The work to be described in this thesis attempts to further the study of the phenomena outlined above.

First, an optical display method for the visualisation of ultrasonic waves in liquids will be presented. The technique allows the sampling of two dimensional sections of complex ultrasonic fields, in a single operation; both standing and progressive ultrasonic distributions may be studied.

Secondly, a new computational technique for the theoretical determination of the radiation patterns of axisymmetric ultrasonic transducers will be presented, in which the size of the surrounding baffle is variable; the method involves the rigorous application of boundary conditions over the plane containing the transducer face, and is capable of wide application.

1.1 The experimental determination of ultrasonic distributions in liquids

Many methods have been described in the literature for the determination of the acoustic variations of an ultrasonic field, present usually in a liquid. These methods will now be reviewed, and fall into several broad categories, namely

   (a)   the use of various types of probe;

   (b)   optical methods;

   (c)   chemical methods;

   (d)   others.

1.1.1 The use of ultrasonic probes

Non-directional microphones have been widely used to plot the distribution of ultrasonic fields, sampling the field at a single point at a time. To do this effectively, they must be small in size, preferably a fraction of the ultrasonic wavelength in the field to be investigated. Additionally, their characteristic impedance should be as close as possible to that of the surrounding medium, reducing the disturbance to the ultrasonic field and the tendency for standing-wave production.

Several workers have attempted to reduce the size of their probes to acceptable limits. Romanenko's miniature piezoelectric receiver(1) had a diameter of 0.2mm, the detector element being a spherical layer of ceramic barium titanate deposited on a platinum sphere. The author used the device at frequencies of up to 10MHz for pulsed fields, but continuous-wave investigations were limited to 750kHz. Saneyoshi et al(2) described a probe in which ultrasonics were conducted along a thin wave-guide to give the sound pressure at a point; their smallest probe had an effective diameter of 1.0mm.

Schmitt(3) showed that ceramic transducers had the potentiality of being extremely small and inexpensive, although his probes were not used at frequencies above 100kHz.

Another approach was demonstrated by Aveyard(4), who collimated a large transducer to a small aperture; additionally, Christie(5) collimated a barium titanate probe with the use of a cork masking ring. Both these probes were used to plot pulsed fields.

The above are all piezoelectric probes. Filipczynski(6) described electrodynamic and capacitance transducers for use in the lower MHz region; the former measured particle velocity, the latter particle displacement. Smith(7) used a probe, utilising the inverse magnetostrictive effect, whose diameter was 0.4mm; it was used to investigate standing waves at 570kHz.

Yeager(8) showed that if a copper wire was immersed in an
electrolyte containing an ultrasonic field, an alternating
voltage at the ultrasonic frequency was set up between the wire
and the solution. Investigations at 200kHz yielded a good
sensitivity in KCl solution. Fox et al(9) measured the
variation in electrolyte conductivity between two wires in
another approach.

Radiation pressure results in a force on an obstacle placed
in an ultrasonic field, and this can be related to the ultrasonic
intensity producing it. Probes based on this phenomenon have
been suggested by Wells et al(10) and Fox and Griffing(11).

The above probes all have one thing in common - their characteristic
impedence differs from that of water. This property was
eliminated in a calorimetric probe described by Fry and Fry(12),
utilising a fine thermocouple wire, surrounded in a castor-oil
medium and contained in a thin polythene case. This probe
minimised interference due to reflection and diffraction; however,
it was insensitive and inaccurate for radiation containing higher
ultrasonic harmonics.

Characteristic impedence problems can also be overcome by the use
of polymer electrets, polarised films of these exhibiting piezoelectric
properties. An example of such a polymer is polyvinylidene
fluoride (PVDF)(13).

It has been indicated that many types of probe are available. They all have one major drawback, however; they only sample ultrasonic variations at a single point. The three-dimensional distribution of a complicated ultrasonic field would require mechanical scanning of the probe, and Christie(5) and Aveyard(4) have shown how this may be achieved.

Although not strictly a probe, Sokolov tubes(14) are worthy of mention in that they can sample extended areas in one operation. Their drawback is that they will inevitably cause a large disturbance to the ultrasonic field to be visualised.

1.1.2 Optical methods

Optical methods have the immediate advantage that disturbance to the ultrasonic field is minimised, as long as the method relies simply on an interaction between light and sound.

Several methods have been evolved which rely on the various mechanisms of light diffraction by ultrasonic waves in liquids; other methods rely on variations in liquid and solid surfaces, and Doppler effects.

The most well-known application of light diffraction to ultrasonic visualisation is in Schlieren systems. These rely on the local periodic variations in refractive index of a medium as an ultrasonic wave passes through it; the refractive index tends to be greater in regions of compression that in those of rarefraction.

In a typical Schlieren system, monochromatic light is shone through the region to contain the ultrasonic distribution, and is focussed on a stop; thus, with zero ultrasonic intensity present, no image is seen. The presence of an ultrasonic beam, with its associated refractive index variations, causes light intensity to be diverted passed the stop and an image created.

Use of the above technique results in the production of a bright image where ultrasonic intensity exists, and the visualisation of ultrasonics in solids(15), liquids(16) and gases(17) has been demonstrated. Additional use of a stroboscopic light source allows individual compressions and rarefractions within a progressive wave to be observed(18). The Schlieren technique has found wide application(19 - 22), further considerations permitting sound pressure measurements to be made(23, 24).

Schlieren systems are quite sensitive, requiring only finite $mWcm^{-2}$ of ultrasonic power. They have, however, a drawback - they cannot be used to sample two-dimensional sections of an ultrasonic field exhibiting variations in three dimensions; this is because the incident illumination must be shone through the whole thickness of the field. Schlieren systems are thus not capable of analysing complicated, three-dimensional fields.

There exist, however, other visualisation systems based on ultrasonic light-diffraction phenomena. Debye-Sears diffraction imaging is an example, use being made of an acoustical slit and an optical

filtering device. Sato and Ueda(25) have demonstrated the effect and Defebvre(26) has examined it theoretically. The technique was applied to the imaging of acoustically irradiated objects. A more applicable system, recently proposed by Cook(27) also made use of conventional light diffraction, and demonstrated the potential determination of the cross-sectional distribution of a progressive ultrasonic wave. A digital computer and data-acquisition system were required, and the method seemed to be limited to axisymmetric sound distributions.

Bragg diffraction imaging is another approach, the effect having been used to sample two-dimensional sections of ultrasonic fields(28). This approach, however, has only been used for ultrasonic frequencies in the tens of MHz region.

Ultrasonic waves have the property that they can cause variations in the contours of interfaces between two media; this is especially the case with liquid/gas interfaces, where levitation of the liquid surface may occur due to the presence of ultrasonics.

Use of this phenomenon has been made in acoustic holography(29) to visualise stationary intensity variations. The technique has recently been refined to a state whereby observation of the progress of acoustic pulses may be made(30); this utilised pulsed laser interferometry. The fringes produced, however, merely gave intensity contours of the gross ultrasonic intensity beneath the liquid surface.

The variations in the surface of a thin membrane have been used in a device known as a pellicle(31). A thin, metallised circular membrane was placed in the path of an ultrasonic field; the displacement amplitude of the ultrasonic wave passing through it was then determined by interferometrically measuring the motion of the pellicle. A scanned laser system was used which also provided brightness modulation of a cathode ray tube to provide an image.

The method is very sensitive (better than $5nWcm^{-2}$ was quoted by the authors) and is useful up to 10MHz. It has been used to study the intensity distribution in front of ultrasonic transducers, but cannot provide instantaneous acoustic information which would allow progressive waves to be studied.

Taylor(32) has used the Doppler Effect to measure variations in absolute acoustic particle velocity of an ultrasonic field; this was done by examining laser light scattered from small particles, suspended in the supporting medium. It was stated that the results obtained were reliable at frequencies in excess of 50kHz. Limitations of the method were that the vibrations of the suspended particles became less representative of the particle velocity as the frequency was increased, and that the field was only sampled at a point. Again, instantaneous acoustic information was not obtained.

1.1.3 <u>Chemical methods</u>

These rely on the fact that ultrasonics may cause the occurance of a chemical process or the modification of a chemical state. Rust et al(33) showed that ultrasonics caused the evolution of iodine from KI solution, noticeable colouration being observed. Another classical reaction, shown by Bennet(34), caused the occurrence of a blue tint on a starch-covered plate by irradiation with 1-3MHz ultrasonics; the plate was in water containing a small amount of 3% iodine solution in methanol.

The above methods were insensitive, needing finite Wcm^{-2} of acoustic power. Rust(35) reported the use of thermosensitive dyes, but $1Wcm^{-2}$ was still needed at 560kHz. Peterman(36) improved on this again by making use of luminescence, $0.1 - 0.5Wcm^{-2}$ of approximately 4MHz ultrasonics being needed. Ernst and Hoffman(37) have shown several additional chemical methods, again using thermosensitive dyes and phosphors, whilst Iizuka(38) made use of the effect of ultrasonics on polaroid films.

The temperature - sensitive properties of certain cholesteric liquid crystals have permitted their use in mapping intensity distributions of ultrasonic fields(39). These liquid crystals were reported to exhibit irridescent colour effects at various temperatures, and intensity mapping of transducer radiation patterns was achieved.

The above methods all rely on variations in acoustic intensity to produce varying degrees of chemical change. Their response time is too slow, however, to enable their use in determining instantaneous values of acoustic parameters.

1.1.4 Other effects

It is well known that ultrasonics may cause alignment of non-spherical particles suspended in the irradiated medium; thus was used in the Pohlman cell(40) to visualise stationary ultrasonic fields, the reflectance of suspended aluminium flakes being observed.

Various molecules constituting a liquid may also be non-spherical in shape, and may be caused to become preferentially orientated by ultrasonic waves. The resulting effect may give rise to double refraction, and this phenomenon has been observed in many liquids. Some of the most sensitive effects have been seen in liquid crystals(41) and the use of these substances for ultrasonic visualisation has been described(42). The main area of application seems to be in the visualisation of surface waves(43); their use for ultrasonic distributions in liquids, however, seems to be limited to intensity mapping. Greggus(44) has shown how a thin layer of such substances can sample intensity distributions at a plane.

The sampling of instantaneous distributions by this method does not seem to have been described, presumably because typical orientational relaxation times are in the ms region. Bertalotti et al(45) have shown, however, that these relaxation times may be improved by the

addition of a surfactant; further investigation into this phenomenon is thus needed.

1.1.5 Conclusions

It is clear from the above review that existing methods for the visualisation of propagating ultrasonic waves are limited in several respects.

Optical methods have the advantage of minimal disturbance to the ultrasonic field, and ultrasonic light diffraction has enabled propagating fields to be visualised quantitatively by Schlieren systems. The drawback, as stated previously, is that Schlieren systems are unable to sample two-dimensional sections or single points of complex three-dimensional fields; their use for the visualisation of the latter is thus limited.

Bragg diffraction is limited to frequencies in the tens of MHz region, and other diffraction processes seem to be complicated experimentally.

The pellicle method [31] has been used to study displacement amplitudes, and hence intensities, at a given plane; extension of the technique to stroboscopic illumination may yield results applicable to the determination of instantaneous values.

Various types of miniature probes have been described, and many are capable of giving the instantaneous value of an acoustic parameter at a point. Disturbance to the ultrasonic field has been minimised in some designs; however, the problem of mechanically scanning the probe to build up a three-dimensional distribution remains.

Chemical methods have been shown to be capable of mapping intensity distributions of ultrasonic fields. The relaxation times of the mechanisms involved are, however, too slow to provide instantaneous values of acoustic parameters.

The above suggests that a new method, capable of sampling two-dimensional sections of complicated ultrasonic distributions, would be welcome, preferably with little disturbance to the ultrasonic field. The work to be described was designed so that the above might be achieved.

1.2 The proposed optical display technique

The essence of the proposed technique lies in the concept of an index layer - a thin sheet of material in which an optical effect is produced when an ultrasonic wave passes through it.

Consider such a layer, positioned in a suitable liquid, as shown in Fig 1.1. A field of propogating ultrasonic waves, travelling from right to left, exists in the volume of liquid concerned; in its

path is an index layer, as shown, in which an ultrasonic wave
will be induced by the ultrasonic field.

Suppose now than an optical property, associated with the layer
material, is capable of showing up ultrasonic waves as moving
light patterns; steady illumination of the layer will produce
a dynamic optical display, invisible to the eye as the velocity
of ultrasonics in both the liquid and layer media is too great.

Convenient viewing of this light pattern may be achieved by use
of the stroboscopic technique. For continuous-wave ultrasonics,
a static display will be achieved by amplitude modulation of the
incident illumination at the ultrasonic frequency. Additionally,
a slight difference between the ultrasonic and light modulation
frequencies will cause the optical display to move slowly through
the index layer.
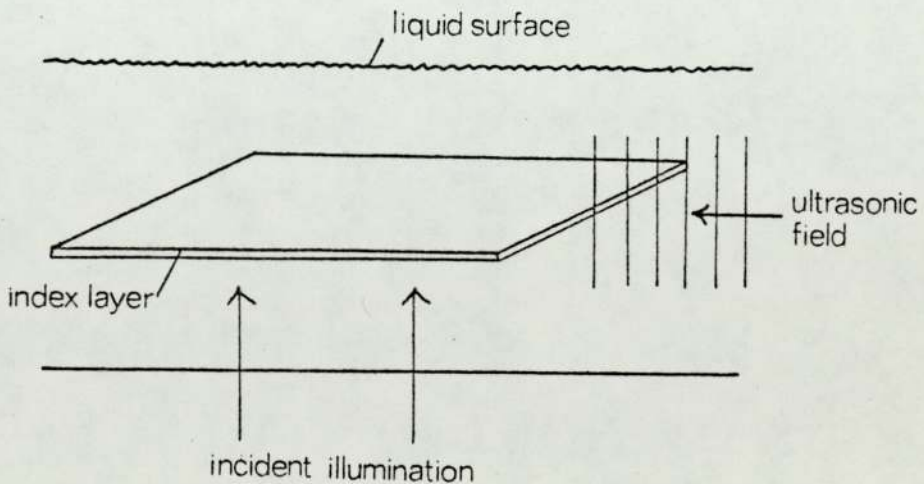
FIGURE 1.1   The use of an index layer

The stroboscopic effect thus allows convenient viewing of
an instantaneous light pattern, caused by the passage of ultrasonic
waves through the index layer. Note that only the portion of the
ultrasonic field covered by this layer produces a display, the
liquid surrounding it producing no visible effect. The technique
thus allows two-dimensional sections of the ultrasonic field to
be sampled. Movement of the layer to various positions in the
sound field then allows the three-dimensional ultrasonic distribution
to be built up from a series of two-dimensional sections.

The advantages of such a scheme over other visualisation systems
may be summarised as follows:

> (i)   the system would be relatively cheap and easily
>   constructed;
> (ii) the system would sample two-dimensional sections
>   instantly, without the need for time-consuming
>   scanning and signal analysis;
> (iii) the use of stroboscopy would provide either moving
>   or stationary images, from which instantaneous
>   values of acoustic parameters could be obtained.

Possible drawbacks might arise from disturbance to the ultrasonic
field, and limitations to the validity of the display produced;
these factors would have to be investigated before the overall
range of application of the technique could be established.

1.3   Proposed visual effects for use in layer materials

The proposed visualisation system, involving the use of thin layers, requires a mechanism whereby ultrasonic variations within the layer material may be converted into light patterns.

Two general mechanisms were thought to be of possible use in this application; these were

(i)   optical effects in liquids, caused by the periodic enhancement of optical activity or circular dichroism by ultrasonics;

(ii)   the production of double refraction or photoelastic effects in solids.

The reasons for their selection will now be outlined.

1.3.1 Potential optical effects in liquids

Optical activity is the ability of a medium to rotate the plane of polarization of a plane-polarized light beam. This effect has been observed in both liquid and crystalline media, and it is found experimentally that the extent of the effect in a liquid depends on both its concentration and the wavelength of light used.

Various optically active liquids, when in an ordered state, exhibit an optical activity far in excess of that seen in the isotropic

liquid. This phenomenon is commonly observed in liquid crystals, a class of substance easily orientated into different states by an applied electric field(46). Optical rotations of the order of 50 - 100,000° per millimetre may be observed in the mesomorphic state of such substances(47), whereas that of the isotropic liquid is immeasurably small in comparison.

Circular dichroism is an effect whereby differential absorption of left and right-handed circularly polarized light occurs, and is invariably associated with the optical activity of a given molecule(48). Enhancement of this effect with orientation is again seen.

The proposed visual effects in liquid layers are based on the assumption that ultrasonic waves may produce a varying degree of alignment of molecules exhibiting optical activity or circular diochroism; variations in alignment are proposed as a kinematic equilibrium between orientational tendencies and random thermal motion. The degree of alignment, from the preceeding argument, can affect the magnitude of circular diochroism and optical activity, and could lead to an ultrasonic display mechanism.

The ability of an ultrasonic wave to produce orientational forces on liquid molecules, leading to such a display, is believed to be facilitated by the use of molecules exhibiting mass-asymmetry i.e. molecules in which the centre of gravity G is not at the geometrical centre O. Acceleration of such molecules will cause rotation so

that, at equilibrium, both G and O lie on the line of action of the accelerating force, with G lagging O.

The proposed visualisation mechanism thus involves the enhancement of optical activity or circular diochroism as a function of molecular alignment; variations in the degree of alignment with an acoustic parameter may be caused by the use of mass-asymmetric molecules, already exhibiting the required optical properties in the random state.

1.3.2 Induced double refraction in solids-photoelasticity

A doubly refracting material is one in which, in general, two orthogonally-polarized light beams are produced upon illumination with plane polarized light. These beams travel through the material with different velocities, and on emerging may combine to give a variety of optical effects.

A material is said to be photoelastic if double refraction is produced in it under the action of an applied stress, the extent of the double refraction produced being dependent on the magnitude of the strain in the material. The photoelastic effect has been found to occur in most transparent solids to some extent, but the most sensitive effects occur in various transparent polymers.

Ultrasonics, when passing through a solid, travel as stress waves; this wave can either be longitudinal or transverse. It

may thus be expected that ultrasonics would produce a dynamic photoelastic effect in a suitable solid, and this has been found to be the case by various authors, as indicated in Chapter Two.

1.4   Factors affecting the validity of the technique

It has been indicated that an optical display could be produced within a thin index layer, placed in an ultrasonic field, provided the layer material has suitable optical properties. The factors governing the validity of such a technique must now be considered; the most important are:

(a)   the optical display, produced by a given layer, must be a true representation of the ultrasonic field that would have been present at the sampled plane in the layer's absence;

(b)   the introduction of the layer must not disturb unduly the ultrasonic field to be visualised;

(c)   the layer must be sufficiently thin that variation of the ultrasonic field across its thickness is minimal.

Factors affecting the validity of a resultant display are examined fully in Chapter Four. However, the disturbance that might be caused to an ultrasonic field will now be discussed.

1.4.1 The disturbance to the ultrasonic field

The characteristic impedence Z of a medium may be expressed as

$$Z = \rho c$$

where c is the velocity of sound in a medium of density ρ.
The importance of characteristic impedence is that its values
in two media determine the proportion of sound reflected at
a boundary between them.

Consider two media, characterised by

$$Z_1 = \rho_1 c_1$$

$$Z_2 = \rho_2 c_2$$

in which an ultrasonic wave is incident normally onto the
boundary from the former medium; the resultant intensity in
each medium will depend on the proportion of sound reflected
and transmitted at the boundary.

Let I_i be the incident wave intensity, and I_r and I_t be that
of the reflected and transmitted waves respectively; the three
are governed by the equations (49)

$$\frac{I_r}{I_i} = \left(\frac{Z_1 - Z_2}{Z_1 + Z_2} \right)^2 = \alpha_r \text{, the reflection coefficient}$$

$$\frac{I_t}{I_i} = \frac{4Z_1Z_2}{(Z_1+Z_2)^2} = \alpha_t, \text{ the transmission coefficient}$$

It is clear from these expressions that if Z_1 and Z_2 differ substantially, $\alpha_r \to \pm 1$ and $\alpha_t \to 0$, and the incident wave is almost totally reflected. Conversely, if $Z_1 = Z_2$, $\alpha_r \to o$ and $\alpha_t = 1$; no reflection occurs and the wave is totally transmitted across the boundary.

Expressions for oblique incidence are more complicated(50), but the same general trends are implied.

It is clear from the above that considerable disturbance to the ultrasonic field may result from a difference in acoustic impedence between the liquid and layer media, used in a visualisation system. Disturbance due to this effect could, however, be kept to a minimum if the impedences are matched.

The material used as an index layer will be expected to be attenuating, since sensitive photoelastic materials are invariably viscoelastic polymers, and the mechanisms suggested for use in liquid layers would involve energy absorption.

The existence of attenuation within the index layer material will inevitably cause an attenuation of the ultrasonic field to be visualised, but it might be expected that this effect would decrease if the layer was made thinner.

The velocity of sound in a liquid is given by

$$C = \sqrt{\frac{K}{\rho}}$$

where K is the bulk modulus of the liquid of density ρ. In
a solid, the case is complicated by the possibility of transverse
vibrations.

Consider, however, the case where the velocity of longitudinal
ultrasonics in bulk samples of the liquid and layer media are
not the same, and where such a layer is placed in the path of
an ultrasonic wave existing in the liquid. It might at first
be thought that a wave, induced within the index layer, would
travel at a velocity differing from that of the ultrasonics
existing in the surrounding liquid.

It has been shown theoretically, however, that the complete system
will adjust itself, so that the velocity of ultrasonics within
both media becomes the same. This implies a departure from
the velocity of sound normally associated with the liquid and
layer media, resulting in a change in wavelength of the ultrasonic
field to be visualised.

A more complete description of the theory involved is presented
in Chapter Four. On further thought, however, one might expect
the equilibrium velocity of the system to be close to that
normally expected within the liquid medium, arising from the
layer's small thickness. The disturbance to the ultrasonic
field by this mechanism will thus be expected to be slight,
and to be further reduced by a decrease in an index layer's thickness.

1.4.2 <u>The index layer thickness</u>

It has been indicated that the disturbance to an ultrasonic field from the introduction of an index layer would decrease if the latter's thickness is reduced. It will be shown in Chapter Four that thinner layers will also result in a more valid display.

The resultant need for thin layers means that any optical effect used must be sufficiently sensitive to produce an adequate display in such small thicknesses. Most display mechanisms, including those outlined in Section 1.3, depend on the light path-length for their effectiveness, and this may have to be taken into account.

1.5   <u>The radiation patterns of ultrasonic transducers</u>

1.5.1 <u>Introduction</u>

Many methods exist in the literature for the theoretical determination of the radiation patterns of vibrating pistons and discs; these involve the use of both exact and approximate expressions.

Various conditions of baffle size, transducer shape and ultrasonic frequency have been examined by these methods, but it seems that single approach, capable of examining a wide range of conditions, including variations in baffle size, has not been described.

It was for the above purpose that an alternative theoretical
approach was designed.

1.5.2 General trends in transducer radiation patterns

The description of the sound field radiated by an ultrasonic
transducer is usually divided into two sections; the first
describes the region close to the transducer, the nearfield
region, and the other deals with the farfield region, the
region beyond the nearfield.

The usual definition of the nearfield region is that portion
of the field characterised by diffraction phenomena, and is
sometimes known as the Fresnel diffraction region. Conversely,
the farfield region   is also known
as the Fraunhofer diffraction region.

Fig 1.2 shows the usual qualitative description of these
portions of the field of an infinitely-baffled disc transducer.
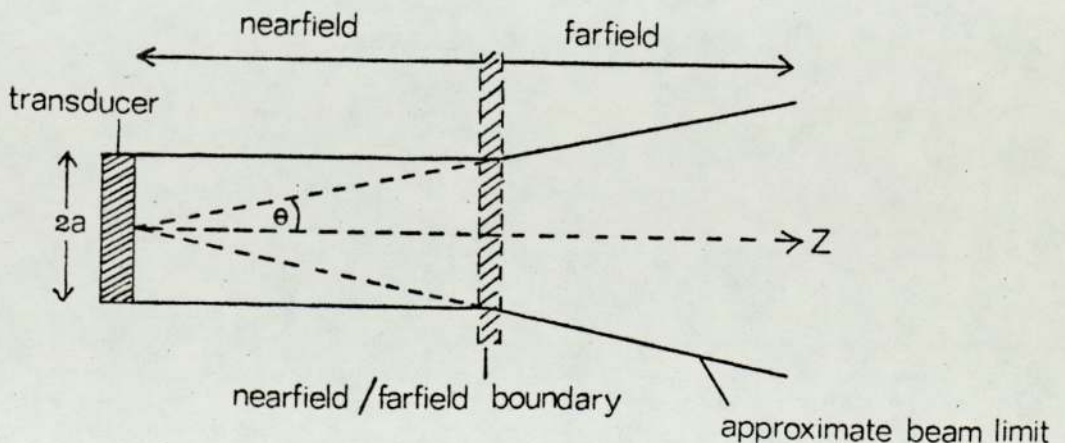
FIGURE 1.2   Radiated field of a disc transducer

The farfield is characterised by a divergence of the ultrasonic beam at the angle θ shown; in the nearfield the beam remains within a roughly cylindrical volume.

The boundary between the nearfield and farfield exists at the position indicated, and this will be at different positions in Z for different ratios of ultrasonic wavelength λ and transducer radius a. In general, it is found that this boundary exists at a distance of approximately a^2/λ from the transducer face; thus, the higher the ultrasonic frequency for a given radius of transducer, the less the diffraction of spread of the resulting beam.

The nearfield region, in which diffraction and interference occurs, is one of great complexity, and until relatively recently, had not been rigorously explored experimentally; in contrast, the farfield region has been described by a variety of techniques in the literature.

1.5.3 Existing theoretical approaches for the determination of these patterns

In general, mathematical analysis of the problem involves finding a scalar velocity potential $\emptyset$, which satisfies the general equation for a compressional wave in a non-attenuating medium, which is

$$\nabla^2 \phi = \frac{1}{c^2} \cdot \frac{\partial^2 \phi}{\partial t^2} = \frac{\kappa}{\rho} \cdot \frac{\partial^2 \phi}{\partial t^2} \qquad (1.1)$$

and which also fits the boundary conditions of the system.
For such a function, the acoustic pressure P and the particle
velocity q are given by

$$P = -\rho \frac{\partial \phi}{\partial t}$$

$$q = \nabla \phi$$

and it is supposed that these parameters are dictated at the
surfaces of the transducer, and those of a baffle and other
obstacles in the irradiated medium.

There are several approaches to the problem. The first involves
the application of Green's Theorem(51), which leads to a
surface integral of the type

$$\phi = \iint_S G \, dS$$

where S is the area over the transducer face, and G is an
appropriate Green's function. G must satisfy equation(1.1)

and must meet the boundary conditions existing over all surfaces in the acoustic medium. In general, G is chosen so as to satisfy a boundary condition extending to infinity in the plane of the transducer face.

The classical expression for the radiation field of an infinitely-baffled disc transducer, using the surface integral approach, was demonstrated by Rayleigh(52). His expression was used by Stenzel(53) to calculate the nearfield axial distribution for such a transducer, whereas McLachlan(54) evaluated it for the pressure distribution across the transducer face. More recently, Zemanek(55) numerically integrated the surface integral to obtain the nearfield distribution.

Schoch(56) showed that Rayleigh's surface integral could be separated into two parts when applied to a vibrating piston, one in the form of a plane wave, the other dependent on the shape of the piston's edge. Schoch's treatment was later elaborated by Dehn(57) and Carter and Williams(58).

The choice of a different Green's function from that used by the above, enables other transducer configurations to be examined. The case of the unbaffled transducer, exhibiting a perfectly absorbing layer across its back face, has recently been examined by Archer-Hall et al(59); the added use of specialist geometry enables the reduction of the surface integral to a single one with fixed limits.

The case of the unbaffled piston, without an absorbing layer, has been examined and the resultant expression for the axial distribution is derived in Appendix 1.

Impulse response techniques(60, 61) have been used for the treatment of both circular and rectangular transducers with infinite baffles; in particular, Lockwood and Willette(62) based their case on a Green's function approach, and have shown three-dimensional nearfield distributions of circular pistons in infinite baffles.

Integral transform methods have been used to solve for the value of $\emptyset$ at a point in the irradiated medium e.g. Junger and Feit(63), starting from Rayleigh's formulation, obtained a single integral to represent the pressure. In contrast, King (64) started from rigid application of boundary conditions to obtain an expression for $\emptyset$.

This expression has been approximated by various authors(65-67) to study circular transducers in infinite baffles.

Integral transform methods seem to be limited in application to this latter case. This arises because finite-baffled or unbaffled transducers give rise to mixed boundary conditions across the plane containing the transducer face; use of this method would involve the simultaneous solution of two separate integrals, which is a lengthy and difficult procedure(68).

Finite baffle problems may, in fact, be solved with the
aid of oblate spheroidal coordinates, and this approach has
been demonstrated by Todamato et al(69), with later contributions
from Devore et al(70) and Laucle(71).

1.5.4 An outline of the proposed theoretical approach

It is clear from the previous section that many different methods
already exist for determining the radiation patterns of disc
transducers; in particular, Lockwood and Willette(62) and Zemanek(55)
have obtained detailed, three-dimensional nearfield pressure
distributions. It might be asked, therefore, why an additional
theory has been developed.

It has been indicated that the nearfield of an ultrasonic transducer
is a region of great complexity, and the above authors have
investigated it for the case of disc transducers in infinite baffles.
The cases of finite-baffled and unbaffled nearfield distributions
seem, however, to be less well investigated; indeed, it appears
that detailed, three-dimensional nearfield distributions of these
configurations do not seem to have been described.

The theory to be presented was developed with a view to establishing
the three-dimensional nearfield distributions of ultrasonic disc
transducers, the baffle conditions being variable; the theory was

also designed to take into account variations in ultrasonic

frequency and transducer dimensions. Thus, the theory would

be capable of wide application, and this would be its main

advantage over existing techniques. In addition, the theory

was also designed to be simple in application, and to be

easily adapted to computer evaluation and graphical techniques.

The theory that has been developed consists of expressing

the scalar velocity potential $\emptyset$ in the form of a limited

series, each term of which is a solution to the relevant wave

equation. All problems that will be dealt with involve axisymmetric

cylindrical symmetry, and so the wave equation to be solved

is the Helmholtz Equation expressed in cylindrical polar

coordinates (r, Z ,θ) which is

$$\frac{1}{r} \cdot \frac{\partial}{\partial r} \left(r \cdot \frac{\partial \emptyset}{\partial r} \right) + \frac{\partial^2 \emptyset}{\partial Z^2} + k^2 \emptyset = 0 \qquad (1.2)$$

where variation with θ is zero, Z is an axial coordinate and r

is a radial coordinate.

A solution to equation (1.2) must be chosen so that its form enables

easy adaptation to a series representation. A solution of the form

$$\emptyset = \frac{A \ J_0 \ (c.r)}{j \sqrt{k^2 - c^2}} \ e^{j \sqrt{k^2 - c^2} \cdot Z} \qquad (1.3)$$

may be shown to be a solution of equation (1.2) by the Principle
of Separation of variables (Appendix 2). Time dependence has
been omitted, A and c are coefficients, k is a circular
wavenumber and J_o is a zero-order Bessel function of the first
kind.

Solutions of this form may be suitably combined to produce a
series type of solution, of the form

$$\phi = \sum_{n=1}^{m} \frac{A_n J_o (c_n r)}{j\sqrt{k^2 - c_n^2}} e^{j\sqrt{k^2-c_n^2}.Z} \tag{1.4}$$

where ϕ is now expressed as a limited series with a finite number
of terms m. It will be noticed that the solution is in the
form of a series of Bessel functions, whose properties have
been investigated and are well-known(72).

Chapter Six will dictate how equation (1.4) may be applied to
the determination of pressure distributions in front of ultrasonic
disc transducers, and how variations in baffle size are dealt
with. It will be seen that a method has been developed, whereby
the boundary conditions, existing over the plane Z = 0 and containing
the transducer face, may be rigidly applied to derivatives of
equation (1.4); this involves fitting the particle velocity
and/or pressure variations to the required distribution at the
plane Z = 0, and hence finding the appropriate values of A_n and
c_n for each value of n.

The advantage of a series solution is its simple evaluation and application to computer techniques. There are, however, potential limitations to a series form of solution, involving its convergence and the range over which it is valid; this would have to be investigated before the technique could be widely applied.

CHAPTER TWO

PROPOSED METHODS FOR ULTRASONIC/LIGHT INTERACTION

The concept of an index layer requires that there be an optical
effect within a thin sheet of suitable material, introduced
into the liquid medium in which exists an ultrasonic field.

Further, there is to be no optical effect in the liquid medium
itself, so that only the induced wave in the sheet will
contribute to the display.

Several mechanisms, as outlined in the Introduction, were thought
to be capable of producing the required optical effects; these
were

      (a)   photoelasticity;

      (b)   the enhancement of optical activity or circular diochroism.

Work on visualisation systems based on photoelastic effects in
solid sheets has been pursued to a useable state; the theoretical
background concerning the photoelastic visualisation of
ultrasonics will be presented.

The dynamic enhancement of optical activity and circular diochroism
by ultrasonics has been examined theoretically, but time factors
prevented experimental verification of these effects.

2.1   Proposed visual effects based on molecular alignment

2.1.1 Introduction

The proposed visualisation mechanism involves a variation in
the degree of alignment of the molecules of a liquid, which
follows the acoustic variations of an ultrasonic wave.

Ultrasonically-induced alignment of liquid molecules, to
produce an optical effect, has been observed in acoustic double
refraction, first reported by Lucas(73). Various theories
for the effect have been put forward(74-76), but all agree
that alternating compressions and rarefractions of an ultrasonic
wave subject the molecules to a flow gradient; orientation, causing
double refraction effects, then follows if the molecules are non-spherical.

The extent of double refraction, produced in this way, alternates
with the ultrasonic frequency; Peterlin(76) attributed this
effect to a kinematic equilibrium between the flow gradient, set
up by the ultrasonic waves, and thermal agitation.

The magnitude of the $\overset{\text{acoustically - induced}}{\diagdown}$ double refraction produced is, however,
very weak, and is dependent on the ultrasonic intensity and
frequency(77). The weakness of the effect is presumably due to
the fact that the degree of alignment, produced by the flow
mechanism, is small; this is easily understood when the ultrasonic
particle velocity at the intensity used ($0.1Wcm^{-2}$ at 1MHz) is

several orders of magnitude less than that due to random

thermal motion of the liquid molecules.

It is thought that the production of a more visible optical

effect, based on the dynamic orientation of liquid molecules,

may result from

      (a)   the use of an optical effect which is more sensitive

             to the orientation of its constituent molecules than

             double refraction;

      (b)   an improvement in the degree of alignment produced

             by the ultrasonic waves.

A more sensitive optical effect might result from the alignment

of molecules exhibiting optical activity or circular dichroism

in the random state, this alignment process enhancing these

optical effects. Improvement in the tendency for orientation to

occur under ultrasonic irradiation will be proposed by the use

of molecules, exhibiting the required optical properties, which

possess an asymmetric mass distribution.

2.1.2 <u>Orientational enhancement of optical activity and circular dichroism</u>

The reason for expecting these optical effects arose from the

consideration of various phenomena. Liquid crystals, already

discussed in the Introduction, show enhanced optical activity and

circular dichroism when caused to be in the ordered or mesomorphic

state; comparison here is with the random state, induced by raising

the temperature.

Liquid crystals have, in fact, been used to visualise ultrasonic standing waves and gross intensity variations(44), and shear waves on surfaces(43). The orientation, due to their cigar-like shape, which produces these optical effects is thought to be of little use in visualising a propagating wave, since the randomisation times of such molecules is too slow, being in the ms region.

Support for the proposed optical effects has arisen from analogue experiments conducted with microwaves.

Metal coils of suitable size and pitch will rotate the plane of polarization of a plane-polarized microwave beam. It is found that the rotation produced by orientated coils on the microwave beam is greater than that produced by coils at random angles to the beam(78). Additional experimental work has suggested that the rotation produced also depends on the angle between the axis of orientation of the coils and the microwave polarization axis.

The analogy here is that the coils represent optically-active molecules and the microwave beam plane-polarized light. Indeed, strong analogy is seen with molecules such as hexahelicene, which exhibits a marked optical activity because of its helical shape(79).
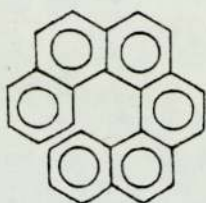
HEXAHELICENE

These microwave experiments also show effects commonly observed
in optically active crystals, where the optical activity
may vary with illumination direction, and where the magnitude
of the effect is invariably greater than a solution of that
substance.

It is thus considered that the alignment of molecules, already
exhibiting optical activity and circular dichroism in the random
state, would lead to an enhancement of these effects. Use of
molecules with a substantial initial optical activity would give
rise to an effect which is particularly sensitive to their degree
of alignment.

In order that the above effect be useful in displaying a
progressive ultrasonic wave, the latter must cause a varying degree
of molecular alignment within a suitable liquid. Further, these
variations must follow those of an acoustic parameter within the
ultrasonic wave.

It is proposed that these effects will occur if the liquid molecules
concerned exhibit mass-asymmetry.

2.1.3 The use of mass-asymmetric molecules

2.1.3.1   General considerations

Consider a liquid molecule, roughly spherical in shape, whose mass is not evenly distributed throughout its volume, as could occur if a highly dense group of atoms is present in such a molecule; the result may be a molecule whose centre of mass G is not at its geometrical centre O.

If such a molecule is accelerated by some external force, the nett force acting through O, the molecule will tend to rotate, as the line of action of the force does not act through G.

The application of an external force to a collection of such molecules, initially randomly orientated, would cause them to accelerate and, by the process outlined above, to swivel about their geometrical centres until both G and O lie on the line of action of the force. This process is shown in Figs 2.1(a) and (b). If the accelerating force is now removed, the molecules would tend to randomise themselves once more by thermal motion.

The presence of an accelerating force in the opposite direction would again result in alignment, this time differing by 180° from the previous case (Fig 2.1(c)).

It is proposed that the accelerations required to produce such orientational effects could be provided by a propagating ultrasonic wave. A degree of alignment that would follow the
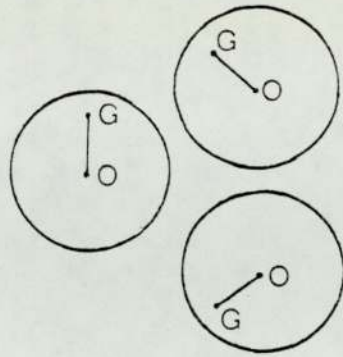
(a) INITIAL RANDOM ORIENTATION
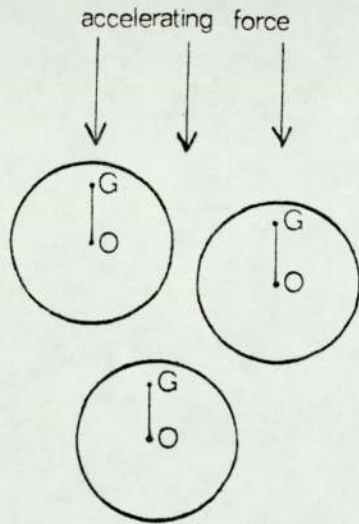
(b) AFTER ACCELERATION
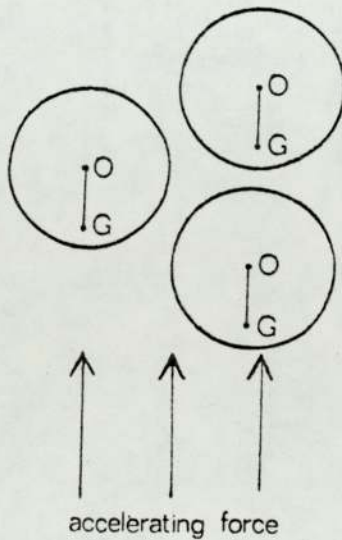
(c) ACCELERATING FORCE DIFFERING BY 180°

accelerating force

accelerating force

FIGURE 2.1 THE EFFECT OF ACCELERATION ON MASS - ASYMMETRIC MOLECULES

acoustic variations of such a wave is proposed as a

kinematic equilibrium, between orientation and randomisation.

The occurence of the above orientational effects is dependent

on several factors:

(a)   effects such as streaming and radiation pressure

       should not produce a permanent orientation of the

       molecules;

(b)   both orientation and randomisation should be fast

       enough to follow the acoustic variations.

Streaming and radiation pressure effects would not be expected

to produce permanent orientation of such molecules; they may

cause orientation of large particles of irregular shape, but

the effects of intermolecular bombardment on small particles

of roughly spherical shape would make these effects unlikely.

The expected times of orientation and randomisation will now

be examined for various molecular sizes and masses.

2.1.3.2   Randomisation relaxation times

The Kerr Effect(80) is the production of double refraction in a

liquid by the application of an electric field, the optical effect

arising from induced orientation of the liquid molecules. It

is thought that the orientation produced is dependent on the dipole

moment associated with the molecules in question, although
a Kerr Effect is seen in molecules without a permanent
dipole by the production of an induced dipole on application
of the electric field.

It is thought that the relaxation time of the Kerr Effect for
molecules without a permanent dipole would give an indication,
within an order of magnitude, of the randomisation relaxation
times to be expected from the type of molecules under consideration.

Some Kerr Effect relaxation times of such molecules are shown in
Table 2.1, and it is evident that they are heavily dependent
on the molecules' mass and dimensions. From this table, it
might be expected that molecules with sizes less than 200Å and
molecular weights less than approximately 10^5 may give rise to
randomisation relaxation times in the μS region or less; this
would be needed for the visualisation of progressive MHz
ultrasonic waves.

SYSTEM	RELAXATION TIME (S)	APPROX. SIZE / M.W.
biomacromolecules (81)	$10^{-2} - 10^{-4}$	3000Å / 10^7
proteins (82)	$10^{-6} - 10^{-8}$	200-300Å / 10^5
molecular liquids (83)	$10^{-10} - 10^{-12}$	—— / $< 10^3$

TABLE 2.1   Kerr Effect relaxation times

2.1.3.3   Orientational response times

The basic model for studying this problem will be a molecule,
having an asymmetric mass distribution, such that the point
through which the accelerating force acts is not the centre
of mass.

The molecule will be considered as cylindrical in shape, and
rotation about the central axis will be studied. The asymmetric
mass distribution is represented by a thin rod of dense
material, positioned at the edge of the cylinder and parallel
to its axis. A section through such a molecule is shown in
Fig 2.2.
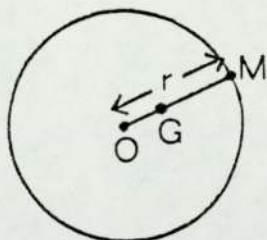
FIGURE 2.2   A mass asymmetric molecule

A cylindrical shape to the molecules has been chosen to
simplify the subsequent mathematics.

The molecule is of radius r and volume $\pi r^2 h$, having a total
mass m + M, of which M represents a dense atom or group on the

circumference. Point O is the geometrical centre of the
cylinder, whereas G is the centre of gravity, now displaced
from O.

Although the molecules under consideration are not spherical,
it is thought that the rotational times obtained will give an
order of magnitude result, applicable to various mass-asymmetric
molecules of differing shape.

Consider then an assembly of molecules, without mass asymmetry,
of mass m and density ρ. Scattered amongst these are mass-
asymmetric molecules, similar to these, but with the extra added
mass M on their circumference.

Let an ultrasonic wave, having a scalar velocity potential $\emptyset$,
exist in the liquid; the force acting on a symmetrical molecule
will be given by

$$F = m \cdot \frac{\partial q}{\partial t} = \rho \pi r^2 h \cdot \frac{\partial q}{\partial t}$$

where $\frac{\partial q}{\partial t}$ is the particle acceleration derived from q, the
instantaneous particle velocity.

A similar force is deemed to act on the mass-asymmetric molecules
also, and may be supposed to act through the centre O. This may be
replaced by a force F acting through the centre of gravity G

(where OG = b), and a couple of moment $FbSin\theta$, where θ is assumed to be measured from the direction of action of the force.

By moments about G,

$$mb = M(r-b)$$

$$\therefore b = \frac{Mr}{M+m}$$

The moment of inertia of the molecule about O is

$$I = Mr^2 + \frac{mr^2}{2}$$

treating the molecule as having an overall cylindrical shape. Hence, the moment of inertia about G (I_G) is

$$I_G = \frac{(M+m)r^2}{2} - (m+M)b^2$$

$$\therefore I_G = \frac{(M+m)r^2}{2} - \frac{M^2}{(M+m)}r^2$$

Let $M = nm$, n then representing the inherent mass asymmetry within the molecule in question; the previous equation becomes

$$I_G = (n+\tfrac{1}{2} - \frac{n^2}{(1+n)})mr^2$$

$$\therefore I_G = \frac{(\frac{3n}{2} + \frac{1}{2})mr^2}{1+n}$$

The equation of motion of the molecule will be derived from $M_f = I\ddot{\theta}$, where M_f is the moment of the external forces. The equation of rotational motion is thus

$$\frac{(\frac{3n}{2}+\frac{1}{2})mr^2}{(1+n)} \frac{d^2\theta}{dt^2} = -\frac{mnr}{(1+n)} \cdot \frac{\partial q}{\partial t} \sin \theta \qquad (2.1)$$

which is derived from

$$\text{Moment of external forces} = Fb\sin\theta = \rho \pi r^2 h \cdot \frac{\partial q}{\partial t} \cdot b\sin\theta$$

Equation (2.1) reduces to

$$\left(\frac{3}{2} + \frac{1}{2n}\right) \frac{d^2\theta}{dt^2} = -\frac{1}{r} \cdot \frac{\partial q}{\partial t} \cdot \sin\theta$$

As this theoretical investigation into the expected time of rotation can only give an order of magnitude result, we may put $\sin \theta = \theta$; thus

$$\frac{d^2\theta}{dt^2} + \frac{1}{r\left(\frac{3}{2} + \frac{1}{2n}\right)} \cdot \frac{\partial q}{\partial t} \cdot \theta = 0$$

There will, in practice, be an effect due to what may be treated as the viscosity of the solution or suspension, acting at the molecular level, which will introduce a damping term into the equation, making it of the form

$$\frac{d^2\theta}{dt^2} + 2k \cdot \frac{d\theta}{dt} + \omega^2\theta = 0$$

The period T of the motion governed by this equation is

$$T = \frac{2\pi}{\sqrt{\omega^2 - k^2}}$$

where, in our case,

$$\omega^2 = \frac{1}{r\left(\frac{3}{2} + \frac{1}{2n}\right)} \cdot \frac{\partial q}{\partial t}$$

If we assume that in all cases $\omega > k$, we may approximate this

expression to

$$T = \frac{2\pi}{\omega} = \frac{2\pi}{\sqrt{\frac{1}{r\left(\frac{3}{2} + \frac{1}{2n}\right)} \cdot \frac{\partial q}{\partial t}}} \tag{2.2}$$

which now ignores any effect due to viscosity.

Equation (2.2) gives the expected period of motion under investigation.

The actual time taken for orientation to occur will be over a

quarter of the complete cycle of motion i.e. the mass-asymmetric

molecules will completely align themselves in a time given by

$$T^* = \frac{\pi}{2 \cdot \sqrt{\frac{1}{r\left(\frac{3}{2} + \frac{1}{2n}\right)} \cdot \frac{\partial q}{\partial t}}} \tag{2.3}$$

where r is a molecule's radius, and where n $= M/m$.   Inspection

of equation (2.3) yields

(i)   T* increases as r increases

(ii)   T* decreases as $\frac{M}{m}$ increases

both of which would be expected. Thus, to produce as small

an orientational time T* as possible, molecules of small size

and large mass-asymmetry should be used.

(iii)   T* decreases as the frequency and intensity of

the ultrasonics increases

This arises because $\left|\frac{\partial q}{\partial t}\right|$ depends on both the intensity and

frequency of the ultrasonics used, $\left|\frac{\partial q}{\partial t}\right|$ increasing with each.

Equation (2.3) may now be used to predict the limits to the

size and mass-asymmetry which a molecule would need, to produce a

given value of T*; this would need to be at least in the μS

region for the visualisation of MHz ultrasonics.

To this end, consider a molecule such as iodobenzene, which has

an approximate radius of 3×10^{-10} m and a value of n given by

$$n = \frac{MW.\ iodine}{MW.\ C_6H_5} = 1.65$$

We are thus dealing with a small molecule with a large inherent

mass asymmetry. Substituting the above values into equation (2.3) gives

$$T* \simeq 10^{-7} S \quad \text{at 200kHz}$$

$$T* \simeq 5\times10^{-8} S \quad \text{at 1MHz}$$

$$T* \simeq 1.5\times10^{-8} S \quad \text{at 10MHz}$$

with an ultrasonic intensity of $1 Wcm^{-2}$. At a lower intensity of $0.1 Wcm^{-2}$,

$$T* \simeq 1.5\times10^{-7} S \quad \text{at 1MHz}$$

and the dependence of T* on the ultrasonic intensity is evident.

Assume, however, an intensity of $1 Wcm^{-2}$, and a molecule with only a moderate mass asymmetry, given by n = 0.5; a molecular radius of $10^{-9} m$ gives

$$T* \simeq 2\times10^{-7} S \quad \text{at 200kHz}$$

$$T* \simeq 10^{-7} S \quad \text{at 1MHz}$$

$$T* \simeq 3\times10^{-8} S \quad \text{at 10MHz}$$

Thus, the use of

(a) a molecular radius $< 10^{-9} m$

(b) a mass asymmetry given by $n \geqslant 0.5$

(c) an ultrasonic intensity $\geqslant 1 Wcm^{-2}$

(d) an ultrasonic frequency $\leqslant 10MHz$

would produce a system, involving mass asymmetric molecules, in which molecular orientational times are sufficiently fast for the

dynamic visualisation of ultrasonic waves.

These figures, however, represent the worst possible case, as they assume that complete alignment of all the mass-asymmetric molecules would be needed within the period T*.

The use of an optical effect that is very susceptible to changes in the degree of alignment, however, may mean that complete alignment may not be needed to produce a visible effect; the value of T* required in this case could then be considered to be greater than that predicted by equation (2.3). This would result in a beneficial effect on the ultrasonic intensities, and the molecular mass-asymmetry and radius needed. In particular, lower ultrasonic intensities could be used to produce a visible effect with a given molecule, thus raising the sensitivity of the technique.

2.1.4 General Conclusions

A mechanism has been proposed, whereby the visualisation of propagating ultrasonic waves by a liquid medium may be achieved. The mechanism involves the use of molecules, exhibiting substantial optical activity and circular dichroism in the random state, which have an asymmetric mass distribution.

The action of ultrasonics has been shown to result in a possible variation in the degree of alignment of a collection of such molecules, this variation following the ultrasonic cycle producing it. Further, the extent of optical effects mentioned above is

expected to be dependent on this variation, being enhanced in regions of increased alignment.

It has been shown that optical activity and circular dichroism may both be sensitive to changes in molecular alignment.

This change in alignment would follow an ultrasonic cycle, provided the conditions outlined in the previous section are met. These were judged to be broad limits; in practice, the use of an optical effect, sensitive to changes in alignment like those proposed, could lead to the use of lower ultrasonic intensities.

Investigations into suitable molecules were centred on organo-metallic compounds, and those singled out were derivatives of olefines in the form of osmate esters. These are readily formed by the reaction of ethylenic bonds with osmium tetroxide. These esters, notably their dipyridyl complexes, have been found to exhibit a strong circular dichroism and optical activity within the visible region(84).

Two examples of these osmate esters are 5α - cholest - 1 - ene and 5α - cholest - 2 - ene (Figs 2.3(a) and 2.3(b) respectively). The osmate group imparts a mass-asymmetry to each molecule, due

to the very dense osmium atom. The high degree of initial

optical activity and circular dichroism meets the required

optical conditions.

Although the size and mass-asymmetry of these molecules probably

approaches the theoretical limits imposed, it is thought that

their usefulness should be investigated.

In conclusion, the display of propagating ultrasonic waves

has been proposed by the use of a liquid, which contains optically

active and mass-asymmetric molecules. Substances with such

properties have been described. Unfortunately, these were not

readily available, and needed to be synthesized; time considerations

did not allow this. It remains, however, for experimental

verification of an observable effect to be carried out.
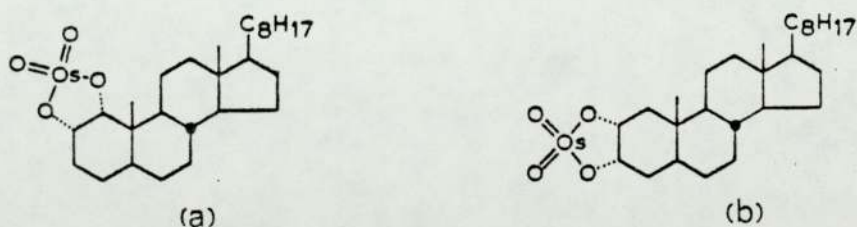
FIGURE 2.3 Osmate esters

2.2   Photoelasticity - the effect for use in solid layers

Photoelasticity has been used for many years in the study
of stresses in materials, and the effect is well-documented.
Recently, the technique has been applied to the study of
ultrasonic waves in solids, mainly for application to the area
of non-destructive testing.

The presence of an index layer, exhibiting photoelastic
properties, in the path of an ultrasonic field would be expected
to produce the type of display sought in this investigation.
The remaining sections of this chapter will thus be devoted to
basic photoelasticity, and the application of the technique to
the display of ultrasonics.

2.2.1 Basic photoelastic theory

A transparent solid, when subjected to a simple stress P,
behaves like a uniaxial crystal, the direction of P corresponding
to the optic axis of the crystal. When monochromatic light
is shone through such a solid in the form of a thin plate, it
is resolved into two polarized beams, vibrating parallel and
normal to P respectively. These travel at different speeds
through the solid, so that a phase difference exists between
them on a solid's far side. This phase difference, or retardation,
is usually measured in fractions of the wavelength of light used.

The above, known as artificial double refraction, can be extended
to a two-dimensional stress in a body by recognising that at
a single point, the state of stress will be characterised by two
Principal Stresses, mutually-perpendicular stresses acting at
that point; in this case, the axes of polarization of the two
light waves passing through the solid are parallel to these
stresses, and are known as the principal axes at that point.

Let us now consider the effect produced when a thin, stressed
plate is placed between crossed polaroid filters, as shown in
Fig 2.4. Plane-polarized light is incident normally onto a point
on the plate, at which the stress distribution is characterised
by two principal axes, X and Y, parallel to the resultant
principal stresses P_1 and P_2; one of these axes is at an angle θ
to the axis of the polarizer.

    Plane -polarized light of the form

    $A = a \sin \omega t$
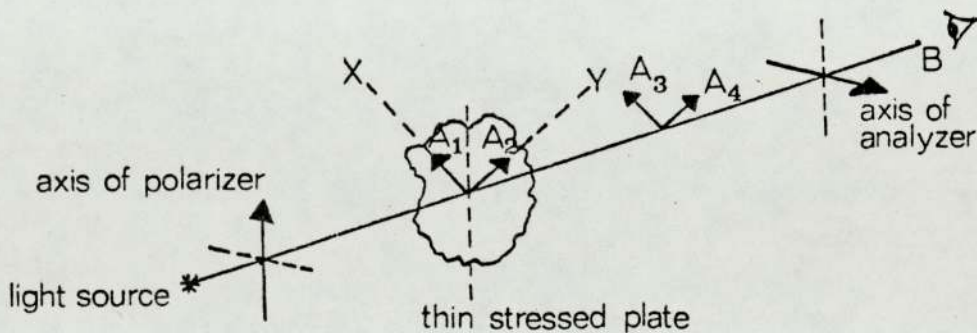
FIGURE 2.4

emerges from the polarizer and is incident onto the stressed

plate; on entering the plate, the light vector is resolved

into two components, A_1 and A_2, given by

$$A_1 = a \sin \omega t . \cos \theta$$

$$A_2 = a \sin \omega t . \sin \theta$$

which travel at different speeds. These components emerge

with a phase difference α to give

$$A_3 = a \sin \omega t . \cos \theta$$

$$A_4 = a \sin (\omega t + \alpha) . \sin \theta$$

The resulting wave transmitted by the analyser will be given by

$$
\begin{aligned}
A_5 &= A_4 \cos \theta - A_3 \sin \theta \\
&= a \sin (\omega t + \alpha) . \sin \theta . \cos \theta - \sin \omega t . a . \cos \theta . \sin \theta \\
&= a \sin 2\theta . \sin \frac{\alpha}{2} \cos (\omega t + \frac{\alpha}{2})
\end{aligned}
$$

Thus, the intensity of the transmitted beam seen at B will be

given by

$$I = k \sin^2 2\theta . \sin^2 \frac{\alpha}{2} \qquad (2.4)$$

where k is a constant. Equation (2.4) gives the expected variation

in the light intensity at the point under investigation,

and it can be seen that the variation

is dependent on two factors, namely the respective values of
θ and α.

(a)   the effect of θ

θ is the angle that exists between a principal axis of the stressed
plate and the axis of the polarizer. In effect, equation (2.4)
thus predicts that the amount of light transmitted through such
a system depends on the direction of the stresses in the plate.
No light will be transmitted when $\theta = n\pi/2$, where n is an integer
i.e. when the direction of a particular stress is parallel or
perpendicular to the axis of the polarizer. The maximum light
intensity will be transmitted when $\text{Sin}^2 2\theta$ is a maximum i.e. when
$\theta = n\pi/4$.

The effect at a point seen by an observer is thus dependent
on the direction of stress at that point, and is a maximum when
the direction of stress is at 45° to the axis of the polarizer.

(b)   the effect of α

α is the phase difference in radians, or retardation in
wavelengths, produced between two components A_1 and A_2 (Fig 2.4)
and is dependent on the magnitude of the stresses at a given
point. Variation in the amount of stress at a point thus produces
a variation in the transmitted light intensity. Examination of
equation (2.4) shows that no light will be transmitted when α is

zero or $2\pi n$ i.e. whenever the retardation produced is an integral number of wavelengths of the light used ($\lambda \equiv 2\pi$ radians).

The value of α at a point will also depend on the wavelength of light used, the material from which the plate is made and its thickness, these quantities being related in the expression for the retardation, given by

$$\text{retardation in wavelengths} = \frac{\alpha}{2\pi} = C(P_1 - P_2).d \qquad (2.5)$$

where C is known as the stress optical coefficient and is characteristic of the material used, P_1 and P_2 are the magnitudes of the principal stresses at that point, and d is the plate's thickness. This expression reduces to

$$\text{retardation} = C.P.d$$

for a single stress P at a point.

In summary, stress in a photoelastic material, placed between crossed polaroids, will cause a light pattern to be produced, this pattern being dependent on the magnitude of the stresses present and their direction. The light patterns produced by variations in the magnitude of the stresses present are known as isochromatics, whilst those produced by the directional dependence of stress are known as isoclinics.

2.2.2 The removal of isoclinics

The photoelastic pattern produced by the plate in Fig 2.4 changes if the plate is rotated about an axis perpendicular to its face; this is a consequence of isoclinic pattern changes. If the pattern in a specimen is required to be independent of the direction of stress, the isoclinic pattern must be removed to leave the isochromatics. This may be achieved in various ways, namely:-

      (a)   by the use of a double exposure technique;

      (b)   by rotating a pair of crossed polaroids in unison;

      (c)   by the use of circularly-polarized light.

(a)   Consider a system such as that shown in Fig 2.4, and let a photographic plate be placed at B. Suppose now that a double exposure is undertaken, with the polarizer/analyzer system being rotated by 45° between each; it can be shown(85) that if half the exposure time is taken in each position, the total intensity at a point exposed to the film is

$$I = k \, \mathrm{Sin}^2 \, \frac{\alpha}{2} \qquad\qquad (2.6)$$

where k is a constant. Thus, the recorded intensity is no longer a function of the directions of stress, and the isoclinic pattern has been eliminated.

(b)   If, in Fig 2.4 the crossed polaroids are rotated in unison
about the axis of the stationary specimen, the isoclinic
pattern moves, but the isochromatic pattern remains stationary.
Thus, continuous rotation of the crossed polaroids will result
in the blurring out of the isoclinics, leaving a record of
the isochromatic pattern only.

(c)   Quarter-wave plates are sheets of material with the property
that their double-refraction causes a retardation of $\lambda/4$ for the
wavelength of light used. Plane-polarized light, whose axis is
incident at 45° to a principal axis of such a plate, will cause
the resultant emergent beam to be circularly-polarized(86).

This result can be used to remove isoclinic patterns if a system
such as that shown in Fig 2.5 is used. Here, Q_1 and Q_2 are
quarter-wave plates with their principal axes in the directions
shown.
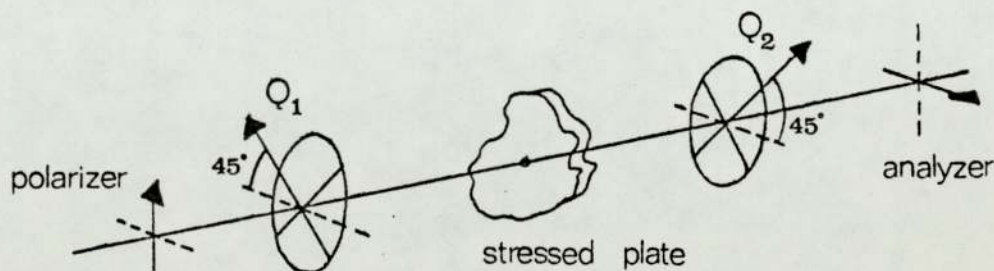
FIGURE 2.5

Circularly-polarized light, produced by the polarizer $/Q_1$

combination, passes through the stressed plate and is

'analyzed' by the Q_2/analyzer combination. The use of

similar mathematics to that used in Section 2.2.1 can be

shown(87) to result in a light intensity at a point being

given by

$$I = k_1 \ Sin^2 \alpha /2$$

which is similar to equation(2.7). θ dependence has been

removed, and isoclinics will not be present.

Quarter-wave plates, however, have a limitation - they only

produce circularly-polarized light over a narrow range of light

frequencies; the use of monochromatic illumination is thus

desirable. Use of light which is not of the required wavelength

will result in a loss of contrast in the photoelastic display

produced.

2.2.3 The study of ultrasonic waves by dynamic photoelasticity

Dynamic photoelasticity involves the study of propogating stress

waves, which will produce patterns in the same way as static

stresses, with the exception that the patterns will not be

stationary. The dynamic fringe patterns so formed have been

recorded in various ways; very high-speed cameras(88) or

streak cameras(89) may be used, or the pattern may be made

stationary by a short duration light flash(90). Alternatively,
use may be made of a stroboscopic light source(91).

The extension of photoelasticity to ultrasonic visualisation
was first proposed by McNamara and Rogers(92), who studied
continuous ultrasonic waves in quartz. In contrast to this,
Pih and Synders(90) used a short duration light flash to
obtain a stationary photoelastic pattern of ultrasonic waves in
an epoxy ring.

The use of a stroboscopic light source to visualise ultrasonic
pulses has been shown by Wyatt(93) and Hanstead(94). Short
duration light flashes were used, at a repetition rate
determined by the need for multiple reflections to die away between
each ultrasonic pulse. Fused quartz or unstrained glass was used
as the visualisation medium. Subsequently, investigators (95-98)
have visually studied the properties of ultrasonic pulses in extended
solid media, usually glass; various types of ultrasonic waves
(i.e. longitudinal, shear and surface waves) may be distinguished.

2.2.4 Further considerations

The quantitative use of photoelasticity in ultrasonic visualisation
requires the consideration of additional factors; these include

    (a)   the display produced should be independent of the
            direction of travel of the ultrasonic wave;

(b)   the wave's acoustic variations must be well-

represented by the photoelastic pattern produced;

(c)   the distinction between longitudinal, shear and

surface waves must be made;

(d)   the approximate sensitivity must be determined.

(a)   The principal stress direction associated with a longitudinal

stress wave is parallel to its direction of travel; isoclinics

will thus arise in the photoelastic display of ultrasonics. The

most effective display, under illumination with plane-polarized

light, will be expected when the wave travels at 45° to the axes

of the polarizer and analyzer, as in this case isoclinics will

not mar the isochromatic pattern. Conversely, travel in a

direction parallel to these axes will result in no display being

produced.   Isoclinics may be removed by any of the methods listed

in Section 2.3.2.

(b)   It is expected that the photoelastic display of a progressive

wave will contain two bright bands per ultrasonic wavelength.

This process is illustrated in Fig 2.6(a). The strain in a

material will be expected to follow the variations in the particle

displacement ξ of the ultrasonic wave. The same brightness of

display will be expected at positions A and B, although the strain

directions differ by 180°. Regions of zero strain produce no

photoelastic effect.
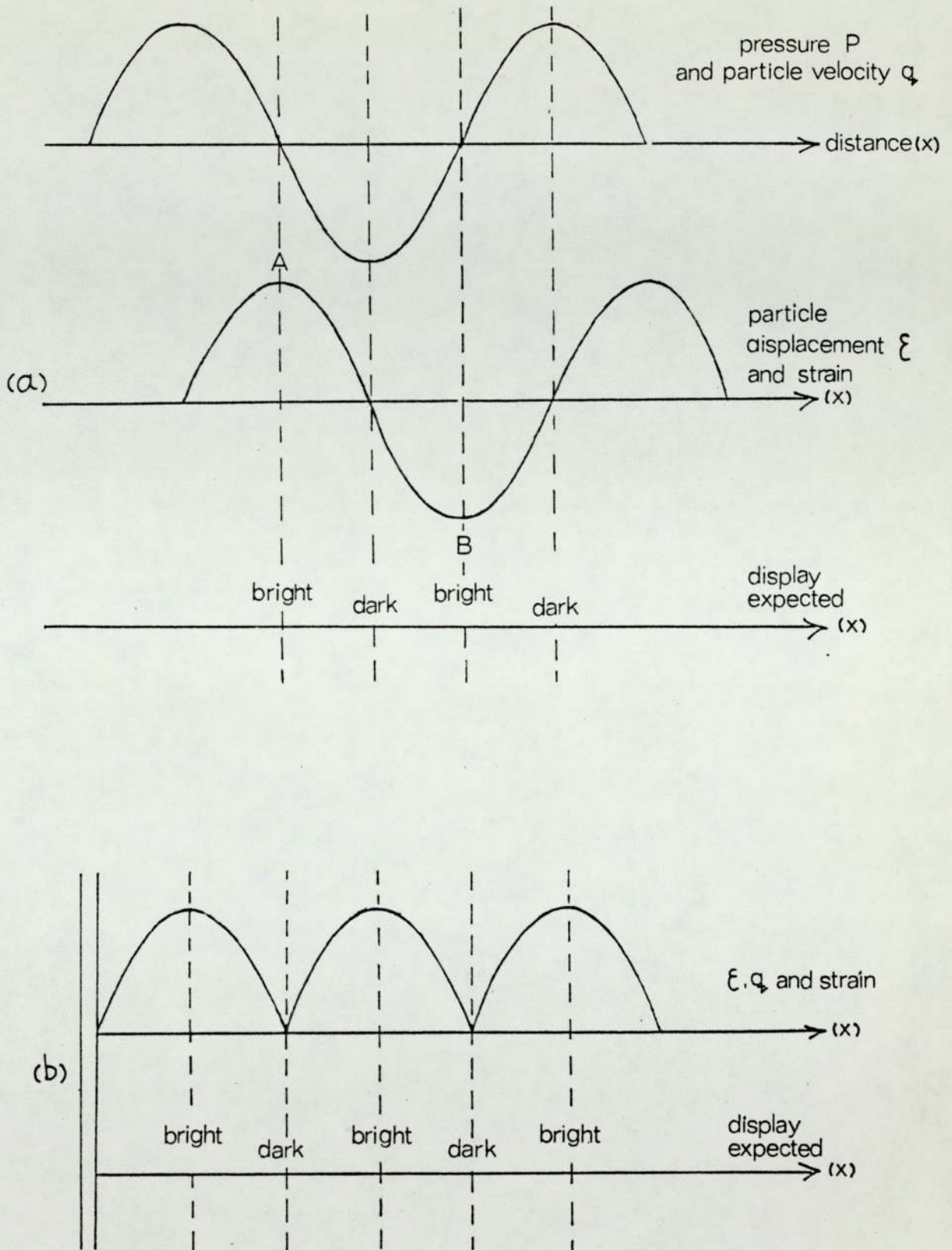
FIGURE 2.6 THE LINKING OF PHOTOELASTIC DISPLAYS
TO ACOUSTIC VARIATIONS.
(a) PROGRESSIVE WAVES (UNDER STROBOSCOPIC ILLUMINATION).
(b) STANDING WAVES (UNDER STEADY ILLUMINATION).

The photoelastic display of a progressive wave may thus be linked to variations in particle displacement, particle velocity and pressure. It should be noted that P and q are 90° out of phase with ξ, and so bright regions will be expected at positions corresponding to the maximum pressure and particle velocity gradients of the wave.

Fig 2.6(b) shows the photoelastic display expected from a standing ultrasonic wave. In this case, variations of particle velocity, particle displacement and strain are all in phase; pressure variations are 90° out of phase with these. Again, two bright bands per ultrasonic wavelength will be expected.

Quantitative measurements will depend upon the knowledge of the strain-optic coefficient, analogous to the stress-optical coefficient of equation(2.5), of the material in question. It should be noted that the photoelastic sensitivity of the material may vary with ultrasonic frequency(99), and calibration at the desired frequency may be required.

(c)   Ultrasonic waves within solids may exist as longitudinal, shear or surface waves, and the photoelastic displays produced by these various wave-types differ. Essentially, the dependence on the direction of travel under plane-polarized illumination may differ, together with the sensitivity and the displayed wavelength of each.

The principal stress directions associated with shear waves are at 45° to those associated with longitudinal waves, travelling in the same direction; thus, a longitudinal wave travelling at 45° to the axis of a plane polarizer will be clearly visible, whereas a shear wave will not. In addition, the velocity of longitudinal waves is usually approximately twice that of shear waves, resulting in the longitudinal wavelength being approximately twice as long in comparison.

Consideration of these phenomena allow the distinction between longitudinal and shear waves in a specimen to be made.

The stresses associated with Rayleigh waves have been described by Viktorov(100); the waveform is elliptical, inducing compressive, tensile and shear stresses in the medium. The photoelastic pattern produced is, however, quite distinctive(98).

(d)   The minimum ultrasonic intensity for photoelastic visualisation in glass has been put at $0.3Wcm^{-2}$(94); this was for a pulsed ultrasonic beam in a glass sample several inches thick. Hall (96) has also indicated that a 300V feed needed to be used for the pulsed transducer used in this type of work.

Glass is fairly insensitive photoelastic material; more sensitive materials include epoxy and columbia resins, polyesters and

polyurethane rubbers, these all being viscoelastic polymers.
These were not used in the work cited as their attenuation
of ultrasonics would be too high; their use, however, would
raise the sensitivity of the photoelastic visualisation of
ultrasonics.

2.2.5 Application to the proposed technique

The proposed technique for the display of ultrasonic waves in
liquids involves the use of thin layers of photoelastic material,
whose acoustic properties should be as close as possible to those
of the liquid, usually water; glass and fused quartz are not
suitable in this respect.

Photoelastic polymer materials, such as those listed in the
previous Section, are particularly applicable to the proposed
system, in that their acoustic properties are much closer to
water than those of glass or fused quartz, and they have a higher
sensitivity. Their use will thus be described.

The conditions of stroboscopy, used by previous workers, were short
duration light flashes at low repetition rates, for the study of
pulsed ultrasonic fields in solids.

The stroboscopic conditions, chosen for the proposed display of
continuous-wave ultrasonics in liquids, were light modulation at

a frequency centred on that of the ultrasonic field, as will

be described in the next chapter.   This was found to give

an adequately visible display, and was judged convenient for

additional reasons to be described.

CHAPTER THREE

APPARATUS AND ITS OPERATION

3.1   Preliminary experiments

The proposed visualisation system makes use of a layer of suitable
material, whose optical properties may be modified by the presence
of an ultrasonic field.   The effectiveness of such materials
needed first to be determined, before a full-scale apparatus was
built which utilised their properties; to this end, a preliminary
apparatus was constructed.

Chapters 1 and 2 have indicated that an effective display would
be expected if modulated, polarized light was used as the
illumination, use being made of the visualisation mechanisms
outlined in Chapter 2; the apparatus for these preliminary
experiments was designed so that this illumination was simply
achieved.   An ultrasonic frequency of 200kHz was chosen, giving
a convenient ultrasonic wavelength for viewing purposes of 7mm
in water.   The frequency of light modulation was designed to
be the same as, or differing by a fraction of Hz from, that of the
ultrasonics.   The stroboscopic effect would then allow a static
or slowly-moving display to be produced.   The system was
designed so that optical effects in both liquid and solid media
could be investigated.

3.1.1 <u>The apparatus</u>

The apparatus used for these preliminary experiments is shown

schematically in Fig 3.1. A 200kHz, PZT-4 ceramic transducer,

positioned at the base of a small cell, produced a plane wave

in a suitable liquid. Pulsed illumination, provided by a set

of six light-emitting diodes (LED's) was polarized and passed

through the cell. Transmitted light was viewed by eye from

the far side of an analyzer, with polarizer and analyzer

crossed so that no light was transmitted with zero ultrasonic

intensity. The liquid contained in the cell would be either

that under investigation, or water; the latter was used for

the investigation of solid media, lowered into the cell in layer

form.

An exploded view of the cell is shown in Fig 3.2. Two of its

sides were constructed from strain - free glass, allowing simple

observation of any optical effect. The rest of the cell was

constructed from materials which would not be attacked easily

by any corrosive chemical under investigation; the two

remaining sides were constructed from P.T.F.E. blocks with

stainless-steel edges, with the PZT-4 transducer producing

ultrasonics within the cell via transmission through a thin

nickel sheet. The whole construction was rendered leak-proof

with silicone-rubber cement.
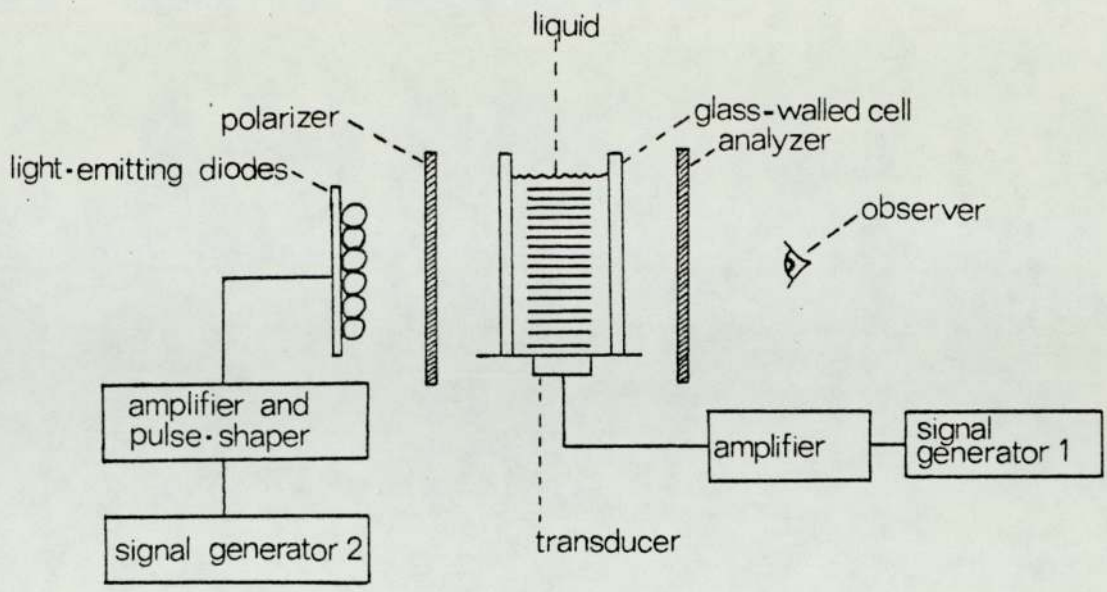
FIGURE 3.1   The preliminary experiment
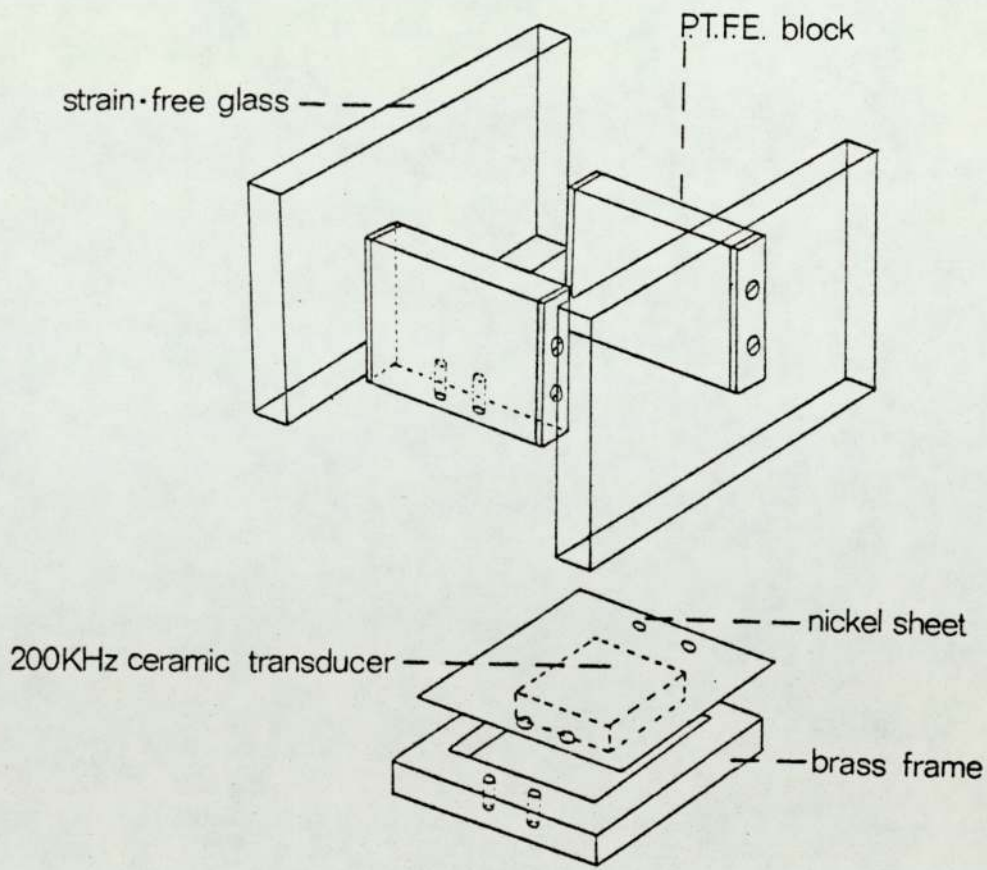
FIGURE 3.2   The standing wave cell

The electronic circuit used to drive the transducer is shown
in Fig 3.3(a). It was basically a transistor amplifier,
incorporating a Darlington arrangement, with a transformer
feed to the transducer. This transformer was designed to
operate adequately at 200kHz, the nominal resonant frequency
of the PZT-4 transducer block.

The pulsed voltage waveform, used to feed the six L.E.D.'s
was produced via the electronic circuit shown in Fig 3.3(b).
This waveform (positions A) was derived from the amplified output
of a signal generator, operating at approximately 200kHz.
The L.E.D.'s were chosen for their light-directivity, emission
frequency (in the green) and fast rise-time. The pulse-like nature
of their light output was confirmed by use of a photomultiplier.

3.1.2 Operation of the apparatus

The apparatus was designed so that either liquids or solids
could be investigated for their suitability as visualisation media.

For solids, the arrangement was as follows. A thin sample, say
3mm thick, was lowered into the top of the cell, which contained
water. The polarizer and analyzer had their mutually-crossed
axes at 45° to the expected principal direction of the ultrasonics
i.e. at 45° to the vertical, allowing the maximum visible effect
to occur (Section 2.2.4).

(b)

waveform produced at A =

← 5 μs →

15 V

(a)
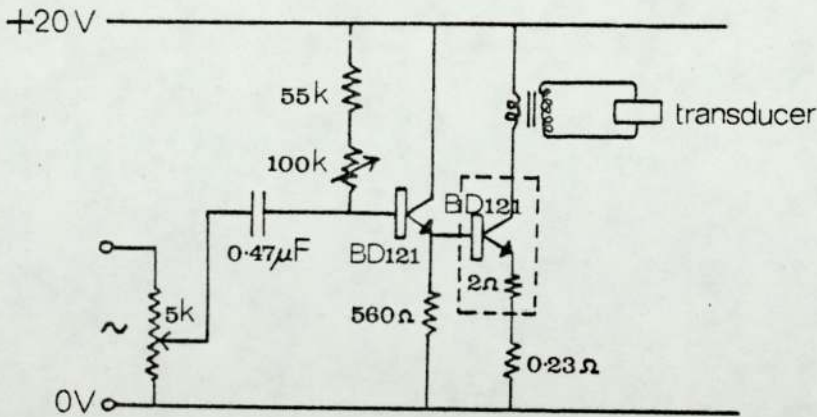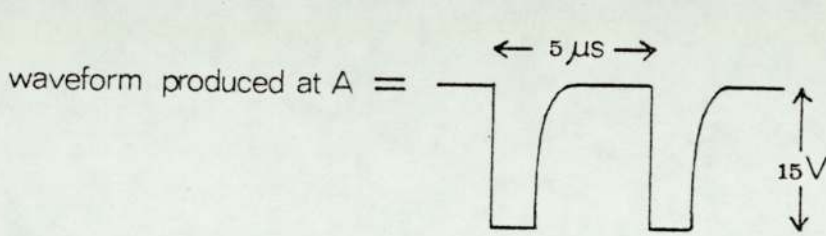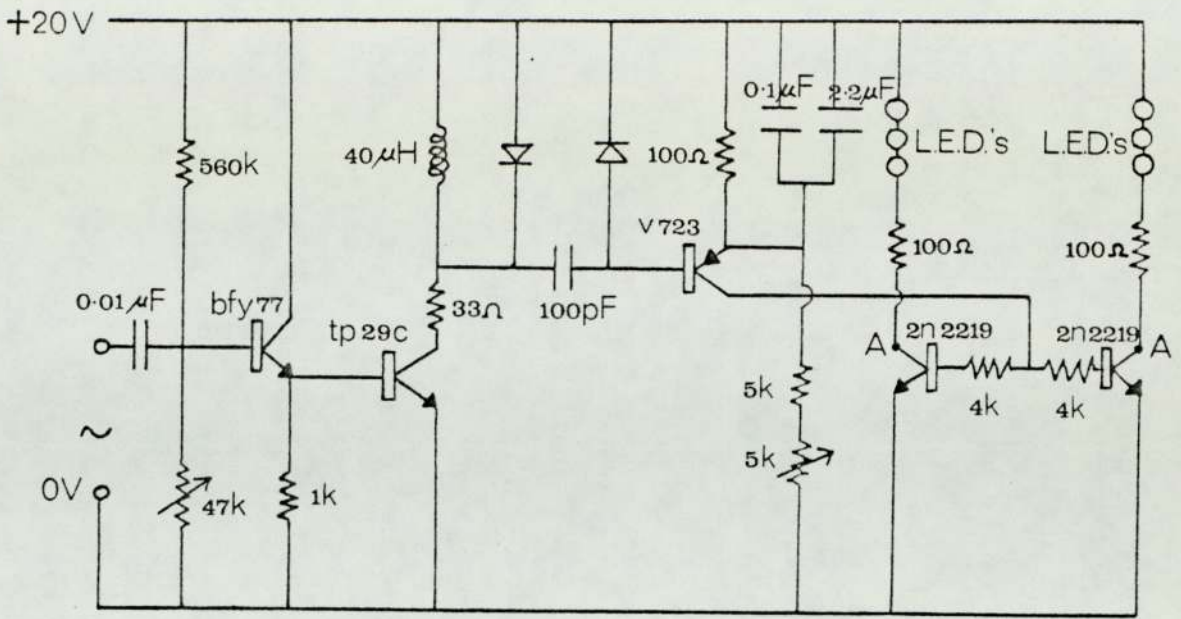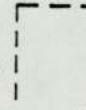
where [ ] = 4 units of the type shown in parallel.

FIGURE 3.3   (a) The transducer driving circuit
             (b) The L.E.D. driving circuit

Adjustment of the depth of water in the cell allowed various

ultrasonic distributions to be produced; predominantly,

however, standing waves were caused to exist by reflection

from the water/air interface.

Referring to Fig 3.1, signal generator 1 was first adjusted so

that resonance of the transducer occurred. Signal generator 2

was then adjusted so that the frequency of light pulsation was

close to that of the ultrasonics. It should be noted that

inspection of a standing wave did not need the use of stroboscopy;

progressive waves, however, could only be viewed conveniently

if the frequency of light pulsation was within one Hz of that

of the ultrasonics.

Under these conditions, visual effects were indeed seen in

various photoelastic materials of thicknesses up to 3mm, when

lowered into the cell in sheet form. Progressive and stationary

fields could be viewed, the former being seen as moving light

patterns when a slight difference between ultrasonic and light

pulsation frequencies existed.

The comparison of different photoelastic materials was thus

readily accomplished with this simply-constructed apparatus,

and their relative sensitivities determined.

The same apparatus, with the addition of quarter-wave plates,

would also have allowed the investigation of ultrasonic enhancement

of optical activity and circular dichroism, had suitable liquids

been readily available. This would have been achieved

by simply putting the liquids concerned into the cell.

The apparatus, however, still allowed confirmation of the

occurance of suitable photoelastic effects in various solid

sheets. This led to the decision to build a full-scale

visualisation apparatus, based on photoelastic effects within

thin sheets, which was capable of the visualisation of extended

three-dimensional ultrasonic fields. Such an apparatus will

now be described.

3.2   The properties required of a full-scale apparatus

The apparatus to be described was designed to follow various

criteria. The prime requisite was a system capable of sampling

two-dimensional sections of a complex ultrasonic field over a

wide area; an index layer of thin photoelastic material was

selected for this purpose. The preliminary experiments described,

and other published work (94,96) had indicated, however, that

the photoelastic visualisation of ultrasonics was likely to be

an insensitive process; it was thus decided to design a system

whereby progressive ultrasonic waves could be generated at an

intensity approaching cavitation levels in water.

An ultrasonic frequency of 200kHz was selected for reasons

explained in Section 3.1. The frequency of light modulation

was proposed to be adjustable around this nominal 200kHz, so that

use of the stroboscopic effect could be made. Short duration
light flashes, at a repetition rate of several hundred Hz
were not considered as suitable, although these have been
effectively used for the visualisation of ultrasonic pulses(95).

Flexibility in the wavelength of illumination was considered
desirable, allowing the display produced to be studied with
either monochromatic or broad-band illumination; this was
thought to be best achieved with a broad-band light source
and a selection of filters.

3.3   A brief description of the full-scale apparatus

A schematic diagram of the full-scale apparatus, constructed
to meet the criteria outlined above, is presented in Fig 3.4.

Light from a 100W, high pressure mercury arc-lamp is collected
and focussed onto a photoelastic light modulator by a series
of bloomed achromats. A sinusoidal voltage, fed to this
modulator via a suitable power amplifier, allows amplitude
modulation of the light beam, in a variety of waveforms, about
a 200kHz nominal frequency. The diverging light beam is then
deflected vertically and made into a parallel, cylindrical beam
for illumination of an index layer.

The ultrasonic field to be visualised is produced by an air-backed
transducer, radiating into an extended volume of water contained
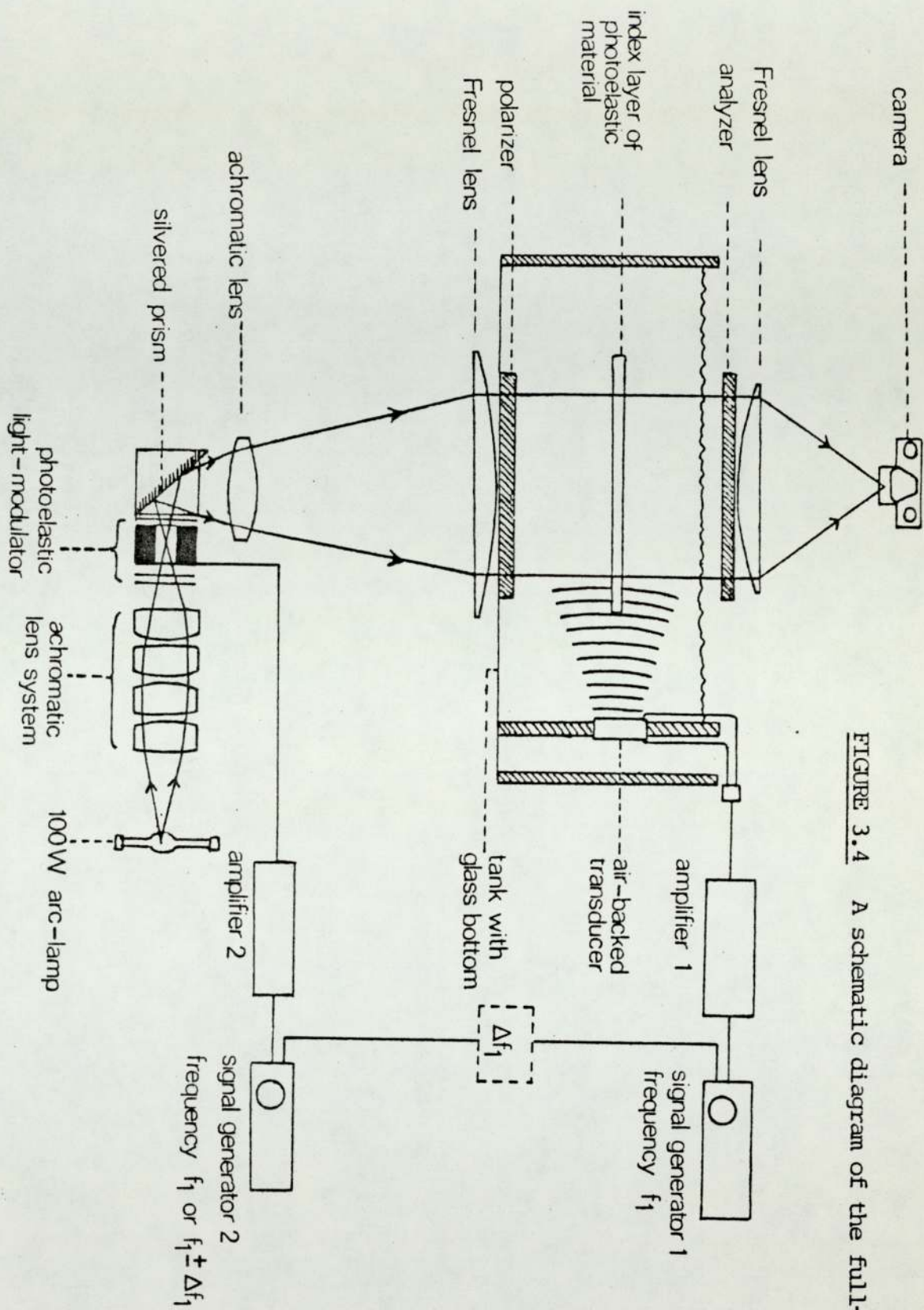
FIGURE 3.4 A schematic diagram of the full-scale apparatus

in a glass-bottomed tank. The sinusoidal voltage supplied
to the transducer via a power amplifier is adjustable in
frequency about 200 kHz until resonance is produced.

The cylindrical light beam, plane-polarized by the polaroid
filter positioned on the tank's bottom, passes through the
index layer of thin photoelastic material, the latter supported
horizontally in the ultrasonic field. The light beam is then
analyzed by a further polaroid filter, its axis being at 90°
to that of the polarizer. A Fresnel lens finally focusses the
resultant beam into either the eye or the lens of a camera.

Control over the difference in frequency between the light
modulation and ultrasonic generating systems is achieved by
first interlocking the frequencies of the two signal generators
shown in Fig 3.4, and then introducing a known frequency
difference between the two. This allows either stationary
or moving displays to be viewed by control over the rate
of stroboscopy.

The constituent components of this apparatus will now be described
in greater detail.

3.4   The optical system

3.4.1 The light source and light collecting system

The chosen light source is a Wotan 100W high-pressure mercury

arc-lamp, which gives a high intensity output with a broad
spectral distribution.   A continuum besides the mercury
lines extends over the ultra-violet, visible and infra-red
spectral regions, with a resultant bluish-white light output.
The total luminous flux of the lamp is 2,200 lm, thought to be
ample if only a fraction of this light is collected and used.
A useful feature of this type of lamp is its small area of
arc, o.25mm x 0.25mm, which allowed the subsequent optics
to be designed on the assumption of a point source.

The arc-lamps are supplied with a non-adjustable electrode
spacing, and thus a high voltage is required to start them.
This is supplied via a modified vacuum leak detector, essentially
a Tesla coil device, whose output is fed to an ignition electrode.
A d.c. supply is used to give 20V across the lamp under
running conditions, the lamp taking a current of 5A after settling
down from starting.

The complete lamp assembly is contained within a water cooled
jacket, fitted with an exit port through which light is collected
via an assembly of lenses. This lens system was designed so
that as large a fraction as possible of the arc-lamps output
could be collected, and directed onto the next optical element
with acceptable freedom from aberrations.
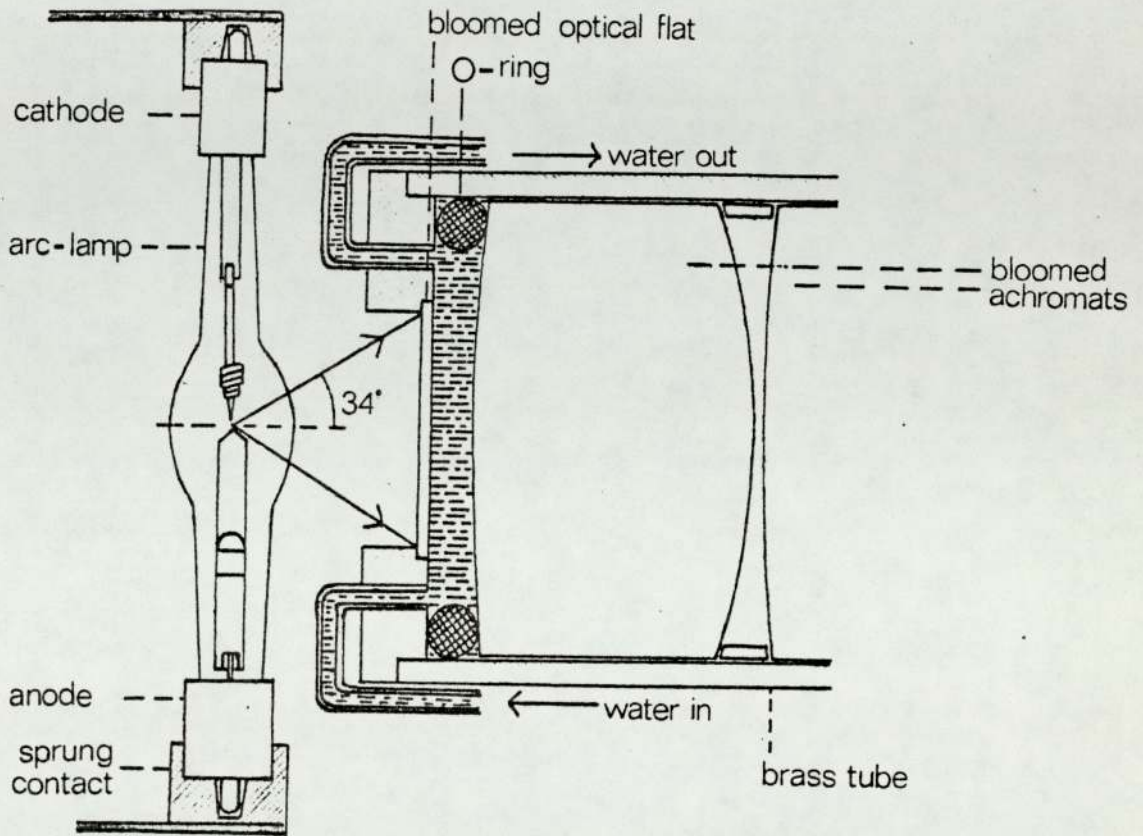
FIGURE 3.5   The arc-lamp and light-collecting system

Fig 3.5 shows how the first of these lenses collects a 34° half-cone angle of light from the lamp; water cooling is provided, via a peristaltic pump, so that the light's infra-red component is filtered out, avoiding damage to the following lens system. This water-cooling serves an additional purpose in that dyes, added to the water, allow the convenient selection of any desired wavelength band from the lamp's output.

The lens system consists of four bloomed achromats, the first two of which were shown in Fig 3.5. These are held coaxial in a brass cylinder, mounted on an optical bench. This lens system, having been designed to be well-corrected for spherical aberration, produces a good, focussed image of the lamp's arc. The resultant convergence of the light beam is a 20° half-cone, suitable for incidence onto a photoelastic light modulator.

3.4.2 The light modulator

The features considered desirable in the modulator to be chosen were:

    (i)   the production of 200kHz amplitude modulation of the incident beam;

    (ii)   adjustment of the modulation frequency either side of this value by a small amount;

(iii) the production of either pulse-like

or sinusoidal modulation waveforms, allowing

the stroboscopic effect by these two to be

compared;

(iv) a large angular aperture.

Various types of light modulator were originally considered

for use, although Pockels Cells were ruled out from aperture

considerations, and Kerr Cells from the difficulty and expense

of producing kV driving signals. A modulator, based on the

photoelastic effect, was then designed and constructed which

would exhibit the required properties.

Fig 3.6 shows a schematic diagram of the design chosen for the

modulator. Light from the arc-lamp is focussed onto the centre

of an optical element, constructed from a suitable photoelastic

material. The output from two 200kHz ceramic transducers is

fed into this optical element to produce a photoelastic effect.

This will cause a variation in light intensity to be seen at P,

provided a suitable combination of polaroid filters and

quarter-wave plates is positioned either side of this element,

as shown.

Plane, elliptically or circularly-polarized light may be incident

onto the optical element by positioning of the quarter-wave

plate at positions A, B and C respectively; this allows the

modulation produced under these various illumination conditions

to be compared.
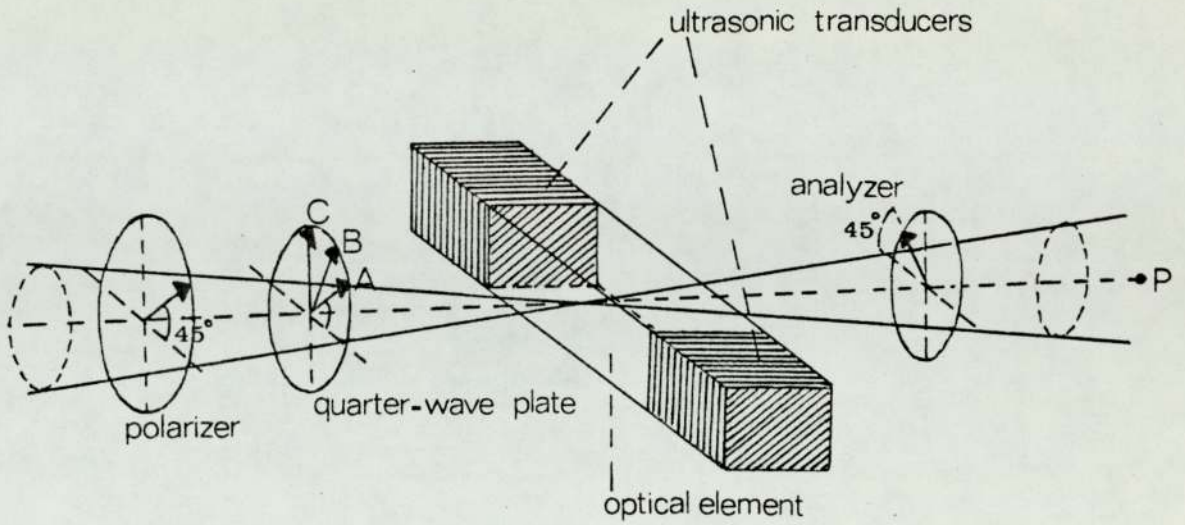
FIGURE 3.6   The design of the modulator
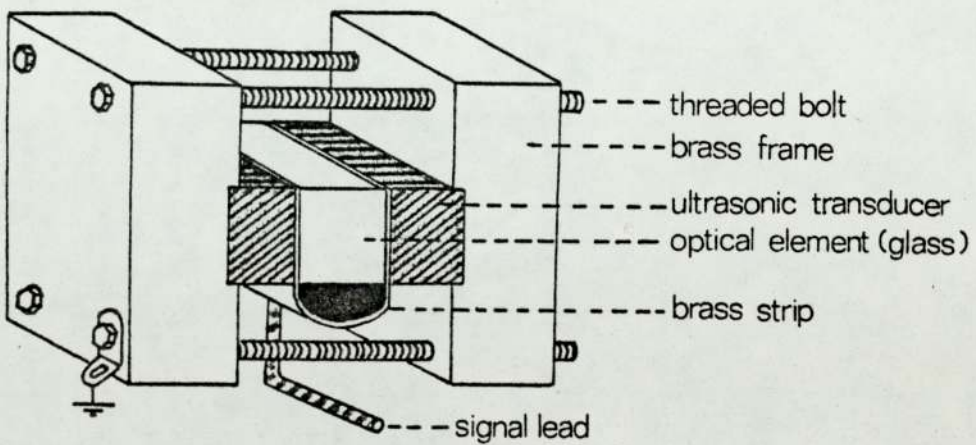
FIGURE 3.7   The modulator's construction

The modulator was constructed so that neither the optical element's thickness, nor the effective path through the completely assembled structure, corresponded to an integral number of ultrasonic half-wavelengths; this was to avoid resonance at 200kHz, and thus to enable operation over a fairly wide frequency band-width. It was also hoped that this design would enhance the production of non-sinusoidal light modulation, by the presence of an increased ultrasonic harmonic content within the optical element.

Fig 3.7 shows the modulator's construction in greater detail. The two transducers are PZT-4 ceramic blocks, these and the optical element being held together in a suitable frame. The initial pressure of the transducers against the optical element may be adjusted by means of the four threaded bolts shown. Electrical connection to the transducers is provided by a brass strip in contact with their inner faces, the brass blocks being earthed. A 200kHz sinusoidal voltage of up to 150Vp-p may be supplied to the transducers via a circuit essentially similar to that shown in Fig 3.3(a).

Initial experiments used various polymers as the optical element; these, however, were found to distort and exhibit permanent strain from heating by the ultrasonics. An initially strain-free glass block, with polished ends, was then tried and found to produce satisfactory results.

Fig 3.8 shows the observed amplitude modulation waveforms,
obtained with the device under illumination with the
focussed beam of the arc-lamp. Here, the upper trace is the
transducer driving voltage, the lower trace being the
light modulation waveform, both displayed on an oscilloscope
screen; the latter was achieved via a specially-constructed
light detector, incorporating a photo-emissive tube. Beside
each set of waveforms is the polarization form of the light
incident on the modulator, produced by the polarizer/quarter-wave
plate combination (Fig 3.6).

Some interesting features arise from these traces. The use
of a plane-polarizer and analyzer results in frequency doubling
i.e. sinusoidal modulation at 400kHz with a 200kHz driving
frequency (Fig 3.8(a)). Sinusoidal modulation at 200kHz results
from the use of circularly-polarized light as the incident
illumination, a plane analyzer being used as before. (Fig 3.8(c)).
Pulse-like modulation at 200kHz is produced, however, with elliptically
polarized incident illumination. 80% amplitude modulation is
achieved for both waveforms at 200kHz, 400kHz modulation being
less efficient at 25%.

It is found that the above modulation characteristics hold
over quite a wide frequency range, and the non-resonant design
of the modulator is thus successful in this respect; in
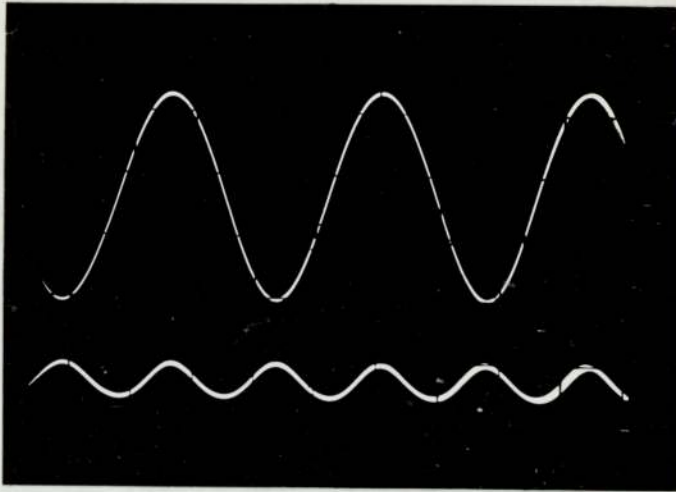
PLANE·POLARIZED
INCIDENT ILLUMINATION
(a)
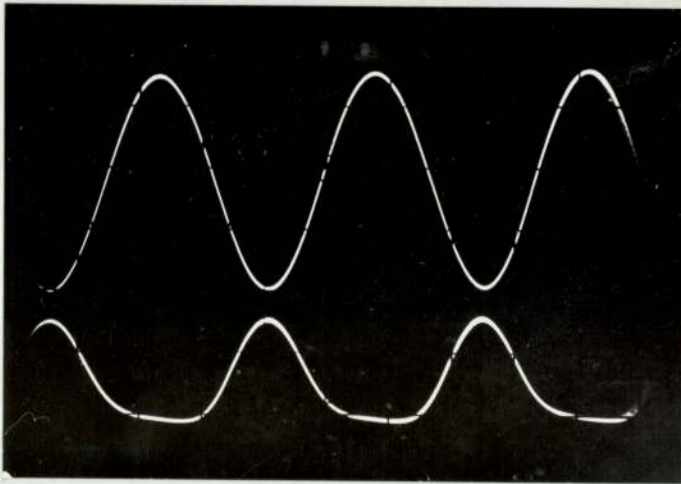
ELLIPTICALLY·POLARIZED
(b)
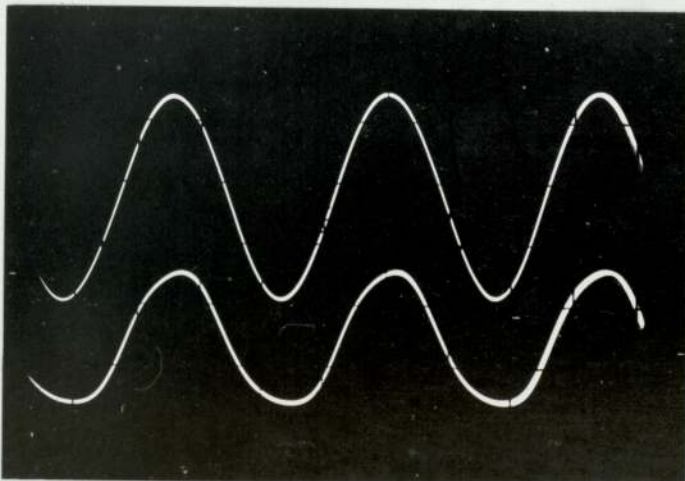
CIRCULARLY· POLARIZED
(c)

FIGURE 3.8   Modulation waveforms, produced by the modulator under
various conditions of incident illumination.
Upper trace: voltage signal to modulator
Lower trace: light modulation waveform

practice, these characteristics hold to within 10% of
the amplitudes quoted between 197 and 203 kHz. This non-resonant
design is also thought to contribute significantly to the
production of 200kHz pulse-like modulation, by the interaction
of elliptically-polarized light with an enhanced ultrasonic
harmonic content within the optical element.

It has been found that photoelastic light modulators have been
used by other authors, especially Kemp(101) who predicted
that frequency doubling would occur under plane-polarized light
conditions, and that sinusoidal modulation at the ultrasonic
frequency would occur if a quarter-wave plate was inserted.
Both these observations agree with those described above. As
with other authors (102, 103) no mention was made of pulse-like
modulation at the ultrasonic frequency. In all three references
cited, the modulator's design incorporated an ultrasonic standing
wave within its optical element, resulting in a high Q device
which was capable of satisfactory operation over only a very
small frequency range.

The modulator constructed, and described above, has a much lower
Q, allowing an extended frequency range of operation, and the
potential of producing pulse-like modulation at the ultrasonic
frequency. The only drawback is that quite high ultrasonic
powers are needed to produce the effects described, a resonant
design requiring much lower powers.

The photoelastic light modulator, described above, thus
meets the criteria outlined at the beginning of this Section;
pulse-like or sinusoidal amplitude modulation, adjustable
in frequency either side of 200kHz, may be produced by the
action of the modulator on the focussed beam from the
arc-lamp.

3.4.3 The subsequent optics and the complete optical system

The need to illuminate an index layer normally with modulated,
polarized light meant that the output from the modulator needed
to be deflected vertically. This is achieved by a silvered
prism, the silvering being present to deflect parts of the .
conical beam which are not within the critical angle. A bloomed
achromat, mounted immediately above this prism, reduces the
angle of divergence of the now vertical beam from 20° to 9°.

Fig 3.9 is a photograph of the optical system up to this point;
clearly seen is the lamp housing, followed by the brass tube
containing four achromatic lenses. Mounted at the far end of
this tube is the polarizer and quarter-wave plate of the photoelastic
light modulator. The latter, together with the deflecting
prism, is mounted on a horizontal plate, with the analyzer of
the modulator placed between the modulator and prism. Above
this prism, the first convering lens can be seen.

FIGURE 3.9   The optical system, including the arc-lamp, lens system, modulator, prism and converging lens
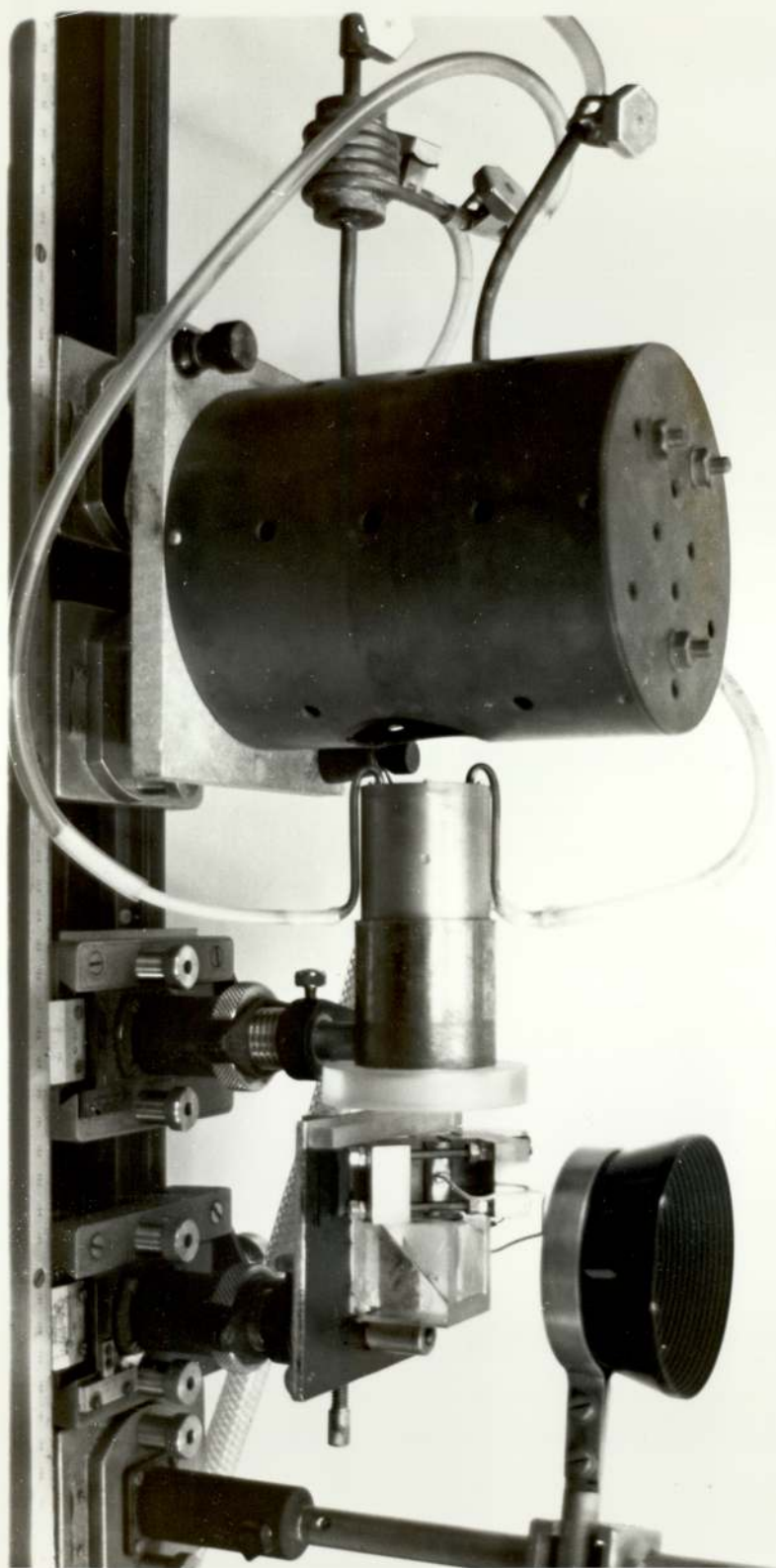
Conversion of the vertical but still diverging beam into
an approximately 20cm diameter cylindrical beam, for illumination
of an index layer, is achieved by a 61cm focal length Fresnel
lens, 40cm in diameter. Fresnel lenses have the advantage of
low cost, large diameter and relatively low spherical and
chromatic aberrations, making them ideal for this application.

The now parallel beam passes through the glass bottom of the
water tank, the other side of which is a polaroid filter,
acting as the polarizer to the index layer. The analyzer
is mounted at the far side of the index layer, above the
water's surface (Fig 3.4). A good image, for the eye or
camera, of events taking place in the index layer is produced
by a field lens, which focusses the transmitted beam to a point.
A Fresnel lens is again used for this application, a 25cm
diameter and 32cm focal length being found suitable. A field
lens is essential if a uniform illumination over the whole
field of view is required.

Fig 3.10 is a diagram showing the states of polarization of the
light beam at various stages in its path through the system.
The cone of light, emergent from the modulator's analyzer A_1,
will be depolarized by reflection at the prism's reflecting
surface unless its plane of polarization is parallel to the latter
i.e. horizontal. A more efficient system will result if
depolarization does not occur; this dictates the orientation of
the axes of the various components of the light modulator,
as shown. It should be noted that the positions A, B and C
indicated ocrrespond to those of Fig 3.6.

analyzer A$_2$

index layer

polarizer P$_2$

tank bottom

Fresnel lens

achromatic lens

silvered prism

analyzer A$_1$

optical element of modulator

45°

A
B
C

quarter-wave plate
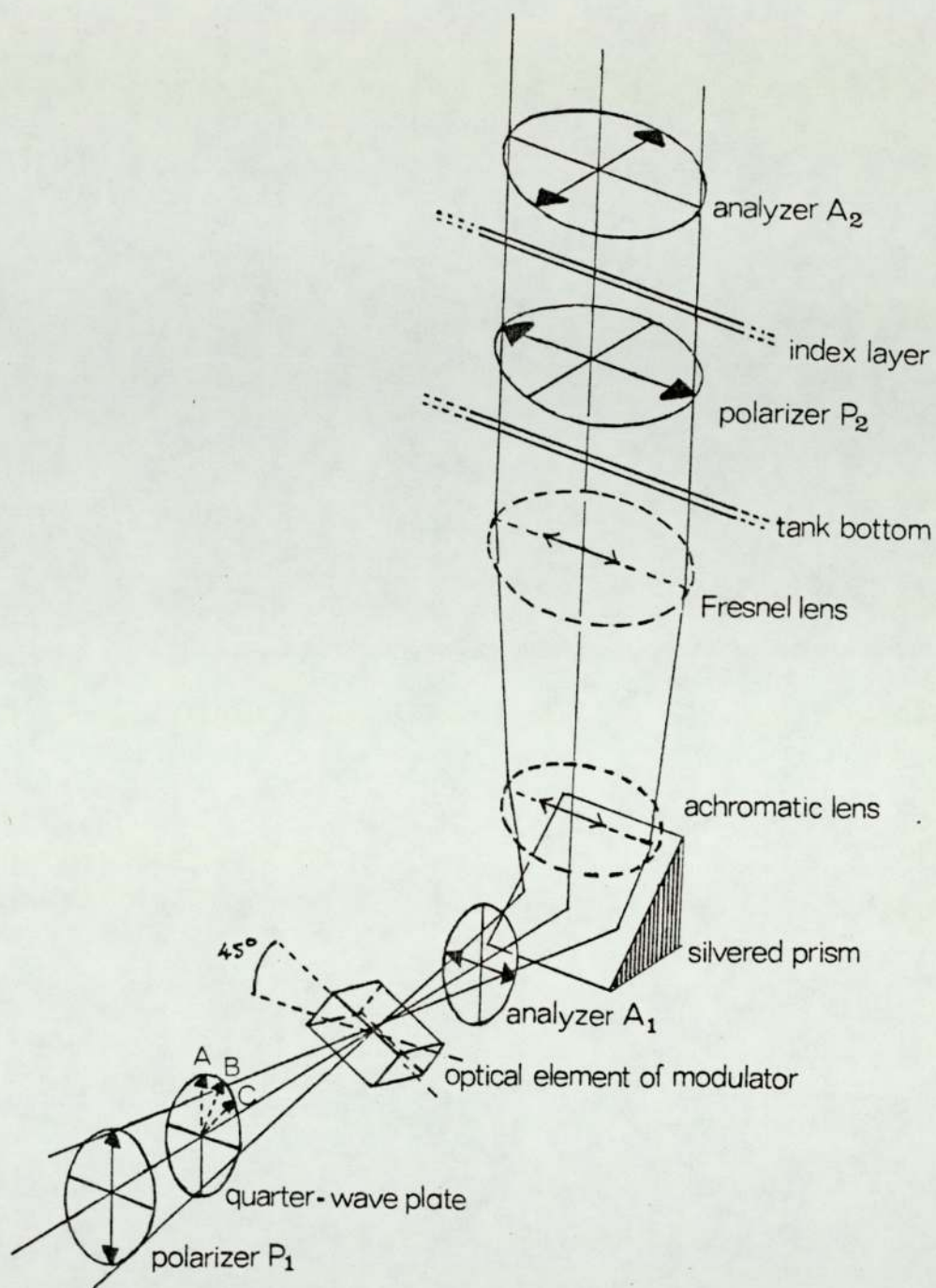
polarizer P$_1$

FIGURE 3.10   States of polarization throughout the optical system

The polarization axis of the polarizer P_2 on the tank's
bottom is arranged to be parallel to the incoming plane-
polarized light beam, again the condition for maximum
efficiency. P_2 is needed to remove any visible effect of
strain within the tank's glass bottom. Finally, analyzer
A_2 is orientated with its axis at 90° to that of P_2,
allowing photoelastic effects within the index layer to
be observed.

The complete optical system, described above, is thus capable
of producing amplitude-modulated, plane-polarized light, of
adequate intensity, for the normal illumination of an index
layer. An analyzer and field lens produce a good image of
photoelastic phenomena within such a layer, caused by the
passage of ultrasonic waves through it.

3.5   The ultrasonic generating system

3.5.1 Introduction

The photoelastic visualisation of ultrasonics was expected
to be an insensitive technique, as previously outlined;
hence, experiments involving continuous-wave ultrasonics were
designed to be conducted at high ultrasonic powers.

In practice, the power that can be delivered to a liquid
medium is limited by the phenomenon of cavitation. The ultrasonic

power level at which this effect is first seen decreases

with lower frequencies; at 200kHz, the level required is

$2\text{-}3Wcm^{-2}$ for water containing dissolved gases(104).

Investigations into the photoelastic visualisation of

ultrasonics were planned at an ultrasonic intensity of approximately

$1Wcm^{-2}$, i.e. at intensities approaching cavitation levels.

The transducer chosen for use was a PZT-4 piezoelectric ceramic

disc, manufactured by Vernitron Ltd., with an efficiency of

approximately fifty percent; the radius of the disc used was

2.5cm, with a radiating area of approximately $20cm^{2}$. This

meant that the transducer had to be driven with continuous

electrical powers of between 30-40W rms, to produce the required

levels of ultrasonic intensity. An electronic system, capable

of supplying these powers at high voltages, was accordingly

designed and constructed.

3.5.2 The transducer mounting and driving electronics

It was thought that an effective way of producing high intensity,

continuous-wave ultrasonics, in an extended volume of water,

was to mount the transducer through a partition towards one

end of a water tank.

This would achieve several aims. An air-backed transducer,

so formed, would exhibit preferential ultrasonic radiation in

the forward direction, due to a large characteristic impedence difference between air and the transducer's ceramic material; the ceramic/water impedence difference would be smaller in comparison. Further, simple electrical connection to the transducer could then be achieved by earthing its front face.

Fig 3.11 shows a plan view of the transducer mounting, situated in a perspex position towards one end of a water tank. Electrical connection to the two transducer surfaces is made via gold-plated nickel discs, chosen so that contact cement could be used to provide good physical and electrical contact. Silicone-rubber cement and an O-ring provide a water-tight seal.

The circuit used to provide a sinusoidal electrical signal to the transducer is shown in Fig 3.12. It is based on a push-pull arrangement of two sets of power transistors, the outputs of which are fed to the primary of a step-up transformer.
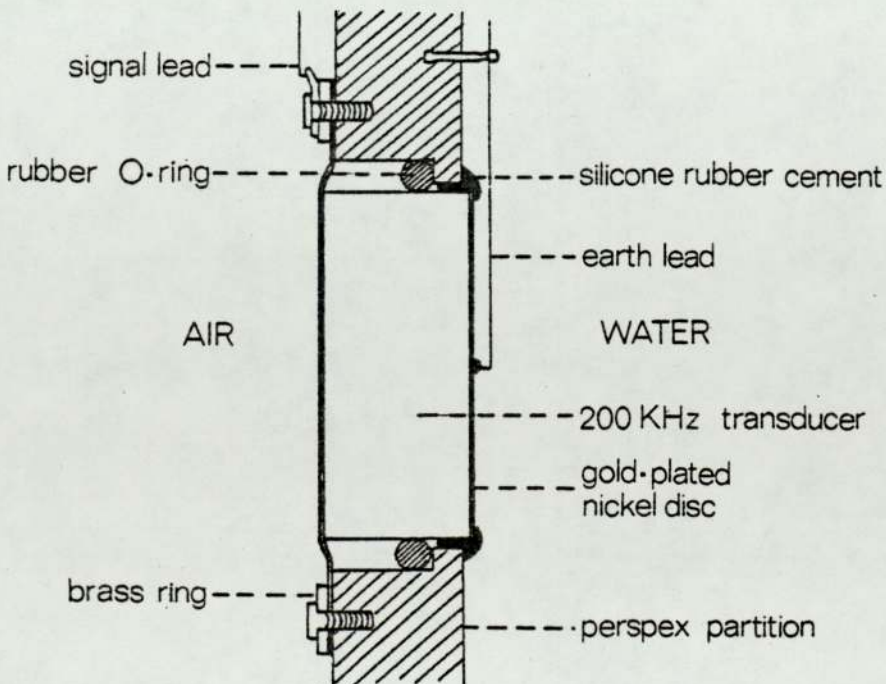
FIGURE 3.11 The transducer mounting
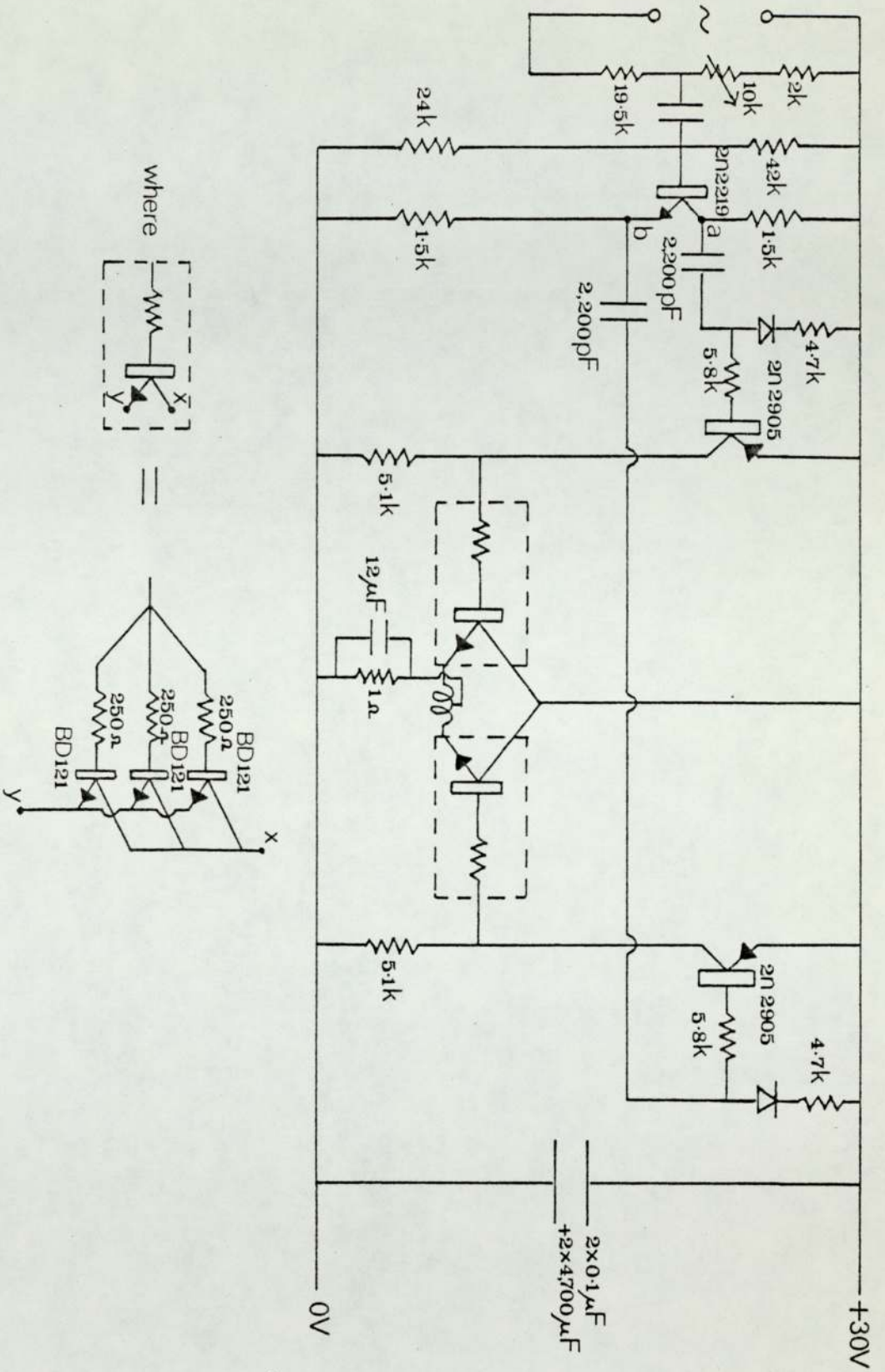
FIGURE 3.12 The transducer driving circuit

There were several reasons for choosing this type of design.
A push-pull configuration would be capable of feeding
large currents, at an acceptably low distortion, into the
primary of the centre-tapped transformer from the low
impedence emitters of the two sets of power transistors. A
transformer turns ratio of 1:34 meant that large sinusoidal
voltages could be produced, with a large secondary impedence
being presented to the transducer, itself a high impedence
device. In addition, the efficiency of the circuit could
be optimised by the use of class C operation for the complete
output stage.

Let us now examine the circuit shown in Fig 3.12 in greater
detail.

A sine-wave input at approximately 200kHz from a signal generator
is fed to the base of a suitably-biased n-p-n transistor, having
equal emitter and collector resistors, and giving unity gain.
The voltage excursion of the input is reproduced at points a
and b, these points feeding the bases of a matched pair of p-n-p
transistors, running in class C mode.

These latter transistors operate in class C push-pull arrangement
i.e. each operates in different halves of a given cycle, being
fed from different leads, either emitter or collector, of the
same transistor. There is, in fact, a time delay between
the periods of operation of each, arising from offset voltage
considerations.

Each 2n2905 feeds a set of three BD 121 power transistors,
arranged in parallel, again run in a class C mode. Each set
has approximately the same current amplification properties,
so that a symmetrical waveform is fed to the primary of the
transformer. The primary is fitted with a centre-tap,
allowing each set of power transistors to feed current into it
in alternate half-cycles, and is wound on a high-frequency
ferrite. A transformer turns ratio of 1:34 is used.

The circuit described is capable of feeding 950Vp-p and 250mAp-p,
in the form of a continuous sine-wave, to the transducer.
Very little distortion of the current and voltage waveforms is
observed. An estimated 33Wrms of electrical power is available
for conversion into ultrasonics, the PZT-4 transducer, with an
approximate efficiency of 50%,producing roughly 16.5W of
ultrasonic power over its radiating area of approximately $20cm^2$.

It is found that streams of bubbles form in the irradiated water
when the full power available is used; further, a hissing noise
is heard, both these phenomena being characteristic of the onset
of cavitation. The ultrasonic generating system may thus be
considered suitable.

3.6   Experimental arrangement of ultrasonic field, index layer and incident illumination

The design of the system required that an index layer should be
supported horizontally within an ultrasonic field, and illuminated
normally by modulated, polarized light.
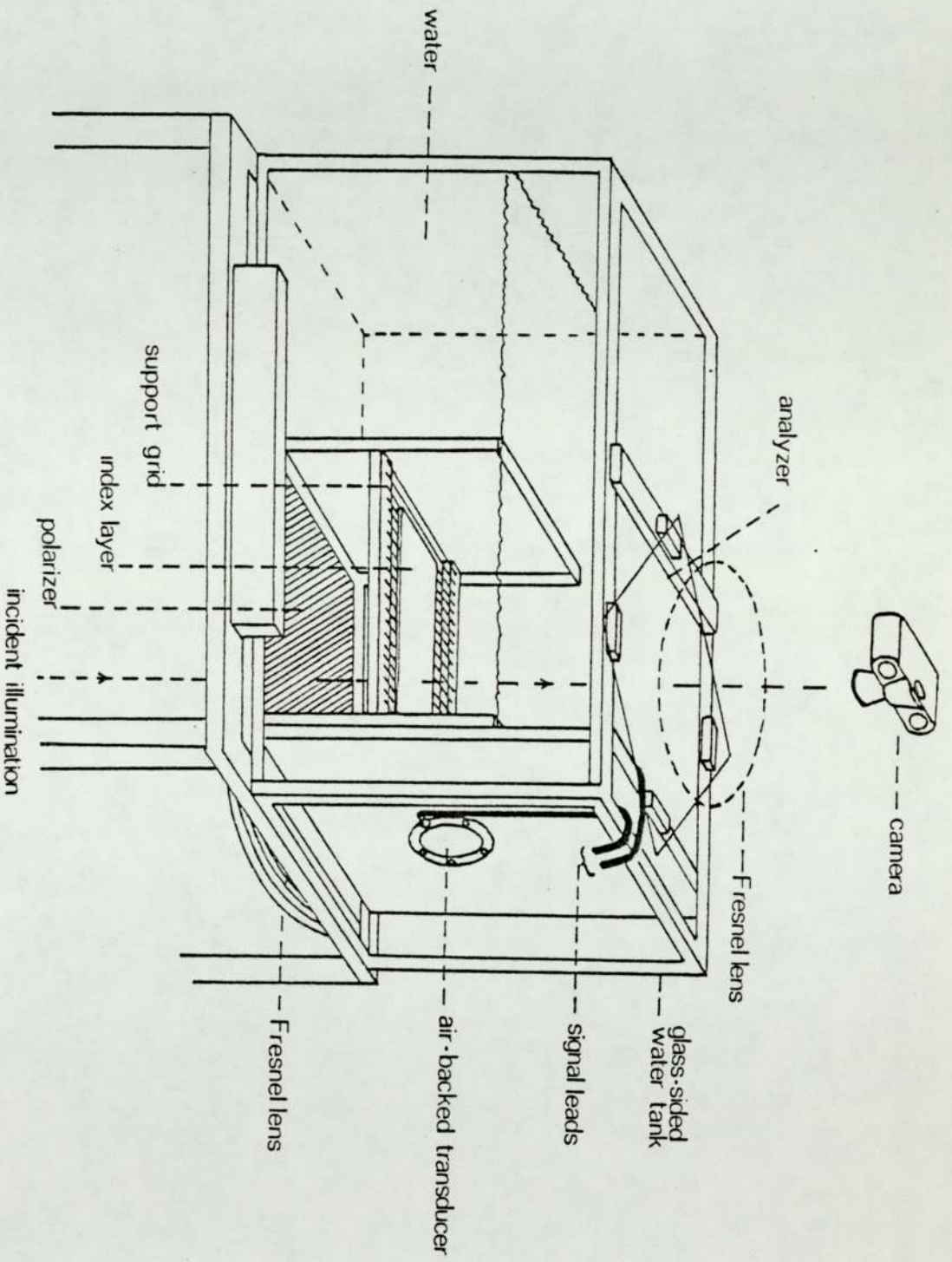
FIGURE 3.13 Experimental arrangement of ultrasonic field, index layer and incident illumination

water

support grid

index layer

polarizer

incident illumination

analyzer

Fresnel lens

glass-sided
water tank

signal leads

air-backed transducer

Fresnel lens

camera

Fig 3.13 shows a schematic diagram of the experimental arrangement used. Ultrasonics are introduced into water, contained in a tank with glass sides and bottom, by the air-backed transducer previously described. The area of tank bottom not taken up by the polarizer is covered with polyurethane foam sheeting, as are the tank's sides, to reduce ultrasonic reflection. The polarizer, a laminated polaroid sheet, is specially waterproofed round its edges to avoid damage from water absorption.

The index layer, a thin sheet of photoelastic material, is supported horizontally by a 0.005 inch diameter tungsten wire grid, strung on a light-weight frame. This grid keeps the photoelastic sheet free from static strain, arising from inadequate support. The plane of the grid is adjustable vertically, so that various horizontal sections may be sampled by the index layer.

The incident illumination, as previously described, passes through the polarizer, index layer and analyzer as a parallel cylindrical beam, being brought to a focus by the field (Fresnel) lens shown.

3.7　Control over the difference between ultrasonic and light modulation frequencies

The primary signals for the ultrasonic and light modulation systems

are provided by two separate generators, as shown in Fig 3.4.

It was found experimentally that frequency drift occurred in both,

so that their frequencies could not be held constant over any

extended period. Additionally, adjustments of a fraction of a Hz

in 200 kHz proved to be extremely difficult. Accordingly, additional

apparatus was designed and constructed which

(a)   Synchronized the two signal generators, so that

they produced the same frequency of output; this

allows a stationary photoelastic display to be

viewed within an index layer;

(b)   produced a steady, adjustable frequency difference

between the two, allowing the observation of

moving displays.

Synchronization of the two frequencies is achieved by feeding the

output of one signal generator into a suitable point of the circuit

of the other; this linkage forces the second signal generator to

operate at the same frequency as the first, provided both are

originally set at approximately the same frequency of operation.

The stroboscopic effect, arising from this interlocking, is then

such that stationary displays are produced.

A system was now constructed, based on the above effect, which

caused the two signal generators to operate at slightly different

frequencies. This involves modifying the frequency being fed from

one signal generator to the other, by a fraction of a Hz say, at

a point in the interlocking lead joining the two. The first still

operates at its original frequency, f_1 say, but the second is now forced to operate at $f_1 + \triangle f_1$, where $\triangle f_1$ is the frequency change imposed. Fig 3.14 illustrates this point.

In practice, $\triangle f_1$ is achieved by inserting a continuously changing phase into the appropriate lead, the second signal generator having been seen to follow a change in phase in a previous experiment.

Let the sinusoidal output of signal generator 1 be given by

$$V = Vo \; Sin \, \omega_1 t$$

and let ϕ be the imposed continuous phase change. The signal then fed to signal generator 2 is given by

$$V = Vo \; Sin \, (\omega_1 t + \phi) \tag{3.1}$$

Suppose now that ϕ changes steadily with time, such that $\phi = \omega t$; equation (3.1) becomes

$$V = Vo \; Sin \left[(\omega_1 + \omega)t \right]$$

and signal generator 2 is now caused, by the locking process, to operate at a frequency given by

$$f_2 = \frac{\omega_1 + \omega}{2\pi} = f_1 + \frac{\omega}{2\pi} = f_1 + \triangle f_1 .$$
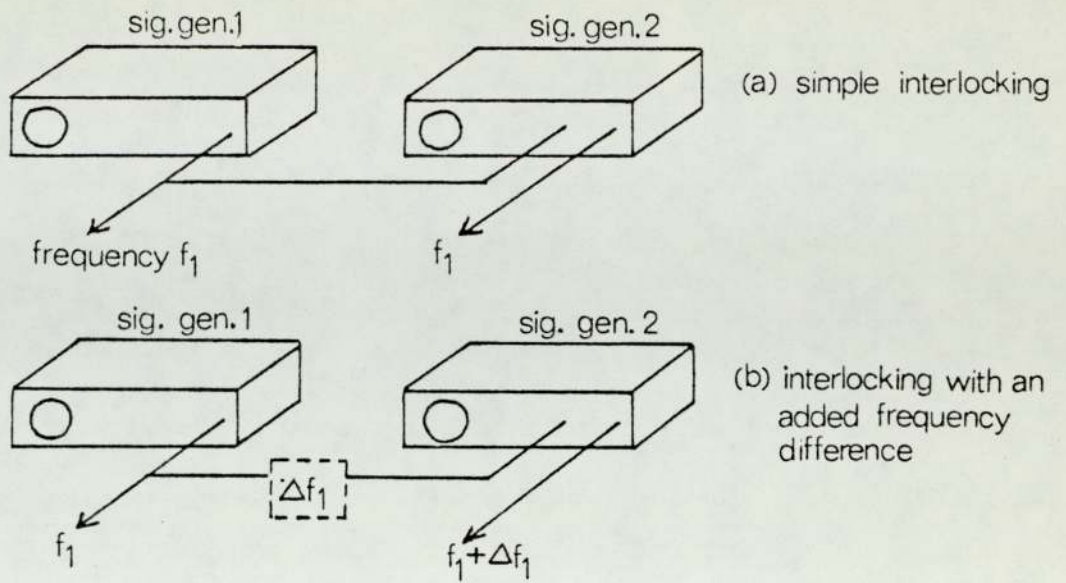
FIGURE 3.14   The interlocking process
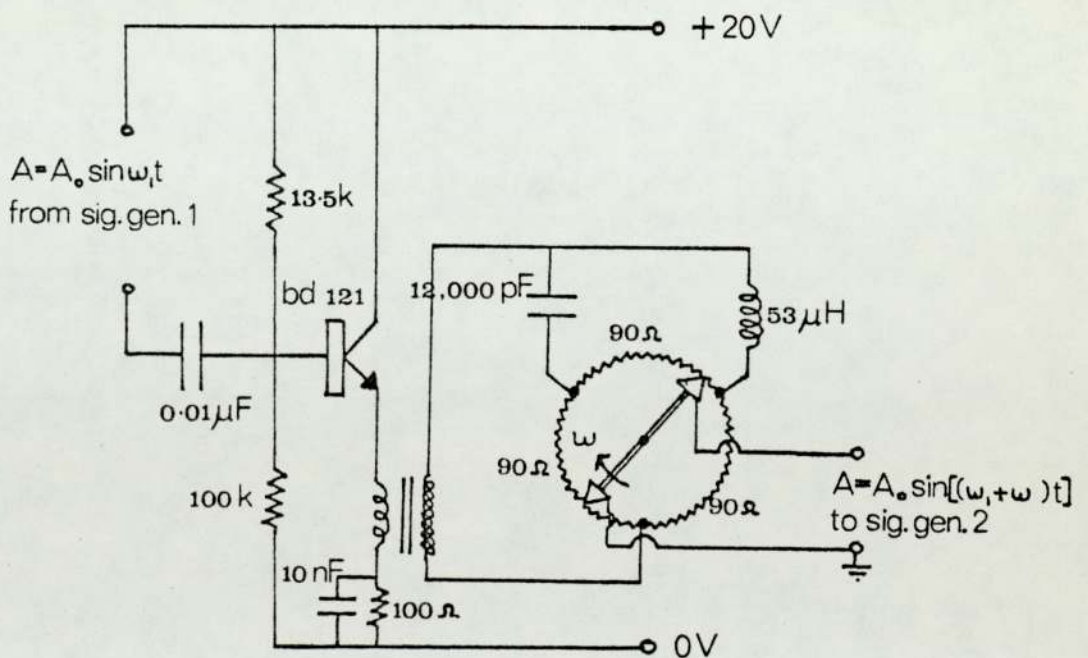
FIGURE 3.15   The circuit producing a continually-changing phase

Adjustment of ω thus allows a controlled frequency difference between the ultrasonic and light modulation frequencies to be achieved.

The circuit which produces a continually changing phase, to be added to the sinusoidal output of signal generator 1, is shown in Fig 3.15.

The incoming signal, represented by $V = V_0 \sin \omega_1 t$, is fed into the base of a buffer amplifier, avoiding excessive loading of the signal generator. This signal is then boosted by a 2:1 step-up transformer, so that the voltage variations, to be fed to signal generator 2, are of sufficient magnitude to produce the required locking phenomenon. Additionally, this transformer isolates the subsequent circuitry from earth.

The transformer is designed to have a low capacity between its primary and secondary by using well-spaced, single layer coils, wound on a ferrite core; this is considered desirable for reasons to be outlined later.

The secondary of the transformer feeds the sinusoidal signal, of frequency $f_1 = \omega_1/2\pi$, into the next stage of the circuit, designed to introduce a continuously - changing phase. It consists basically of a circular, wire-wound potentiometer, fitted with three symmetrically spaced taps and exhibiting a resistance of 90 Ω between each.

In two of the leads to the above taps are placed an inductance
and a capacitance respectively, specially chosen so that in
conjunction with the three $90\,\Omega$ segments, voltages which are
120° out of phase at 200 kHz are produced at each of the three
fixed taps shown. Silvered mica capacitors were chosen to
provide the capacitance needed, their low-loss characteristics
giving a small inherent resistance; such a resistance might
upset the conditions needed to produce the required phase
distribution. Similarly, the inductance was specially constructed
from an air-cored copper winding, designed to have a low loss
and hence again a low resistive impedence. The low capacity
between the primary and secondary of the transformer, mentioned
above, was also necessary to the design, as disturbance to the
required phase distribution would result from any extra capacitance
in the circuit.

The calculation of values for L and C, the inductance and
capacitance needed to produce the required phase distribution in
the chosen rotary potentiometer, follows theory used in the design
of three-phase networks; the method of calculation, which arrived
at the values quoted in Fig 3.15, is presented in Appendix 3.

The wire-wound potentiometer, provided with voltages at each of the
fixed taps which are 120° out of phase, is also fitted with a wiper,
able to rotate axially at a steady speed, by connection to an
electric motor. One end of this wiper is earthed, whilst the other
is used to provide a locking signal to the second signal generator.
Steady rotation of this wiper dictates the frequency of the
sinusoidal signal taken from it. If the wiper rotates at an angular

velocity ω_2, then ϕ in equation (3.1) above will be given by $\phi = \omega_2 t$; thus changing the rate of rotation of this wiper alters the frequency of the sine wave derived from it, which is of the form

$$V = Vo \, Sin \left[(\omega_1 + \omega_2) . t \right]$$

Locking of signal generator 2 onto this signal thus provides a controlled frequency difference between that of the ultrasonic generating system, of frequency $f_1 = \omega_1/2\pi$, and light-modulation system, of frequency $f_2 = f_1 + \omega_2/2\pi = f_1 + \triangle f_1$.

It should be noted that signal generator 2 may be caused to operate at a frequency less than or greater than that of signal generator 1 i.e. at $f_1 \pm \triangle f_1$, by simply reversing the sense of rotation of the wiper.

Fig. 3.16 is a photograph of the apparatus described above. Clearly seen are the large air-cored inductance, and the silvered mica capacitors. Below the inductance, the specially wound 2:1 step-up transformer can be seen. The circular potentiometer is positioned centrally; the rate of steady rotation of its wiper can be selected by means of the a/c motor and pulley system shown.

The apparatus, described above, thus fulfills its function in providing a controlled frequency difference $\triangle f_1$ between two signal generators. The speed and sense of rotation of the potentiometer's wiper allows flexibility in the frequency difference produced. Use of this apparatus thus allows control over the conditions of stroboscopy, used in the visualization system, facilitating the convenient viewing of either stationary
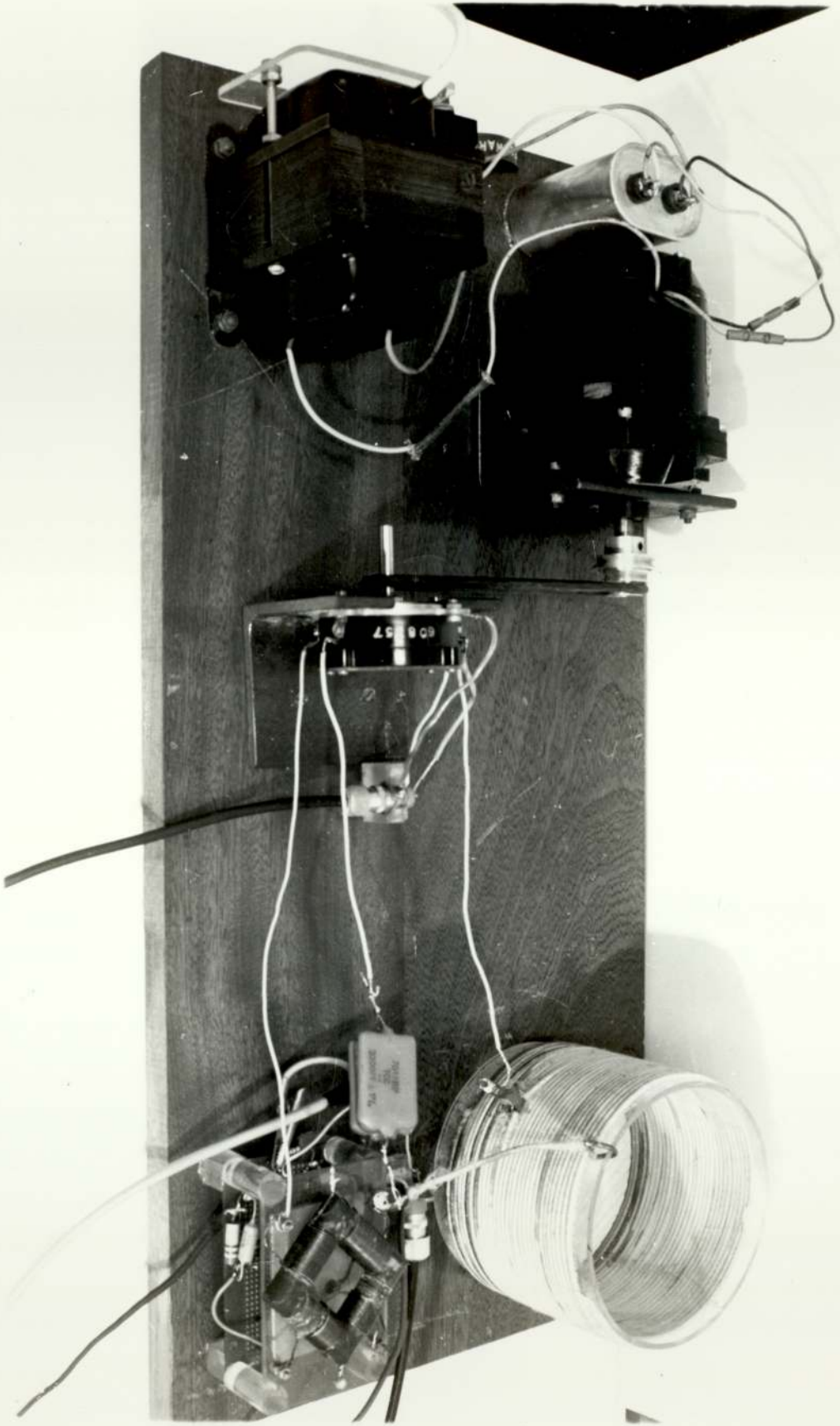
FIGURE 3.16 The interlocking apparatus

or steadily-moving photoelastic displays.

3.8   The complete apparatus and its operation

The light modulation and ultrasonic generating systems have been
described, and have been seen to operate at a nominal 200 kHz;
in addition, the modulator is capable of operation over an extended
frequency range, 197-203 kHz.

It was found, however, that the optimum frequency of operation
of the ultrasonic generating system was at the edge of the above
range. This difference in the frequencies of peak efficiency of
the two systems probably arose from the differing mounting
conditions of the 200 kHz transducers used in each system;
additionally, variations in the resonant frequencies of the
transducers, within the manufacturer's tolerances, would also
contribute.

It is essential that the frequencies of peak efficiency of each
system are close, so that effective use of the apparatus, described
in the previous section, can be made. This was achieved by
modification of the resonant frequency of the transducer used in
the ultrasonic generating system, with a small amount of
capacitance, 700pF, connected in parallel with it. Operation
of the complete apparatus under the optimum conditions could now
be achieved.

Fig 3.17 is a labelled photograph of the complete apparatus in an
assembled state. Clearly visible is the water tank, in which the
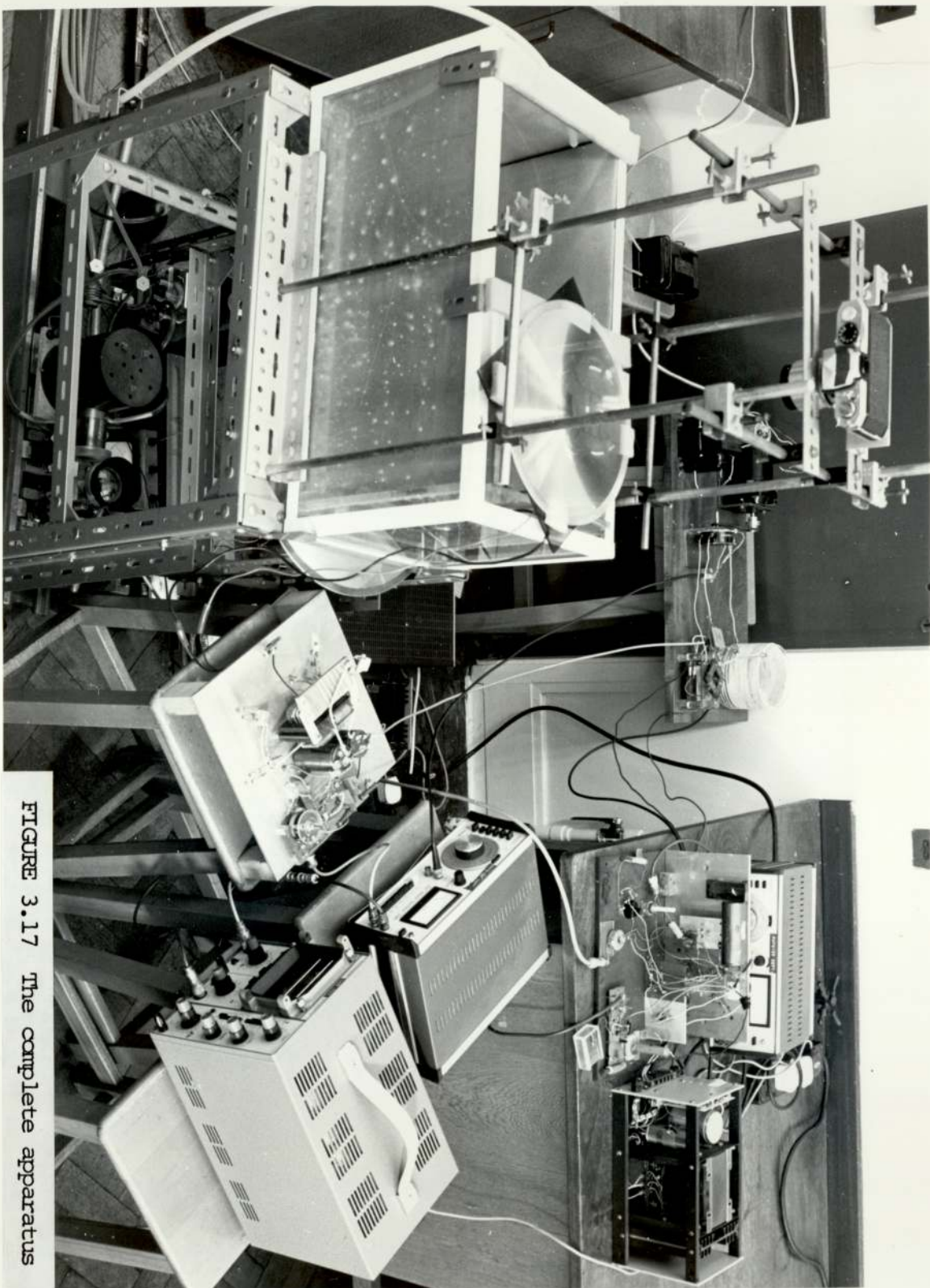
FIGURE 3.17 The complete apparatus

visualization process takes place; mounted above this is the
analyzer and field lens, the latter focussing the resultant
light beam into the camera lens. The arc-lamp and subsequent
optics, for producing the incident illumination, are situated
below the tank. The electronic systems, providing signals to
the light modulator and the water-tank's transducer, are
interlocked by means of the apparatus previously described.

Operation of the equipment proceeds as follows. The frequency
of the ultrasonic generating system is set so that resonance of
its transducer occurs. Next, with the aid of an oscilloscope,
the frequency of light modulation is adjusted so that simple
interlocking with the former system is achieved, via the apparatus
described in Section 3.7; the wiper in this device is stationary
at this stage. The photoelastic display, seen in an index layer
within the water tank, is now stationary also, and can be
conveniently observed through the camera's viewfinder. Still
photography is now possible.

If now the wiper, previously described, is caused to rotate, the
photoelastic display of a progressive ultrasonic wave within an
index layer is seen to move steadily across the field of view; the
oscilloscope now indicates a difference between the light
modulation and ultrasonic frequencies. Cinematography of the
progress of a given ultrasonic distribution can then be
conveniently achieved.

3.9   Preliminary conclusions

An apparatus has been described with which the visualization of
continuous-wave ultrasonics has been accomplished. This involves
placing a thin index layer of photoelastic material into the path
of an ultrasonic field, present in an extended volume of water.
Passage of ultrasonic waves through this layer causes the
formation of a photoelastic pattern, the photography of which
may be accomplished with the aid of stroboscopic illumination.

The high pressure mercury arc-lamp was selected for its
approximation to a point source, and the subsequent lens system
designed on this assumption. The resultant intensity of
illumination of the index layer is found to be adequate for both
visual observation and photography. Stroboscopic illumination
is provided by the use of a photoelastic light modulator, acting
on the arc-lamp's output. This modulator was chosen for its large
angular aperture and flexibility of operation; 80% amplitude
modulation, in either pulse-like or sinusoidal waveforms, is
capable of being produced.

The ultrasonic generating system can produce ultrasonic
intensities approaching $1 Wcm^{-2}$ in magnitude at 200 kHz; this
allows the investigation of potentially insensitive photoelastic
effects.

It will thus be seen that the apparatus constructed fulfills
the requirements laid down for an effective visualization
system, involving the stroboscopic illumination of thin

photoelastic sheets; in particular, this is achieved with a
high degree of simplicity, and at a low cost.

CHAPTER FOUR

THEORETICAL STUDIES INTO THE VALIDITY OF THE TECHNIQUE

4.1   Introduction

The proposed visualisation technique involves the introduction
of a thin layer of material into a liquid containing an
ultrasonic field. The resultant display will only be valid,
however, if it is an accurate representation of the ultrasonic
field that would have existed at the sampled plane in the layer's
absence; additionally, the ultrasonic distribution must not
be unduly altered by the layer's introduction.

The validity of the optical display will depend on

   (a)   the layer being thin enough so that variations
          in the ultrasonic field across its thickness are
          negligable;

   (b)   the display following the acoustic variations of
          the field at the sampled plane;

   (c)   sufficient ultrasonic intensity being present within
          the layer, so that a visible display is produced
          over its whole area;

   (d)   the ultrasonic wavelength, derived from the display
          being characteristic of that normally associated
          with the liquid medium.

Disturbance to the ultrasonic field will occur from

      (e)   its reflection or diffraction by the index layer;

      (f)   energy transfer from the ultrasonic field to the layer,

              with a change in its wavelength and its attenuation.

The above effects will be considered in three discrete sections.
The first considers the effect of characteristic impedence
differences between the liquid and layer media; next,
a difference in ultrasonic velocity and attenuation will be
studied by theoretical analysis. Finally, the reason for
expecting a deficiency in ultrasonic intensity around a layer's
edge will be presented, and the problem examined theoretically
by analogy with a diffraction problem.

4.2   The effect of characteristic impedence

It was indicated in the Introduction that a difference in
characteristic impedence between two media results in reflection
of ultrasonics at their common boundary. For both normal
and oblique incidence, the same general principle was seen to
hold i.e. that the closer the impedences of the two media,
the greater the transmission across the boundary, and the smaller
the reflection from it. It is thus clear that it is desirable to
match the characteristic impedences of the layer and liquid media
as closely as possible in a visualisation system, in order to
reduce the scattering and reflection of the ultrasonic field
to a minimum, and allow as great a transmission of ultrasonic
intensity as possible into the layer.

A difference in characteristic impedence may also produce
an anomolous display by the following mechanisms:

(i)   the presence of mode conversion within a solid
      index layer;

(ii) internal reflection within the layer, possibly leading
      to the formation of resonant modes;

(iii) the presence of insufficient ultrasonic intensity
      within the layer.

The process of mode conversion is illustrated in Fig 4.1. Both
longitudinal and shear ultrasonic waves may be produced within
a solid, by incidence of a longitudinal wave from a liquid,
which travel at different velocities, C_2 and S_2 respectively.
The direction of travel of each, as shown in Fig 4.1, is given
by
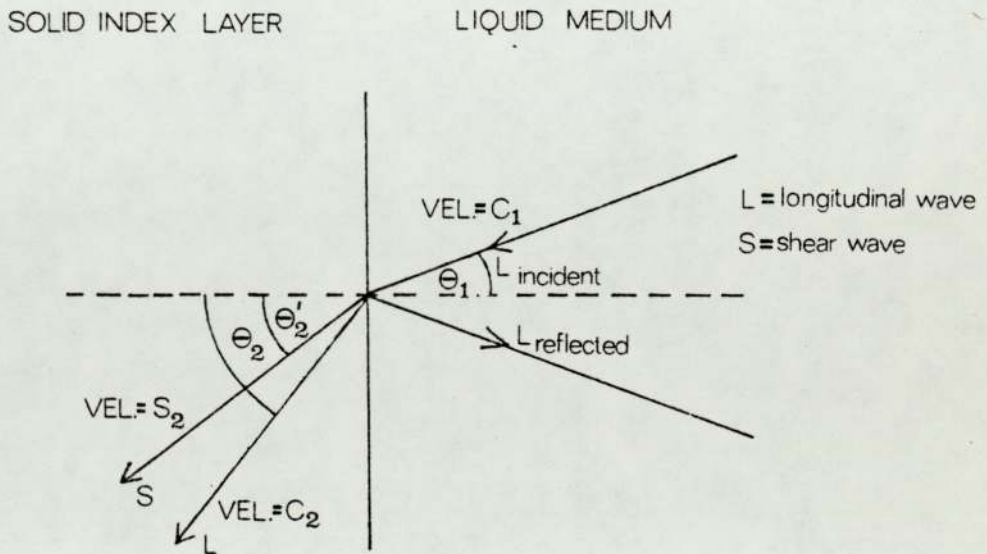
FIGURE 4.1   Mode conversion

$$\frac{C_1}{\sin \theta_1} = \frac{C_2}{\sin \theta_2} = \frac{S_2}{\sin \theta_2'}$$

As, in general, $C_2 > S_2$ and $S_2 > C_1$, the resultant waves in the solid will be refracted away from the normal, the effect being greater for the longitudinal wave. These phenomena will occur until a critical angle is reached; at this angle, the refracted longitudinal wave travels along the boundary between the two media. Increasing θ_1 still more produces complete reflection of the incident longitudinal wave, and transmission of shear waves only occurs. Finally, a second critical angle is reached, above which no ultrasonic waves will enter the solid.

It is clear from the above that an incident field of longitudinal waves from the liquid medium may give rise to a complicated distribution within a solid index layer, with the production of an anomolous display if these waves are all visualised. Mode conversion may be minimised by the use of either a layer medium in the form of a liquid, or in the form of a solid whose Poisson's ratio is close to 0.5; in either case, shear waves will not be supported to any great extent.

Even if there is no production of shear or surface waves, a further form of anomolous display may arise from internal reflection

at the layer's edge. In extreme cases, this may result in the
display of resonant mode patterns; this is particularly liable
to occur within layers having very low attenuation coefficients,
and large values of α_r (section 1.4.1).

An impedence mismatch between the layer and liquid media may
also result in a low level of ultrasonic intensity within an index
layer, which may not be sufficient for effective visualisation
to take place. The sensitivity of the technique will obviously
be enhanced when the impedences are matched.

It may thus be concluded that it is extremely desirable to use
an index layer whose characteristic impedence is close to that
of the liquid medium, reducing the disturbance to the ultrasonic
field and the occurrence of anomolous displays. In the case of
solid layers, the use of a material with a suitable Poisson's
ratio will confine mode conversion to a minimum.

4.3   A theoretical study of a thin, attenuating layer in an
      ultrasonic field

From the foregoing, it may be seen that a difference in
characteristic impedence between the liquid and layer media
can produce undesirable effects. The general case where the
two media are characterised by a different ultrasonic velocity,
and unequal attenuation coefficients, will now be studied.

Consider the ultrasonic distribution, induced within an
index layer by an ultrasonic field in a liquid. The velocity
of the induced longitudinal waves may, at first sight,
be expected to differ from those within the surrounding liquid,
if the two media usually differ in this respect. However, the
waves in both media will be expected to interact, and this process
will lead to an equilibrium. The position of this equilibrium
is important in that it will determine

    (a)   the ultrasonic wavelength, and hence that of the
           display produced, within an index layer;

    (b)   the disturbance to the ultrasonic field, caused by
           the layer's introduction, involving a change in
           its wavelength.

The layer medium will, in general, be an attenuating one,
as outlined in the Introduction. The presence of such a layer
will inevitably attenuate an ultrasonic field, established within
a non-attenuating liquid. In addition, the transfer of energy
from the liquid medium will tend to reduce the attenuation of
a wave, induced within an index layer. Another equilibrium may
thus be expected, which will determine

    (a)   the attenuation to any ultrasonic field to be
           visualised, caused by the layer's introduction;

    (b)   the extent to which the induced wave within the
           layer, and hence the display produced, fades with
           distance.

The theory to be presented attempts to predict these equilibria, the disturbance to the ultrasonic field, and the validity of the display produced.

At the commencement of this investigation, it was thought that the presence of a large extent of ultrasonic field, surrounding a thin index layer, would result in the distribution within the layer being "forced" to be close to that previously existing in the liquid at that plane i.e. the equilibria above would dictate common waves within the two media, whose properties closely resemble those normally expected in the liquid medium; the theory to be presented confirms this view.

The analysis that follows assumes a plane progressive wave to exist in the liquid prior to the introduction of the layer; it is hoped that the predictions obtained will generally be applicable to more complicated distributions.

4.3.1 The system under consideration

Consider the proposed visualisation system, in which an index layer is placed in an ultrasonic field; such a system is depicted in Fig 4.2. A thin, attenuating layer, of finite thickness 2h, is bounded on both sides by a finite extent ℓ of non-attenuating liquid, contained between perfectly-reflecting boundaries. The layer and liquid media are characterised by their densities (ρ_2 and ρ_1 respectively), circular wavenumbers (k_2 and k_1) and the velocity of sound in each (c_2 and c_1).

The ultrasonic field to be visualised, assumed to consist solely of plane waves travelling in the x direction, exists in the liquid and fills its whole volume. With no layer present, these waves will be characterised by a circular wavenumber k_1. The introduction of a layer with differing acoustic properties causes an interaction between the two media, with the result that this value changes from that of k_1. This change is an indication of the disturbance to the ultrasonic field in the liquid.

The ultrasonic wave, induced in the layer by the ultrasonic field, will, in addition, be characterised by a circular wavenumber which differs from k_2, the value normally associated with extended samples of the layer medium. The resultant value will determine the validity of the display produced.

The theory that follows attempts to predict how the values of the circular wavenumber in both media differ from their normal values, k_1 and k_2 respectively, as various parameters are adjusted. It should be noted that circular wavenumbers may be either real or complex in form, the latter case implying attenuation within a given medium.

$y = +\ell$ —————————————————— perfectly reflecting boundary

LIQUID $c_1\ k_1\ \rho_1$

$y = 0$ ———————————————————
$y = -h$ – – – – – – – – – – – – – – – – – – $\updownarrow 2h$ } LAYER $c_2\ k_2\ \rho_2$

LIQUID $\quad \ell$

perfectly reflecting boundary
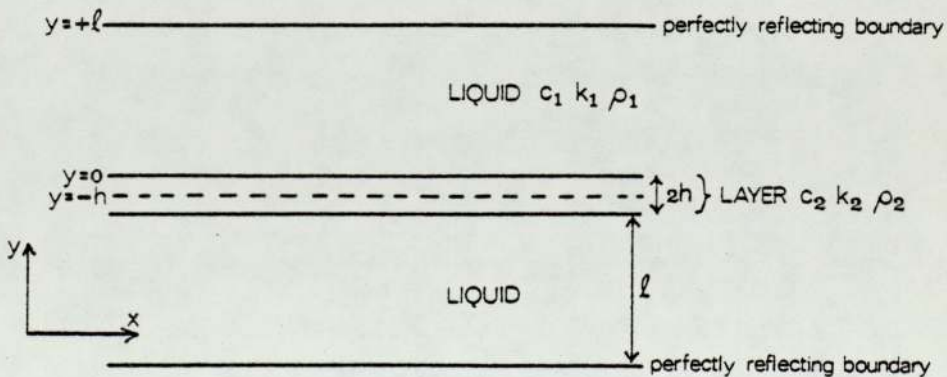
FIGURE 4.2   The visualization system

- 103 -

4.3.2 Assumptions

(i)   Ultrasonic waves in the liquid have a scalar velocity

        potential $\emptyset_1$, and that in the layer $\emptyset_2$;

(ii)   The layer material is an attenuating substance, whose

        attentuation properties are known;

(iii)   It is assumed that attenuation within the bulk liquid

        is so small that it may be neglected in comparison with

        that due to the presence of the layer;

(iv)   The system is infinite in the x direction;

(v)   Perfectly reflecting boundaries exist at the limits of the

        liquid in the y direction;

(vi)   The ultrasonic field consists solely of plane waves,

        assumed to fill the whole volume of the liquid,

        propagating in the x direction; there is no variation

        in the z direction;

(vii)   Only longitudinal compressional waves are produced in

        the layer by the ultrasonic field;

(viii) In the assumed symmetrical system there would be no energy

        transfer across the mid-plane of the layer; hence this

        becomes equivalent to a perfectly reflecting plane;

(ix)   It is assumed that, if it is shown that the disturbance

        produced by a layer on a plane wave is small, the effect

        on a non-plane wave will be acceptable.

4.3.3 <u>Preliminary discussion</u>

The problem to be solved involves the interaction of ultrasonic
waves present simultaneously within the liquid and layer media,
and is investigated by finding an appropriate solution to the
relevant wave equation in either medium, and then applying
the boundary conditions.

The wave present within each medium will, however, differ
from that expected in a bulk unbounded specimen of each; this is
due to the mutual interaction of the waves in each medium.   To
describe this effect, two parameters α and β are introduced,
both of which have dimensions of wavelength $^{-1}$.

Suppose k_1 is the circular wavenumber normally associated with
the unbounded liquid. At equilibrium, the value of k_1 will
change to

$$k(\text{liquid}) = \sqrt{k^2_1 - \alpha^2}$$

where $k(\text{liquid})$ is the equilibrium value of the wavenumber of
compressional waves in the liquid, produced when a given layer
is present. Thus, α represents the modification in properties
of an ultrasonic wave, present in a liquid, due to the
presence of a visualisation layer. The following theory attempts
to show how α , and hence $k(\text{liquid})$, varies with a change in
layer properties.

Similarly, if k_2 is the circular wavenumber normally

associated with an unbounded specimen of the layer material,

the wavenumber of the compressional wave set up in an

index layer may be written as

$$k(layer) = \sqrt{k_2^2 - \beta^2}$$

and β represents the modification of the properties of the

layer due to the ultrasonic wave in the liquid. The theory

will also indicate the expected values of β .

The above forms of k(liquid) and k(layer) are chosen to suit

other factors to be discussed later. However, at first sight

one might expect k(liquid) and k(layer) to be equal when an

equilibrium is reached; this is in fact found to be the case.

The layer is assumed to be attenuating; the result is that

k_2 will be complex. It is further assumed that negligable

attenuation occurs in the bulk liquid; k_1 is thus taken as being

real.

4.3.4 The boundary conditions

Perfectly reflecting boundaries have been imposed at $y=\ell$

and $y=-h$, treating only one half of the system. At such

boundaries, the vertical component of the particle velocity,

$\frac{\partial \varnothing}{\partial y}$, must be zero; thus, two boundary conditions to be obeyed are

(i) $\frac{\partial \varnothing_1}{\partial y} = 0$ at $y=\ell$, for all x ;

(ii) $\frac{\partial \varnothing_2}{\partial y} = 0$ at $y=-h$, for all x .

Ultrasonic waves are assumed to exist in both the liquid and layer media. At the boundary between them, however, the pressure will be the same for both media, i.e.

$$P_1 = -\rho_1 \cdot \frac{\partial \varnothing_1}{\partial t} = -j \omega \varnothing_1 \rho_1$$

$$P_2 = -\rho_2 \cdot \frac{\partial \varnothing_2}{\partial t} = -j \omega \varnothing_2 \rho_2$$

assuming harmonic time dependence. Thus, at the boundary,

$$\rho_1 \varnothing_1 = \rho_2 \varnothing_2, \text{ at } y=0, \text{ for all x}$$

and this is boundary condition (iii). In addition, the vertical component of the particle velocity at this boundary must be the same for both media; thus

$$\frac{\partial \varnothing_1}{\partial y} = \frac{\partial \varnothing_2}{\partial y} \quad \text{at } y=0, \text{ for all x}$$

and this is boundary condition (iv).

4.3.5 The solutions for $\emptyset_1$ and $\emptyset_2$ and the application of boundary conditions

The method of investigation involves finding appropriate expressions for $\emptyset_1$ and $\emptyset_2$, the scalar velocity potentials for the two media. An ultrasonic compressional wave in the unbounded liquid medium is described by the wave equation

$$(\nabla^2 + k_1^{\,2})\ \emptyset_1 = 0$$

where $k_1 = \dfrac{2\pi}{\lambda_1}$ and $\nabla^2 \emptyset_1 = \dfrac{\partial^2 \emptyset_1}{\partial x^2} + \dfrac{\partial^2 \emptyset_1}{\partial y^2}$

The expression chosen for $\emptyset$ must satisfy this equation, involving variations in both x and y. Similarly, the expression chosen for $\emptyset_2$ must obey the equation

$$(\nabla^2 + k_2^{\,2})\emptyset_2 = 0$$

which describes an ultrasonic wave in the unbounded layer medium.

To enable an estimation of the extent of interaction between ultrasonic waves in the liquid and layer media, the solutions chosen for $\emptyset_1$ and $\emptyset_2$ must have the two parameters α and β respectively incorporated in them. Additionally, the two expressions for $\emptyset_1$ and $\emptyset_2$ must obey the imposed boundary conditions. A solution which obeys the wave equation in the liquid medium is, omitting time dependence,

$$\emptyset_1 = A\,e^{-j\sqrt{k_1^{\,2} - \alpha^2}\,.\,x}\ \cos \alpha(y-\ell) \qquad (4.1)$$

This solution also satisfies boundary condition (i); when $y = \ell$, (4.1) becomes

$$\emptyset_1 = A \ e^{-j \sqrt{k_1^2 - \alpha^2} \cdot x}$$

and $\dfrac{\partial \emptyset_1}{\partial y} = 0$.

A similar solution to the wave equation in the liquid medium is

$$\emptyset_2 = B \ e^{-j \sqrt{k_2^2 - \beta^2} \cdot x} \cos \beta(y+h) \qquad (4.2)$$

Such a solution satisfies boundary condition (ii); when $y = -h$, the solution for $\emptyset_2$ becomes

$$\emptyset_2 = B \ e^{-j \sqrt{k_2^2 - \beta^2} \cdot x}$$

and again $\dfrac{\partial \emptyset_2}{\partial y} = 0$

Thus, equations (4.1) and (4.2) are solutions for $\emptyset_1$ and $\emptyset_2$ which contain the factors α and β , which are functions of both x and y, and which satisfy the first two boundary conditions.

It now remains to apply boundary conditions (iii) and (iv). From condition (iii),

$$\rho_1 \emptyset_1 = \rho_2 \emptyset_2 \qquad \text{at } y = 0 \text{ , for all } x$$

$$\therefore \rho_1 A \ e^{-j \sqrt{k_1^2 - \alpha^2} \cdot x} \cos \alpha \ell = \rho_2 B \ e^{-j \sqrt{k_2^2 - \beta^2} \cdot x} \cos \beta h \qquad (4.3)$$

From condition (iv),

$$\frac{\partial \phi_1}{\partial y} = \frac{\partial \phi_2}{\partial y} \qquad \text{at } y = 0 \text{, for all } x$$

Now, $\quad \dfrac{\partial \phi_1}{\partial y} = -\alpha\, A e^{-j\sqrt{k_1^2 - \alpha^2}\,.x} \sin \alpha\, (y - \ell)$

$\therefore \quad \dfrac{\partial \phi_1}{\partial y} = \alpha A e^{-j\sqrt{k_1^2 - \alpha^2}\,.x} \sin \alpha \ell \qquad \text{at } y = 0$

Also, $\quad \dfrac{\partial \phi_2}{\partial y} = -\beta\, B e^{-j\sqrt{k_2^2 - \beta^2}\,.x} \sin \beta\, (y + h)$

$\therefore \quad \dfrac{\partial \phi_2}{\partial y} = -\beta\, B e^{-j\sqrt{k_2^2 - \beta^2}\,.x} \sin \beta\, h \qquad \text{at } y = 0$

$\therefore$ Applying condition (iv),

$$\alpha\, A\, e^{-j\sqrt{k_1^2 - \alpha^2}\,.x} \sin \alpha \ell = -\beta\, B e^{-j\sqrt{k_2^2 - \beta^2}\, x} \sin \beta\, h \tag{4.4}$$

On inspection of equations (4.3) and (4.4) it is seen that

$$k_1^2 - \alpha^2 = k_2^2 - \beta^2 = k_*^2 \qquad \text{say,} \tag{4.5}$$

and it is clear that the waves present simultaneously within the liquid and layer media, characterised by the expressions for ϕ_1 and ϕ_2, will exhibit the same wavenumber k_*. This wavenumber will, in general, be complex, k_2 being complex originally; it may thus be expected, in general, that both α and β are complex.

The implications drawn from equation (4.5) are that ultrasonic waves in both the liquid and layer media will have the same wavelength (derived from the real part of k_*), and will both experience the same attenuation (the imaginary part) as predicted in Section 4.3.3.

Additionally, it is seen that

$$\alpha A \sin \alpha l = - \beta B \sin \beta h \qquad \text{from equation (4.4)}$$

$$\rho_1 A \cos \alpha l = \rho_2 B \cos \beta h \qquad \text{from equation (4.3)}$$

$$\therefore \quad \frac{\alpha}{\rho_1} \tan \alpha l = - \frac{\beta}{\rho_2} \tan \beta h \qquad (4.6)$$

Equations (4.5) and (4.6) may be used to obtain equations which contain terms in either α or β only; e.g. from equation (4.5),

$$\beta = \sqrt{k_2^2 - k_1^2 + \alpha^2}$$

and equation (4.6) becomes

$$\frac{\alpha}{\rho_1} \tan \alpha l = -\frac{\sqrt{k_2^2 - k_1^2 + \alpha^2}}{\rho_2} . \tan \left(h\sqrt{k_2^2 - k_1^2 + \alpha^2} \right) \qquad (4.7)$$

A similar equation may be derived for β .

Equation (4.7) is a transedental equation in a complex variable α, and is thus not amenable to direct solution. This equation

is potentially soluble by iterative methods such as

Newton's method of successive approximations; this process

is, however, extremely time-consuming and tedious.

The situation is complicated in that, on physical grounds,

one would expect more than one solution to such an equation;

this would allow a transient change in k_1 and k_2 to occur,

on the initial interaction between the waves in each medium.

The system would then be expected to settle down to an

equilibrium state.

Thus, although more than one independent solution for both

α and β is expected, these cannot easily be obtained. If

attention is restricted to a single solution for each of α

and β, however, then various physical trends may become

apparent; this would be especially so if a steady-state solution

was obtainable.

Accordingly, approximate steady-state solutions are now

obtained, by the assumption of small values of α and β. This,

by consideration of the physical situation, would mean the

assumption of very thin layers, which would be expected to

exhibit an equilibrium distribution almost instantly; this

assumption thus allows the equilibrium state to be examined.

4.3.6 The approximate solutions for α and β.

It is well known that for a small angle θ, $\tan\theta \simeq \theta$. In addition,

if θ is complex, this approximation still holds i.e.

$$\tan (a + jb) \simeq a + jb$$

if both a and b are small. Use of this approximation on equation (4.6) yields

$$\frac{\alpha}{\rho_1} \cdot \alpha l = -\frac{\beta}{\rho_2} \cdot \beta h$$

$$\therefore \frac{\alpha^2 l}{\rho_1} = -\frac{\beta^2 h}{\rho_2} \qquad (4.8)$$

The above assumes that both αl and βh are small; this is seen to hold if h is very small with respect to l i.e. if very thin layers are placed in large volumes of ultrasonic fields.

As a further simplification, assume that the densities of the two media are equal; combination of equations (4.5) and (4.8) then yields expressions for α^2 and β^2, containing known variables only:

$$\alpha^2 = \frac{k_1^2 - k_2^2}{(1 + \frac{l}{h})} = (k_1^2 - k_2^2) \cdot \frac{h}{(h + l)} \qquad (4.9)$$

$$\beta^2 = \frac{k_2^2 - k_1^2}{(1 + \frac{h}{l})} = (k_2^2 - k_1^2) \cdot \frac{l}{l + h} \qquad (4.10)$$

Approximate solutions for α^2 and β^2 have thus been obtained.

Let us now discuss the significance of equations (4.5), (4.9) and (4.10). Equation (4.5) predicts that the resulting equilibrium is accompanied by equal wavelength and attentuation properties within the two media. Inspection of equations (4.9) and (4.10) further indicates that α^2 and β^2 are of

different sign e.g. if $k_1 > k_2$, α^2 is positive and β^2 is negative; this agrees with the fact that k_* (equation 4.5) is an equilibrium value, which must by definition lie between the value of k_1 and k_2. This process is illustrated in Fig 4.3.

The position of equilibrium will be predicted by equations (4.9) and (4.10), which will determine the relative values of α^2 and β^2. It is clear from these equations that $\alpha^2 \ll \beta^2$, if it is assumed that $h \ll \ell$ i.e. that thin layers are present within an extended volume of ultrasonic field. Thus, the equilibrium wavenumber k_* will lie very close to k_1, as again indicated in Fig 4.3.
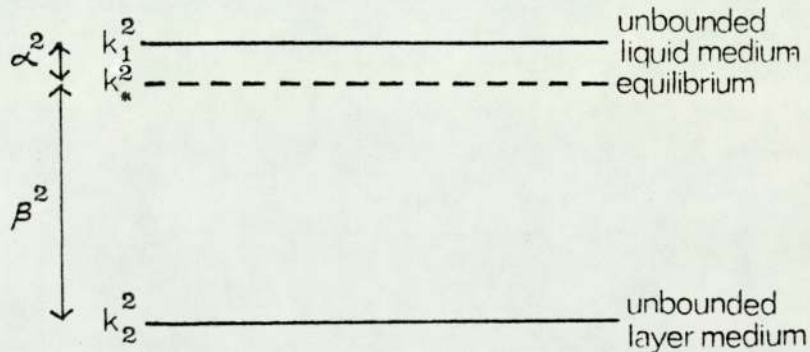
FIGURE 4.3   The theoretical equilibrium

The above results in several general concepts, applicable to the type of visualisation systems proposed. In general, the longitudinal wave induced within an index layer, by the surrounding ultrasonic field, will have properties described by k_* which are close to those normally associated with the liquid medium; in addition, the ultrasonic field will not be affected unduly by the presence of a thin layer, as the difference between k_1 and the equilibrium value of k_* will, in general, be small.

The above concepts would be expected to hold for any
frequency of interest, as the ratio of equations (4.9) and
(4.10) gives

$$\alpha^2 = - \frac{h}{\ell} \cdot \beta^2 \qquad\qquad (4.11)$$

and as long as $\ell \gg h$, the waves within the layer will
always be affected to a much greater extent that those of
the surrounding liquid.

The variation of α^2 and β^2 with various parameters is seen
to agree with that expected physically, noting that the
magnitude of α^2 indicates the extent of disturbance to the
ultrasonic field, and that of β^2 to how close the original
wave in the layer becomes to those normally expected in the
liquid medium:

(a)   both β^2 and α^2 increase as the difference between k_1^2
        and k_2^2 increases; thus, a more desirable equilibrium,
        with k_* lying close to k_1, will occur if k_1 and k_2 are
        more nearly equal i.e. if the layer and liquid media become
        closer in their original acoustic properties;

(b)   increasing the thickness of a layer, i.e. increasing
        h, causes an increase in α^2 with a corresponding decrease
        in β^2; thus, increasing the layer's thickness will

cause an increased disturbance to a given ultrasonic field, the equilibrium wave number k_* moving away from k_1; in addition, the resultant distribution within the layer will become further removed from that normally expected in the liquid medium.

(c) increasing the extent of ultrasonic field in the y direction, i.e. increasing ℓ, causes a decrease in α^2 an increase in β^2, the equilibrium value k_* moving closer to k_1. This is expected, as a greater extent of ultrasonic field would exert a greater influence on any wave within an index layer, whereas the effect of that layer on the field would decrease, together with the disturbance produced.

4.3.7 <u>Application of the theory to the proposed visualisation technique</u>

It has been indicated that a steady-state equilibrium, resulting from an interaction between ultrasonic waves in the liquid and layer media, will have associated properties close to those normally observed in the liquid medium. The tendency for this to occur will be enhanced by

(i)   the use of thin layers in large volumes of ultrasonic field;

(ii)   the use of a layer medium whose acoustic properties are as close as possible to those of the liquid medium.

Consider now the physical consequences, arising from the introduction of a thin, attenuating layer into the ultrasonic field to be visualised. Assume that the liquid and layer media's acoustic properties are not too different, a condition that has been met in practice (chapter 5); an equilibrium will be established, with the properties outlined, and let us now examine the consequences:

(a)   the disturbance to the ultrasonic field

Disturbance will occur, on the layer's introduction, by a change in the field's wavelength and an imposed attenuation. The extent of these phenomena will be judged by the real and imaginary parts of α^2 respectively, both of which will be small; thus, disturbance to the ultrasonic field by these mechanisms will be slight, and will be decreased by attention to (i) and (ii) above.

(b)   the display produced within an index layer

The equilibrium is predicted to be heavily biased in the liquid's favour, equation (4.10) predicting a substantial modification to the layer's original wavenumber k_2; the result is an ultrasonic distribution, within the layer, which will closely resemble the distribution that would exist at that plane in the layer's absence.

This latter statement has important consequences. The
wavelength of the resulting display, determined by the real
part of k_*, will now be virtually independent of the value
of k_2 previously associated with the layer medium; as k_*
is close in value to k_1, this display wavelength will be
characteristic of an ultrasonic wave in the liquid,
despite the fact that the visualisation process is occurring
within the layer. A valid display of the ultrasonic field
in the liquid, at the sampled plane, will thus result.

Attention to the imaginary part of k_*, which will be
small, again because k_* lies close to k_1, indicates that the
shared attenuation between the liquid and layer media will
be slight; this will be true despite the use of layer media
normally exhibiting extensive attenuation properties. The
result is that an ultrasonic wave within an index layer
will continue at a reasonable level of intensity for a greater
distance than normally expected. The display produced
will thus also be expected to remain at a reasonable level
of visibility over extended areas of the layer used.

4.3.8 A further prediction of the layer theory

The theory, outlined in the previous sections, has shown
that an index layer and the surrounding liquid will each
support an ultrasonic wave with a common wavenumber k_*, given
by equation (4.5), which was

$$k_* = \sqrt{k_1^2 - \alpha^2} = \sqrt{k_2^2 - \beta^2}$$

Thus, the solution used for each wave, present simultaneously

within each medium at equilibrium, may be expressed as

$$\emptyset_1 = Ae^{-jk_*x} \cos \quad \alpha(y - \ell) \qquad (4.12)$$

$$\emptyset_2 = Be^{-jk_*x} \cos \quad \beta(y + h) \qquad (4.13)$$

by substitution of (4.5) into (4.1) and (4.2) respectively.

Consider now the wave existing in the liquid medium, as expressed

by (4.12); the instantaneous pressure P, defined as

$$P = - \rho_1 \quad \frac{\partial \emptyset_1}{\partial t}$$

will be given by

$$P = - j\omega \rho_1 \emptyset_1$$

The concept of a simple wavefront is a surface on all points

of which, at a given instant of time, the pressure is

the same; accordingly, a simple expression for an acoustic

wavefront is

P = constant, C say:

$$\therefore \; -j\omega\rho_1 \; \emptyset_1 = C \qquad \text{i.e } \emptyset_1 = -\frac{C}{j\omega\rho_1}$$

Substitution into equation (4.12) gives

$$A e^{-jk_*x} \cos \; \alpha(y - \ell) \; = -\frac{C}{j\omega\rho_1}$$

$$\therefore e^{-jk_*x} \cos \; \alpha(y - \ell) = Q, \text{ another constant} \qquad (4.14)$$

A similar approach for the layer medium gives

$$e^{-jk_*x} \cos \; \beta(y + h) = R, \text{ a further constant} \qquad (4.15)$$

Taking logs of both sides of (4.14), we obtain

$$x_{liquid} = -\frac{1}{jk_*}\left[\log_e Q + \log_e \sec(\alpha(y - \ell))\right] \qquad (4.16)$$

whereas the same procedure, applied to (4.15), gives

$$x_{layer} = -\frac{1}{jk_*}\left[\log_e R + \log_e \sec(\beta(y + h))\right] \qquad (4.17)$$

Consideration of equations (4.16) and (4.17) shows that
ultrasonic wavefronts in both the liquid and layer media
are not plane, the resulting shape that these equations
predict being shown in Fig 4.4. The wavefront in the
liquid, immediately adjacent to the layer, is lagging
that at the $y = \ell$ limit of the liquid. A similar
effect occurs in the layer medium, but here the curve
is in the opposite sense. The complete wavefront shape
will by symmetrical about the $y = -h$ plane.

Various conclusions may be drawn from the above:

(a)   the introduction of an index layer, into an ultrasonic
field consisting solely of plane waves, will cause a
distortion to the ultrasonic wavefronts within the liquid
medium;
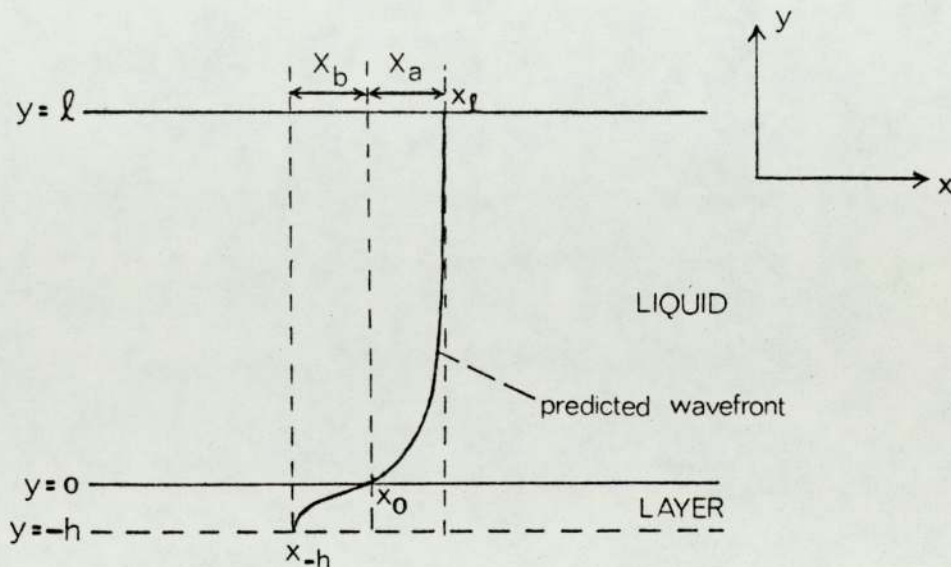
<u>FIGURE 4.4</u>   Resultant wavefront shape

(b)   the visual representation resulting from a wavefront
within the layer medium will be blurred over a finite
distance in the x direction, when viewed parallel to
the y axis;

(c)   this blurred image will lag the wavefront present
in the liquid medium.

To guage the extent of these phenomena, consider equations
(4.14) and (4.15); (4.14) was

$$e^{-jk_*x} \cos \alpha(y - \ell) = Q;$$

At $y = \ell$, this equation reduces to

$$x_\ell = - \frac{\log_e Q}{jk_*}$$

At $y = 0$,

$$\cos \alpha(y-\ell) = \cos \alpha \ell, \text{ and equation (4.14) reduces to}$$

$$x_0 = - \frac{\log_e Q}{jk_*} - \frac{\log_e \sec \alpha \ell}{jk_*}$$

∴. For an ultrasonic wave in the liquid,

$$\left| X_A \right| = x_\ell - x_o = \frac{\log_e \sec \alpha \ell}{jk_*} \qquad (4.18)$$

where $\left| X_A \right|$ is shown in Fig. 4.4; similarly, for an ultrasonic wavefront in the layer we obtain

$$\left| X_B \right| = x_{-h} - x_o = -\frac{\log_e \sec \beta h}{jk_*} \qquad (4.19)$$

Substitution of approximate values into equations contained in Section 4.3.6 has shown that $\alpha \ell > \beta h$, by approximately an order of magnitude. Hence, $\left| X_A \right|$ will be expected to be greater than $\left| X_B \right|$, although the actual amount by which these will differ is difficult to determine, due to the $\sec \alpha \ell$ and $\sec \beta h$ terms.

In general, it may thus be assumed that a display, produced in an index layer, will be blurred over the distance X_B, the previously plane wavefront in the liquid now being distorted over the distance X_A. The extent of these phenomena awaits experimental determination, but it is expected to decrease as the acoustic properties of the layer and liquid media become closer; as this occurs, the values of $\alpha \ell$ and βh become smaller, giving in turn smaller values of X_A and X_B.

4.3.9 <u>Conclusions concerning the layer theory</u>

The theory presented has investigated the case of a thin,
attenuating layer within an ultrasonic field in a liquid,
the latter's attenuation properties being negligable in
comparison. An assumption that the layer's acoustic
properties were not too different from those of the liquid
 led   to the following conclusions, when the theory
was applied to the proposed visualisation system:

(a)   The displayed wavelength within an index layer will
       be characteristic of that of the ultrasonic field;

(b)   the display will continue over an extended area
       of index layer, despite the latter's normal bulk
       attenuation properties;

(c)   a thin layer will not unduly affect the wavelength
       of the ultrasonic field being visualised, nor attenuate
       that field to any great extent;

(d)   these desirable properties will be enhanced by the
       use of as thin a layer as possible, whose acoustic
       properties do not differ substantially from those of
       the liquid medium;

(e)   the ultrasonic field will experience a distortion
       of its wavefronts due to the layer's presence. A further
       distortion in the layer will result in a blurred
       display which lags the ultrasonic distribution. These
       phenomena will be minimised by the use of layers with
       the properties outlined in (d).

The theory arrived at these conclusions by consideration
of the simplest possible case, that of an ultrasonic field
consisting solely of plane waves; it is thought, however,
that the listed conclusions will apply for a wide range
of ultrasonic distributions.

4.4 The build-up of ultrasonic intensity within an index layer

The production of a visible display within an index layer will
be dependent on sufficient ultrasonic intensity being present
within it, and it has been shown that this will be optimized
by the use of an index layer whose characteristic impedence
is the same as that of the surrounding liquid.

Suppose, however, that an impedence mismatch exists; a
substantial proportion of the ultrasonic field may be
reflected by the layer, resulting in an insufficient initial
intensity within the latter. The ultrasonic field, may under
certain circumstances however, cause this intensity to
build up with distance from the layer's edge, by a gradual
spread of its distribution.

This process is illustrated in Fig 4.5. and assumes that the
plane of the layer is parallel to the direction of propagation
of an incident field of plane waves. If this diffusion
process is too slow, a region may exist, around the layer's
edge, at which an insufficient ultrasonic intensity exists.
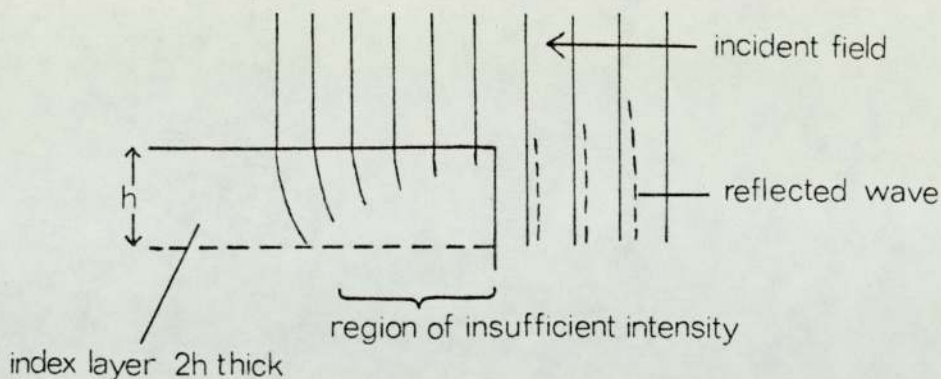
FIGURE 4.5   The spread of the distribution

An approximate estimation of the rate at which such

diffusion processes may occur was thus considered desirable;

this was achieved, as a theoretical approach, by studying

an analogous diffraction problem.

4.4.1 Build-up theory - statement of the proposed approach

The theoretical approach involves consideration of an analogous

situation - the diffraction spread of a plane-wave distribution,

originally contained between two perfectly-reflecting walls,

into a region wider than this by half a layer's thickness.

This process is illustrated in Fig 4.6. The plane wave,

contained between the perfectly-reflecting boundaries Y_2 and Y_3

encounters a widening of the channel at $x = 0$. As the

distribution progresses beyond this position, it diffracts

into the region between Y_1 and Y_2 planes shown. This latter

region, for $x > 0$, represents one half of an index layer, whose

FIGURE 4.6   The theoretical analogue

FIGURE 4.7   The distribution at x=o

thickness is 2h. The Y_1 plane, representing the mid-plane
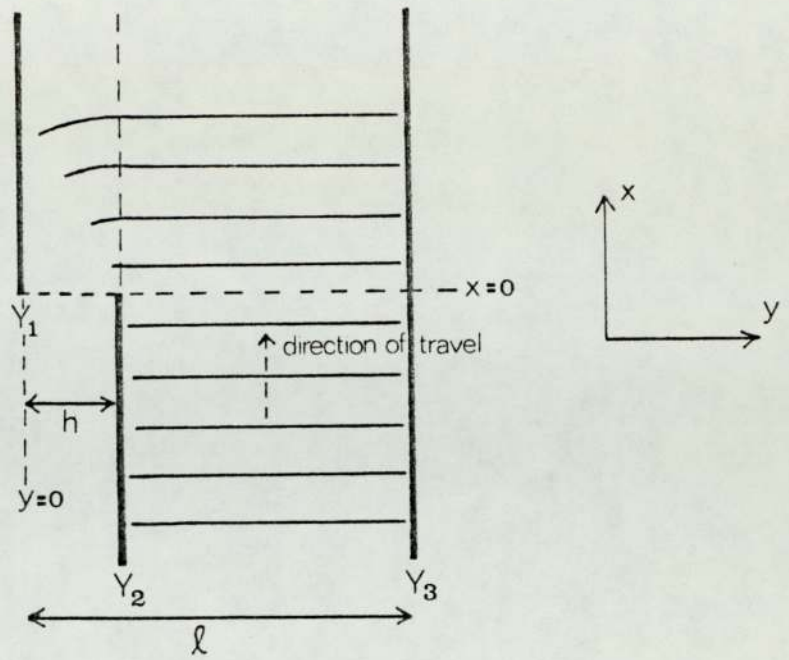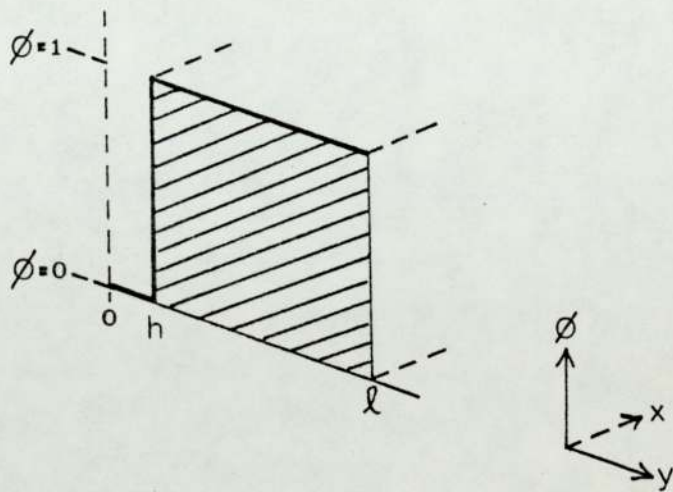of the layer, will be perfectly reflecting as before.

The region between Y_1 and Y_2, for $x > 0$, will hereafter
be known as the layer space, and the rate of diffraction
of the distribution into it will indicate the expected
ultrasonic intensity increase within the analogous index
layer.

The theory to be presented only approximates to the real
process, which will involve different liquid and layer
media; in addition no ultrasonic intensity is assumed within
the layer space initially, whereas in practice transmission
through the layer's edge will cause some intensity to be
initially present. It is hoped, however, that the theory
yields a theoretical approach, capable of predictions
which are within an order of magnitude of the real process.

4.4.2 <u>Synthesis of the ultrasonic distribution at x = 0</u>

Let the scalar velocity potential in the medium under
investigation be $\emptyset$, and consider a plane wave, of amplitude $\emptyset = 1$,
existing between Y_2 and Y_3 at $x = 0$ (Fig 4.6); the distance between
these two planes is $(\ell-h)$. To the left of Y_2 exists a region of
thickness h, in which there is no ultrasonic presence at $x = 0$
i.e. in which $\emptyset = 0$. This distribution is shown in Fig 4.7,
and may be expressed mathematically as

$$\phi = 1 \qquad h < y < \ell$$
$$\phi = 0 \qquad 0 < y < h \Bigg\} \text{ at } x = 0$$

This distribution must be synthesized from equations which obey the boundary conditions, and which are solutions to the wave equation

$$(\nabla^2 + k^2) \; \phi = 0 \qquad\qquad (4.20)$$

where $\nabla^2 = \dfrac{\partial^2}{\partial x^2} + \dfrac{\partial^2}{\partial y^2}$, and k is the circular wavenumber

The boundary conditions to be imposed are that this distribution should be contained within perfectly reflecting boundaries at $y = 0$ and $y = \ell$, at the plane $x = 0$

i.e. $\dfrac{\partial \phi}{\partial y} = 0$ at $x = 0$, for $y = \ell$ and $y = 0$

It was noted that the proposed system lends itself to Fourier synthesis, and so a solution was formulated, incorporating terms readily available for this procedure. It can be shown, by the Principle of Separation of Variables (Appendix 2) that

$$\phi = Ae^{j \sqrt{k^2 - C^2} \, . \, x} \; \text{Cos.} \, C \, y \qquad\qquad (4.21)$$

is a solution to equation (4.20), where A is a coefficient and C is a constant. Writing C as $\dfrac{n\pi}{\ell}$, where n is an integer, (4.21) becomes

$$\emptyset = Ae^{j\sqrt{k^2 - \frac{n^2\pi^2}{\ell^2}} \cdot x} \cos \frac{n\pi}{\ell} y \tag{4.22}$$

Equation (4.22) obeys the prescribed boundary conditions; differentiating with respect to y gives

$$\frac{\partial \emptyset}{\partial y} = -Ae^{j\sqrt{k^2 - \frac{n^2\pi^2}{\ell^2}} \cdot x} \frac{n\pi}{\ell} . \sin \frac{n\pi y}{\ell}$$

and $\frac{\partial \emptyset}{\partial y} = 0$ at $y = 0$ and $y = \ell$

Consider now the type of Fourier Series, needed to synthesize the required distribution in $\emptyset$ at $x = 0$. The required distribution may be expressed as a half-range Fourier Series, containing cosines only, and will be given by

$$F(y) = \frac{1}{2} . a_o + \sum a_n \cos \frac{n\pi y}{\ell} \tag{4.23}$$

where $a_n = \frac{2}{\ell} . \int_0^\ell f(y) . \cos \frac{n\pi y}{\ell} . dy$,

and the function is defined over the period $0 < x < \ell$.

Now, as in Fig 4.7,

$$f(y) = 1 \qquad h < x < \ell$$
$$f(y) = 0 \qquad 0 < x < h$$

$$\therefore \quad a_n = \frac{2}{\ell} \int_h^\ell \cos \frac{n\pi y}{\ell} . dy \tag{4.24}$$

i.e. $a_n = - \dfrac{2}{n\pi} \cdot \sin \dfrac{n\pi h}{\ell}$

The value of a_0 will be given by $n = 0$ in equation (4.24)

$\therefore \ a_0 = \dfrac{2}{\ell} \cdot \displaystyle\int_{h}^{\ell} dy$

$= 2(1-g)$, where $g = \dfrac{h}{\ell}$.

Thus, the full Fourier Series is

$$F(y) = (1-g) - \sum_{n=1}^{n=\infty} \frac{2}{n\pi} \ \text{Sin } n\pi g. \ \cos \frac{n\pi y}{\ell} \quad (4.25)$$

Equation (4.25) may now be used to modify the form of the

original solution for $\emptyset$, which was

$$\emptyset = Ae^{j\sqrt{k^2 - \frac{n^2\pi^2}{\ell^2}} \cdot x} \cos \frac{n\pi}{\ell} y$$

to give

$$\emptyset = (1-g)e^{jkx} + \sum_{n=1}^{n=\infty} - \frac{2}{n\pi} \sin n\pi g. \ \cos \frac{n\pi y}{\ell} \ e^{j\sqrt{k^2 - \frac{n^2\pi^2}{\ell^2}} \cdot x}$$

$$(4.26)$$

where the coefficient A has been replaced by the Fourier Series

F(y). Equation (4.26) has the required distribution in y at

x = 0, and is in the form of a series in which each component
is itself a solution to the wave equation (4.20). At x = 0,
(4.26) becomes

$$\phi = (1-g) - \sum_{n=1}^{n=\infty} \frac{2}{n\pi} \; \text{Sin} \; n\pi g. \; \cos \frac{n\pi y}{\ell} \qquad (4.27)$$

This series, and that in equation (4.26), have been seen to be
fairly rapidly convergent, and a good approximation to both
was obtained by the use of a finite number of terms in each.

The distribution at x = 0, determined by equation (4.27), was
evaluated using the University's ICL 1904S Computer and Fig 4.8(a)
indicates that the fit to the required distribution improves
with a greater number of terms m; a better fit is also seen with
a lower ratio of ℓ to h (not shown). Fig 4.8(b) shows how the
complete distribution at x = 0 may be synthesized and plotted
by the computer and its associated graph plotter.

Having thus shown that the required distribution may be
synthesized at x = 0, the predicted diffraction process may
now be studied.

4.4.3 The distribution for x > o

Progress of the distribution in the x direction, and its
diffraction into the layer space, may be studied by use of
equation (4.26) with a finite number of terms m, enabling the
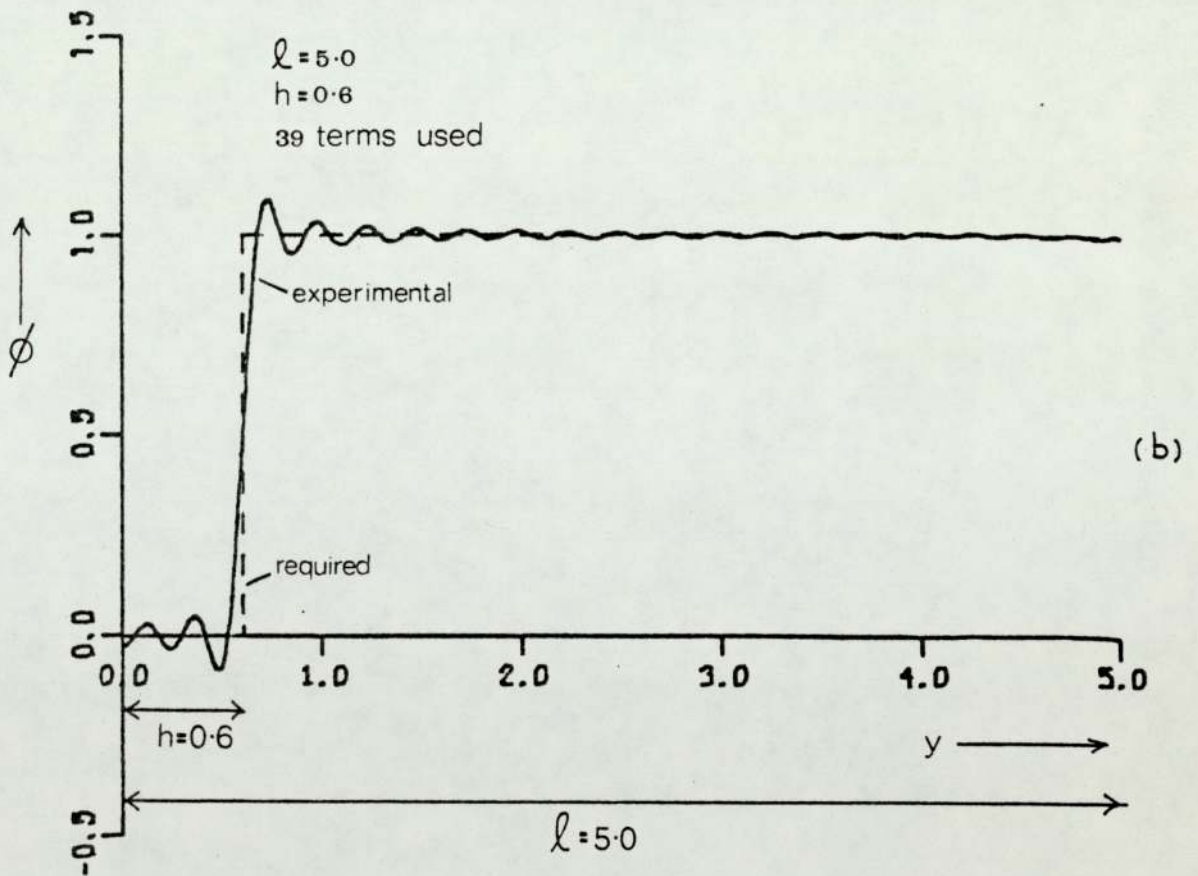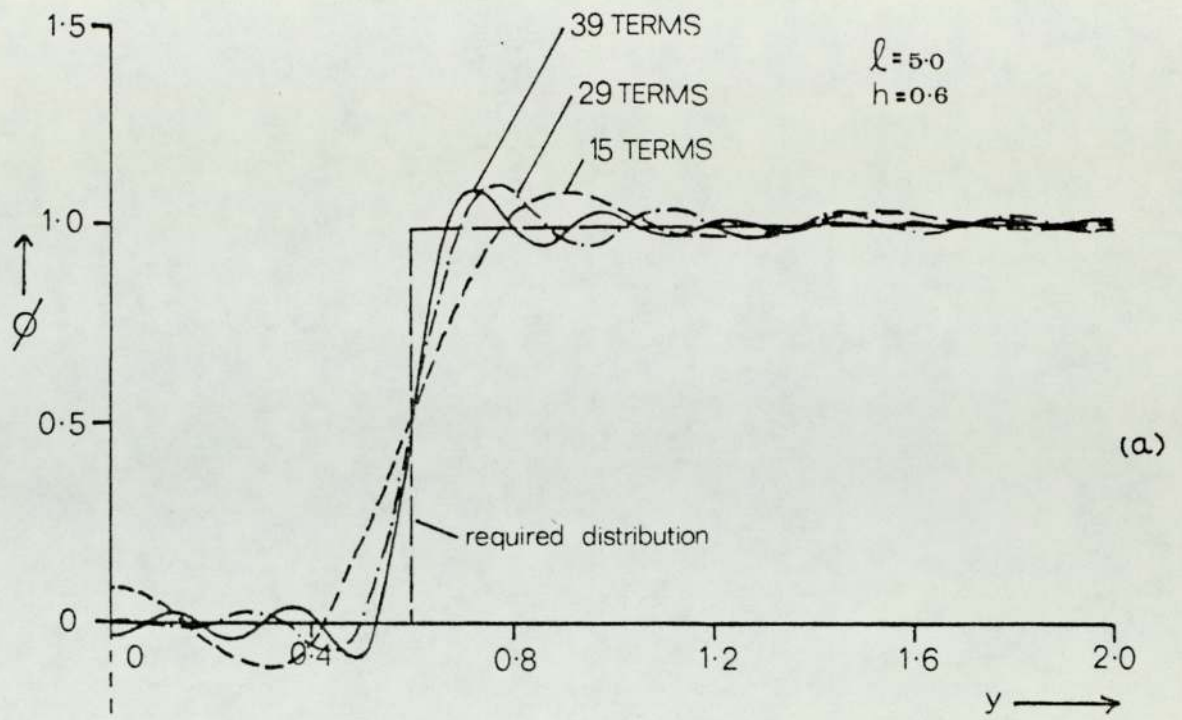
FIGURE 4.8   The computed distribution at x=o

(a) variation with number of terms

(b) a typical distribution

expected build-up of $\emptyset$ in this region to be determined.

Before this is done, however, other factors must be considered.

Equation (4.26) will only be easily evaluated by computer

techniques when expressed in its separate real and imaginary

parts, $\emptyset_{cos}$ and $\emptyset_{sin}$ respectively; these will be given by

$$\emptyset_{cos} = (1-g) \cos kx$$

$$+ \sum_{n=1}^{n=m} - \frac{2}{n\pi} \, \text{Sin} \, n\pi g. \, \cos \frac{n\pi y}{\ell}. \, \cos \sqrt{k^2 - \frac{n^2\pi^2}{\ell^2}} \, . x$$

and

$$\emptyset_{sin} = (1-g) \sin kx$$

$$+ \sum_{n=1}^{n=m} - \frac{2}{n\pi} \, \text{Sin} \, n\pi g. \, \cos \frac{n\pi y}{\ell} \, \sin \sqrt{k^2 - \frac{n^2\pi^2}{\ell^2}} . x$$

and the magnitude of $\emptyset$ will be given by

$$|\emptyset| = \sqrt{\emptyset_{cos}^2 + \emptyset_{sin}^2} \qquad\qquad (4.28)$$

In addition, if $\frac{n^2\pi^2}{\ell^2}$ becomes greater than k^2,

$$e^{j\sqrt{k^2 - \frac{n^2\pi^2}{\ell^2}}.x} \quad \text{becomes} \quad e^{-\sqrt{\frac{n^2\pi^2}{\ell^2} - k^2}.x}$$

and this will only contribute to the real (cosine) series;

thus, when $\dfrac{n^2 \pi^2}{\ell^2} > k^2$, an attenuating term is introduced into

the $\emptyset_{cos}$ series.

Bearing the above in mind, the value of $\emptyset$, given by equation
(4.28), may be found for any positive values of x and y;
this enables the whole diffraction process to be studied.
Fig 4.9 shows the progress of a typical distribution as it
propagates in the x direction, commencing at $x = 0$. Diffraction
into the layer space, of width h, is clearly visible, resulting
in a build-up of $\emptyset$ in this region from its initial negligible
value. The wavenumber used is $10cm^{-1}$, approximately that of
200 kHz ultrasonics in water.

It is found that the rate at which $\emptyset$ increases in the layer
space, as the distribution progresses in the x direction, is
dependent on the relative values of k, ℓ and h; it is found
that

<div style="margin-left:2em">

(a)   increasing the frequency of the ultrasonic wave

         i.e. increasing k, causes the rate of build-up

         of $\emptyset$ in the layer space to decrease;

(b)   the smaller the thickness h of a layer space, the

         more rapid the observed build-up of $\emptyset$ within it;

(c)   the value of ℓ i.e. the extent of initial

         ultrasonic field, does not seem to affect the

         resulting rate of diffraction.
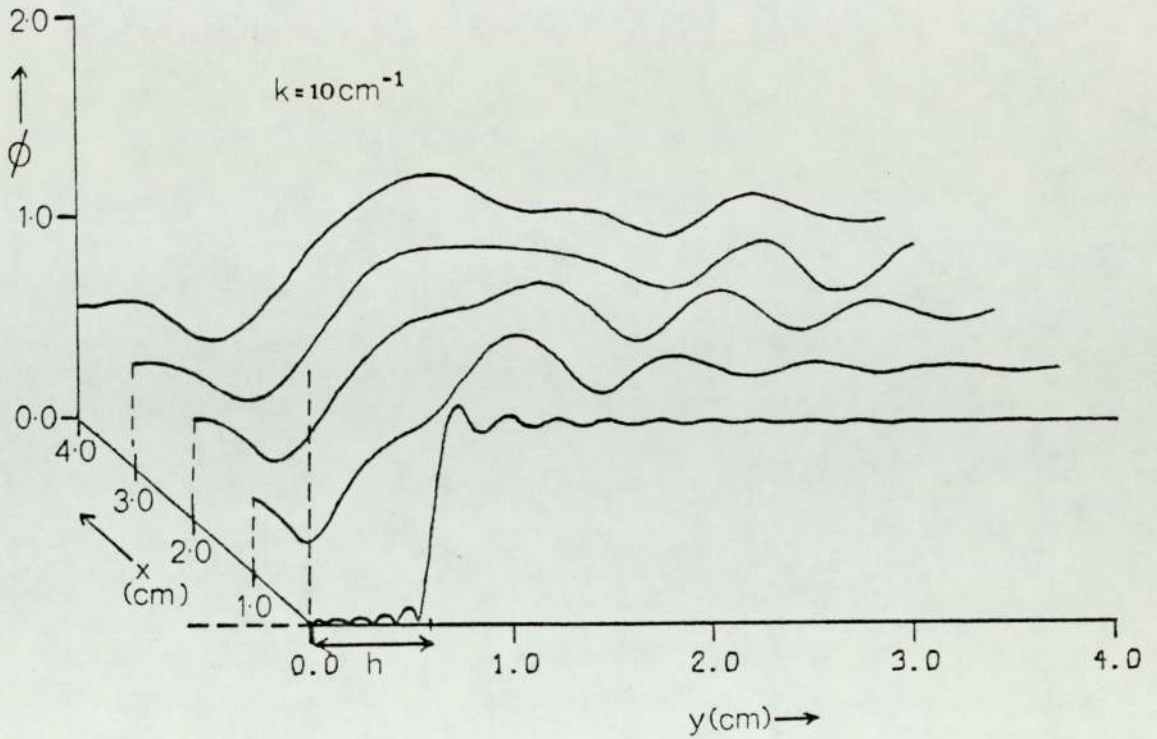
</div>

FIGURE 4.9   Progress of a typical distribution
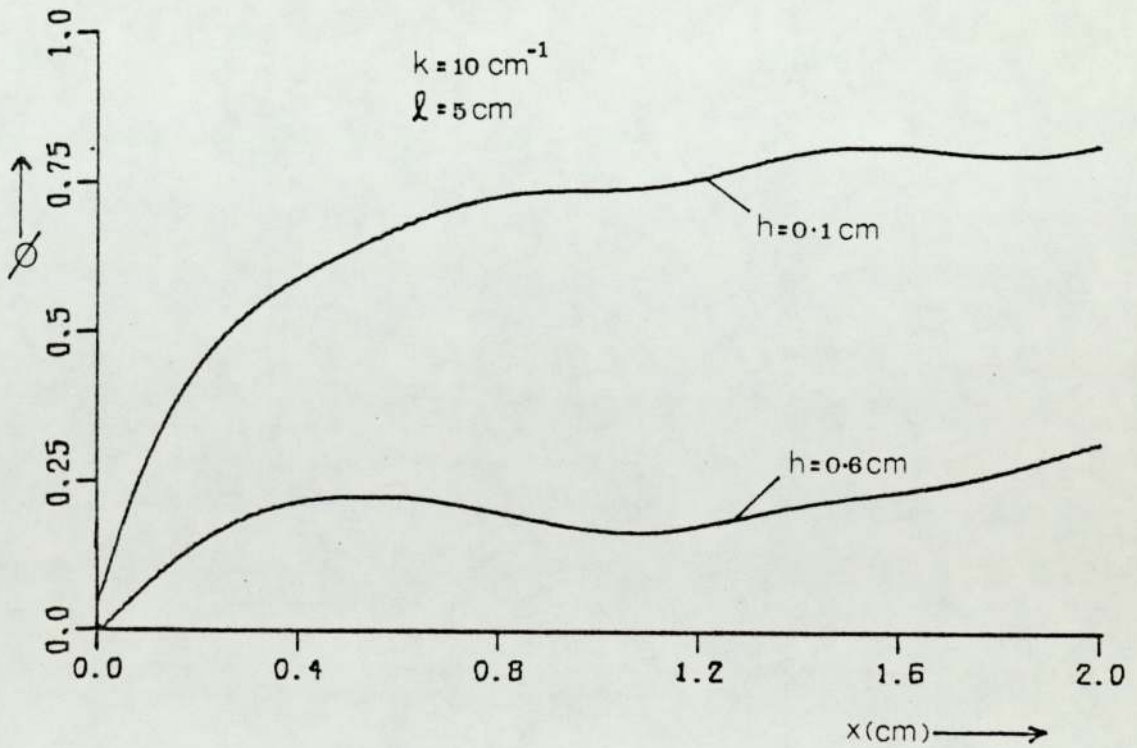
FIGURE 4.10   Build-up of ∅ with distance at the plane y=h/2

Fig 4.10 illustrates the process described in (b) above,
and shows the build-up of $\emptyset$ with distance x at the plane
$y = \dfrac{h}{2}$ i.e. at the mid-section of the layer space; the rate
of diffraction spread with distance is clearly greater in
the case of the thinner layer space.

4.4.4 Application of the theory to practical visualization systems

The analogue theory, involving the study of diffraction
within a continuous medium, has been shown to predict the
rate of build-up of $\emptyset$, and hence ultrasonic intensity,
within a region representing an index layer, the layer space.
A study of this process is believed to give an indication
of the rate of diffusion of an ultrasonic field into an
index layer, assuming the latter's plane is perpendicular
to the incident wavefronts.

As outlined previously, sufficient intensity for the production
of a visible display may not exist within an index layer by
simple transmission from the ultrasonic field; the diffusion
process, predicted by the theory, will then dictate the
distance from a layer's edge at which the ultrasonic intensity
builds up to an acceptable value.

By analogy with the theory, which treats the process as
diffraction, it may be expected that the rate of diffusion of
an ultrasonic distribution into an index layer will

(a)   decrease with an increase in ultrasonic
       frequency;

(b)   decrease with an increase in the layer's
       thickness;

(c)   be unaffected by changes in the extent of
       ultrasonic field surrounding it.

Some idea of the rates of diffusion involved may be obtained

by the analysis of graphs such as those presented in Fig 4.10.

Here, the upper graph predicts that an ultrasonic field,

roughly corresponding to a 200 kHz distribution in water, will

diffract rapidly into a 1mm thick layer space; indeed, $\emptyset$

reaches a value of 0.5, at the plane $y = h/2$, within 3mm of the

discontinuity at $x = 0$ (Fig 4.6); this would correspond to a

distance which is less than half of the ultrasonic wavelength.

This infers that the diffusion process, expected in practical

situations, will be sufficiently rapid at 200 kHz for effective

visualization to take place within layers up to 2mm (2h) thick,

or even more. As the photoelastic index layers, used in the

practical apparatus described in Chapter Three, range from

1-3mm in thickness, the resultant displays will be expected to

fill the bulk of their area.

Extension of the theory to a higher frequency of 1 MHz yields a

prediction that $\emptyset$ will only build up to a value of 0.5, at the

plane $y = h/2$, over a distance of two ultrasonic wavelengths at

this frequency. This may be unacceptable, and the inference is

that at these frequencies and higher, it becomes important to

match the characteristic impedences of the liquid and layer
media, so that the diffusion processes examined become less
important.

In conclusion, the theory presented is intended as an analogous
approach to predicting phenomena not otherwise easily examined.
It must be stated that it only approximates to the physical
reality; index layers will, in general, contain some ultrasonic
intensity by transmission through their edges, the layer may have
different acoustic properties to those of the liquid medium,
and the diffusion process may also be affected by reflection at
the layer's upper and lower faces. Despite this, however, it is
thought that the predictions of the theory lead to an approximate
idea of the rates of the processes studied.

4.5   General Conclusions

The overall validity of the proposed visualization technique,
involving the use of thin layers, depends on two main factors
- the disturbance to the ultrasonic field and the validity of
the display produced.

A difference in characteristic impedence between the liquid
and layer media has been seen to result in various undesirable
effects, including reflection and diffraction of the ultrasonic
field, and internal reflection and mode conversion within the
index layer.

The theory of section 4.3 indicated that if thin layers are used, the display produced will be expected to represent closely the ultrasonic distribution present at the sampled plane in the layer's absence; in addition, the ultrasonic wavelength derived from the display will be expected to be close to that normally associated with the liquid medium. These general concepts were seen to hold as long as the layer and liquid media did not differ too widely in their acoustic properties.

Attenuation within the layer medium is only expected to affect the ultrasonic field slightly; conversely, the display produced is expected to exist for a far greater distance than might be expected from consideration of the layer's attenuation characteristics.

An undesirable phenomenon, predicted by the theory, is that a distortion to the wavefronts of the ultrasonic field may occur on the layer's introduction; additionally, the display produced may be blurred and may lag the distribution being visualized. These effects will be minimized by the use of thinner layers, closer to the liquid in their acoustic properties.

The build-up of ultrasonic intensity within an index layer has been suggested by a spreading of the ultrasonic field into it, superimposed on direct ultrasonic transmission across liquid/ layer boundaries. The latter is enhanced by matching the characteristic impedences of the liquid and layer media, the former by the use of thin layers.

In summary then, both disturbance to the ultrasonic field, and the non-validity of the display produced, may be minimized by

    (a)   the use of layers which are as thin as possible;

    (b)   ensuring that the acoustic properties of the liquid and layer media are as close as possible.

These theoretical considerations thus lay down a basis for an ultrasonic visualization system, using the concept of an index layer, which is capable of wide application.

CHAPTER FIVE

THE VISUALISATION SYSTEM - RESULTS AND DISCUSSION

An ultrasonic visualisation technique has been proposed,
based on the stroboscopic illumination of thin photoelastic
layers, in which two-dimensional sections of an ultrasonic
field may be selected for study; an apparatus, utilising
this concept, has been described and built.

Chapters 1 and 4 indicated that various factors needed to
be considered, before such a technique could be widely
applied; these included the disturbance to the ultrasonic
field, and the validity of the display produced. These
factors will now be examined, and the displays produced by
the described apparatus presented.

5.1   The type of display produced

A typical display, produced by the apparatus described in
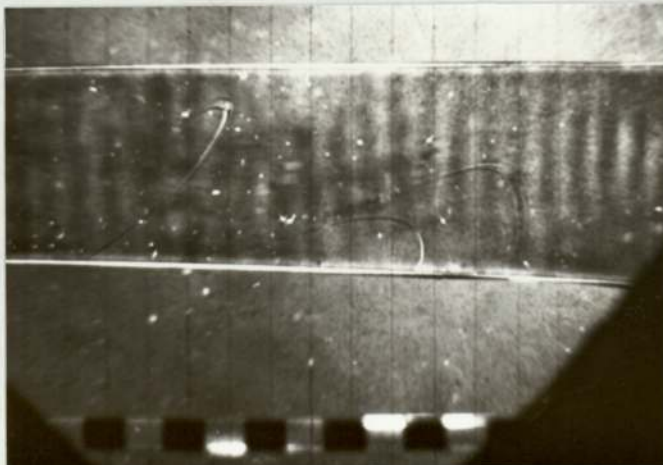Chapter 3, is presented in Fig 5.1. This is the display

FIGURE 5.1
a typical display

produced within a 3mm thick sheet of photoelastic
material, of area 20cm x 5cm. The layer was supported
horizontally by the visible wire grid in the path of
the 200kHz, continuous-wave ultrasonic beam, emanating
from the transducer previously described (Section 3.5.2).

Progressive ultrasonic waves, passing through this index
layer, are shown up as a series of light and dark bands
upon illumination with modulated, plane-polarized light,
the stroboscopic effect 'freezing' the photoelastic
display produced; the curved lines are surface defects.

The polarizer, positioned beneath the index layer on the
tank's bottom Fig (3.13),was orientated with its axis at
45° to the principal direction of ultrasonic propogation
i.e. at 45° to the bands in the photograph; this produced
the optimum conditions for the photoelastic display of
longitudinal waves (Section 2.2.4), the analyzer crossed
with the polarizer. The display shown was photographed
with a still camera, the ultrasonic and light modulation
frequencies being made the same by use of the apparatus
described in Section 3.7. A slight frequency difference
between the two, introduced via the circuit of Fig 3.15,
caused the bands to move steadily through the field of view,
allowing convenient cinematography of the progress of the
distribution.

At the base of the photograph, Fig 5.1, can be seen a reference scale, each section of which is 1cm wide; this allows the distance between each band i.e. the display wavelength, to be determined.

It is evident from the photograph that only the portion of the field of view covered by the layer contains a photoelastic display, the water within the tank producing no visible effect. This will be true in the direction perpendicular to the plane of the layer also. Movement of this index layer throughout the whole volume of the ultrasonic field will thus allow the visualisation of the complete three-dimensional distribution.

5.2 Optimization of these displays

The visibility of photoelastic displays, produced within various index layers, was found to be dependent on various factors, namely

      (a)   the choice of index layer material;

      (b)   adjustment of the optical system;

      (c)   the illumination conditions;

      (d)   the intensity of the ultrasonic field.

5.2.1 Suitable index layer materials

The sensitivity of a material to the photoelastic display
of ultrasonics may be judged by the value of its strain-
optical coefficient, and the materials which seemed of
immediate promise were various photoelastic polymers,
readily available in sheet form. These were additionally
useful in that their acoustic properties were fairly
close to those of water. Those chosen for investigation
were

(i)   polyurethane rubbers

(ii)   epoxy resins

(iii) columbia resins

(iv)   polyesters

These materials, in layer form, were each found to give
visible photoelastic displays within the apparatus described,
with little difference in their sensitivities. The thickness
of each used varied between 1-3mm, and the visibility of
display seemed relatively unaffected by a change in their
thickness within this range. Other polymer materials
with a lower photoelastic sensitivity e.g. perspex, were found
to give inadequate displays.

5.2.2 Adjustment and alignment of the optical system

Good alignment of the optical system was found to be essential
for the production of acceptable displays. This involved

ensuring that the resultant light beam from the modulator
was diverted through 90°, and not at an angle, and that
all the subsequent optical elements were coaxial with
respect to this beam. In particular, the system seemed
to be sensitive to misalignment of the two Fresnel lenses,
the first producing the parallel beam for illumination
of the index layer, the second being the Field lens.
Careful positioning of the camera was also needed, to
produce a uniformly illuminated field of view for photography.

In addition, it was found necessary to ensure that the
polarizer and analyzer were properly crossed; if this was
not so, the contrast of a resultant display was poor.

5.2.3 Adjustment of the illumination conditions

The selection of various wavelength bands of light, via
suitable filters, from the output of the arc-lamp was
found to affect the visibility of a given display. Narrow-
band illumination was found to give a better effect than
white light, and the blue end of the visible spectrum was
found to be the best. The latter fact agreed with photoelastic
theory, the double refraction produced by a strain in a given
material increasing in magnitude with a decrease in
illumination wavelength(105). Accordingly, all the displays
presented were photographed under illumination with blue light,
obtained by the introduction of a blue dye into the lens cooling
system (Section 3.4.1).

The on-time is the fraction of the period for which

the illumination is present.

The conditions of stroboscopy, controlled by the photoelastic light modulator, were variable as indicated in Fig 3.8.

400kHz modulation was found to result in a weak, hardly discernable display, because of the poor performance of the modulator at this frequency; of more interest were the displays produced at the 200kHz nominal frequency. Pulse-like illumination was found to give a better visibility of display than a sinusoidal one, both for static and moving displays. This is understood, when one considers that the effective on-time of the sinusoidally modulated illumination will be greater than that of the pulse-like variety; the display will tend to be blurred by an excessive on-time, and this effect will be greater for sinusoidal modulation.

5.2.4 The intensity of the ultrasonic field

As has been described, an ultrasonic generating system, capable of producing powers of up to $1Wcm^{-2}$, was developed so that investigations into the usefulness of insensitive index layer materials could take place.

In practice, it was found that the full intensity of ultrasonics available was required to produce the most visible display, the brightness increasing steadily with ultrasonic intensity. It was concluded from this that the

Photoelastic effect, produced by the maximum intensity
available, did not reach the equivalent of a half-wave
plate in the brightest regions of display; an increase
in ultrasonic intensity in excess of that producing an
optical half-wave plate would have caused a decrease
in the brightness of the display, and this was not
observed.

Additionally, it may be concluded that ultrasonic intensities
in excess of those used in this investigation might have
yielded more visible displays.

It was found that the minimum intensity needed for the
production of acceptable displays in typical polymer index
layers was roughly $0.2 \mathrm{Wcm}^{-2}$, variations in layer thickness
between 1 and 3mm again producing little observable change.
The above figure thus represents the effective sensitivity
of the technique in its present state.

It should be noted that photoelastic index layers of
thickness less than 1mm were found to produce inadequate
displays at these intensities; this thickness is thus
the lower limit available for use with the index layer
materials investigated.

5.3   The disturbance to the ultrasonic field

Considerations in previous chapters have shown that
disturbance to the ultrasonic field could occur from

      (a)   a change in its wavelength

      (b)   its reflection and diffraction by the index layer

      (c)   its attenuation

and it was considered desirable to use as thin a layer as
possible, whose acoustic properties were as close as possible
to the surrounding medium, in this case water.

An ideal index layer material will thus have an equal bulk
modulus and density to that of water.

The epoxy resins, columbia resins and polyesters used as
index layer media had, in general, a characteristic impedence
that was approximately twice that of water, whereas
the velocity of longitudinal waves in each, judged by
their bulk moduli and densities, was normally greater than
the velocity of sound in water by approximately fifty percent.

Use of these three materials as index layers can thus lead
to a disturbance of the ultrasonic field by the mechanisms
outlined above.

In contrast to these materials, polyurethane rubbers
were found to exhibit acoustic properties close to those
of water, as will now be described.

5.3.1 The properties of polyurethane rubbers

The density of polyurethane rubbers used in this investigation
was very close to that of water, but marginally greater;
this was clearly observed when a sample, immersed in water,
sank only very slowly.

The determination of the velocity of longitudinal waves in
a bulk sample of the material was carried out by a simple
experiment using a clinical A-scan diagnostic set. Ultrasonic
pulses, produced by the transducer, were reflected normally
from a horizontal glass slab, and the resulting echo displayed
on the oscilloscope screen. A sheet of polyurethane rubber
was now placed horizontally on the glass plate and the
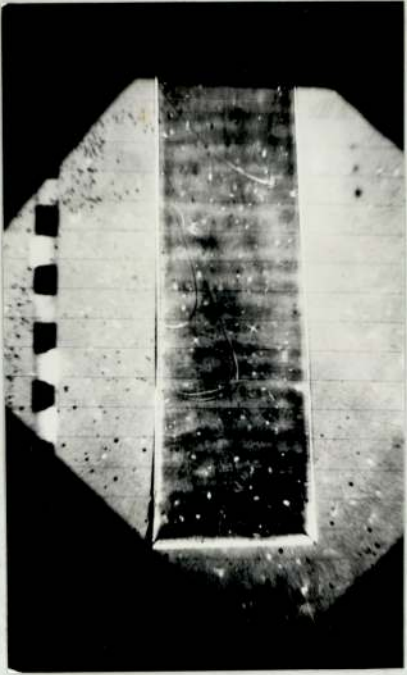procedure repeated. The traces obtained indicated

> (i)   that only minimal reflection was occurring at
>   the interface between water and polyurethane
>   rubber;
>
> (ii)   that the velocity of ultrasonics within the two
>   media was the same, within experimental error,
>   the reflection from the glass block occurring
>   at the same position in each case.

These observations held for sample thicknesses of up to
9mm, although with thicker specimens the reflected
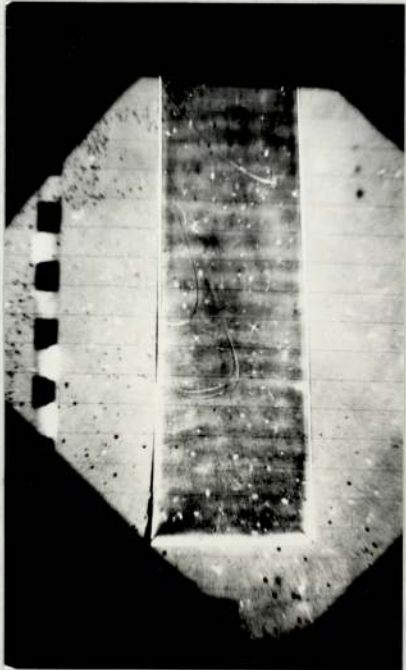echo from the glass was highly attenuated.

It may thus be concluded that both the bulk modulus and
density of polyurethane rubbers are almost identical to
their respective values in water; disturbance to the
ultrasonic field by reflection and diffraction, on such
a layer's introduction, will thus be extremely small.
There will also be no modification to the wavelength of the
ultrasonic field, as might be produced by the mechanisms
treated theoretically in chapter Four.

Experimental proof that a change in wavelength of the
ultrasonic field does not occur, on such a layer's introduction,
is provided by the series of photographs presented in
Fig 5.2. Here, a 3mm layer of polyurethane rubber was moved
through the ultrasonic field, being the farfield of the 200kHz
transducer described, with all other conditions remaining
constant. Figs 5.2(a), (b) and (c) show the displays produced
at three different positions in the ultrasonic field, and
Fig 5.2(d) shows sections through all three set side by side.
Correct positioning was aided by the marker and wire support
grid.

FIGURE 5.2 THE EFFECT OF A 3mm SHEET OF POLYURETHANE RUBBER ON THE ULTRASONIC FIELD'S WAVELENGTH;

(a), (b) and (c), the display produced at various positions;
(d) these displays compared

If the layer was causing the ultrasonic wavelength in the water to change, the display produced at a certain position would be shifted laterally, and not be superimposable, as the layer itself was moved laterally. It can be seen from the photographs that no lateral shift is observable, and that no visible disturbance to the ultrasonic field's wavelength was produced.

Additional evidence of an impedence match between polyurethane rubbers and water came from the observation that the display, produced by a given index layer, was not visibly altered by introducing a sheet of the material into the ultrasonic field.

The attenuation within polyurethane rubbers is rather high. However, theory (Chapter 4) has indicated that the resultant attenuation to an ultrasonic field, due to a thin, highly-attenuating index layer, will not be excessive; indeed, attenuation is considered a benefit.

Thus, with respect to the disturbance to a given ultrasonic field, polyurethane rubbers may be regarded as an almost ideal material. In addition, the material has other desirable properties e.g. its Poisson's Ratio is close to the ideal of 0.5, and thus shear wave production (see next section) will not be a problem.

5.4   The interpretation of the displays

5.4.1 The attenuation properties of the layer material

An observable feature of the displays hitherto presented
is that they exist over the whole area of the index layers,
and do not fade with distance; this is despite the fact
that the photoelastic material used in each was polyurethane
rubber, a material exhibiting a high attenuation coefficient
for 200kHz ultrasonics.

This observation agrees well with the theoretical considerations
of Chapter 4, which concluded that the ultrasonic wave,
induced within a thin index layer, would not be attenuated
to the degree predicted from the layer's bulk attenuation
coefficient at that frequency. This phenomenon has, in
fact, been observed in a wide range of index layer materials,
and thus theory and practice agree in this respect.

5.4.2 The photoelastic display wavelengths

3mm sheets of polyurethane rubber, epoxy resin and columbia
resin were used as index layers in the apparatus described.
Fig 5.3(a) shows sections taken from the photoelastic displays
in each material. The displays are propagating, longitudinal
waves, photographed under stroboscopic illumination, each
section being enlarged to the same scale, as indicated by the
match obtained in the wire support grids.

It is clear that similar display wavelengths were produced
in each material, and were measured to be identical within
experimental error.

The velocity of sound in polyurethane rubber has been
determined to be close to that of water (Section 5.3.1);
it may thus be concluded that the displayed wavelength in
each was characteristic of that of the ultrasonic field in
the surrounding water, despite the fact that the velocity
of sound in epoxy and columbia resins is normally greater
than that of water. The display wavelength was measured
at 0.74 cm, within experimental error of the wavelength
normally associated with 200kHz ultrasonic waves in water.

It will be remembered that the theoretical analysis of
Chapter 4 predicted that the ultrasonic wave, induced within
a thin index layer, would have a wavelength close to that
normally expected within the liquid medium, provided the
acoustic properties of the liquid and layer media did not
differ too widely. These predictions have been born out in
the above observations.

Fig 5.3(b) shows the display wavelength of a progressive
wave within a 3mm glass sheet, reproduced to the same scale
for comparison. The display wavelength is visibly greater
than those within the polymer materials, and is in fact
mid-way between the wavelengths normally associated with
200kHz ultrasonic waves in glass and water respectively.
Despite the fact that the acoustic properties of glass and
water differ widely, it seems that again some sort of

epoxy resin

FIG. 5.3 (a)
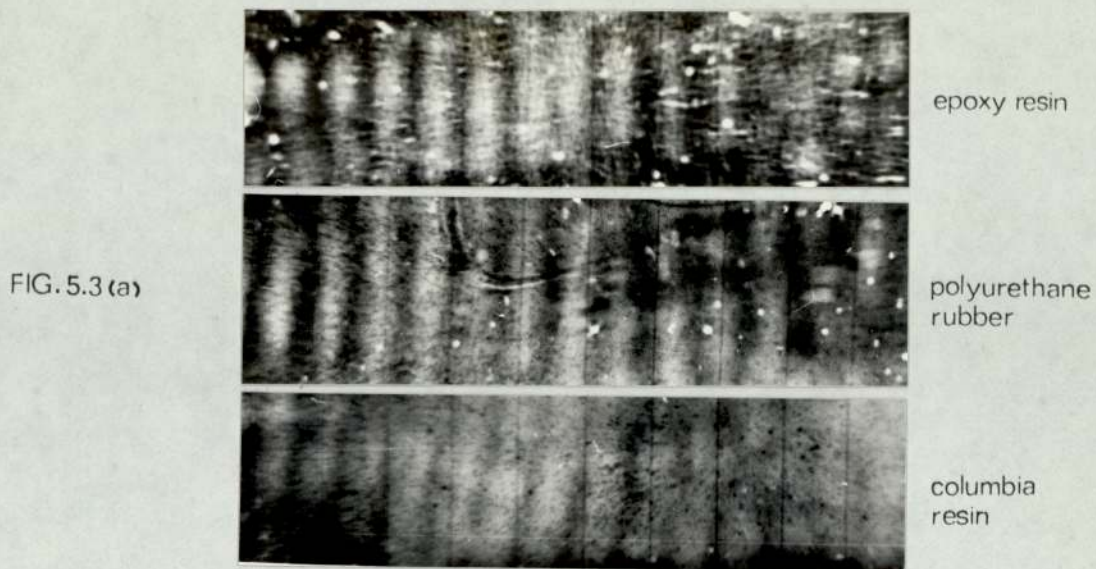
polyurethane
rubber

columbia
resin

FIG. 5.3 (b)

glass

FIGURE 5.3   Display wavelength of progressive waves produced in various
layer materials
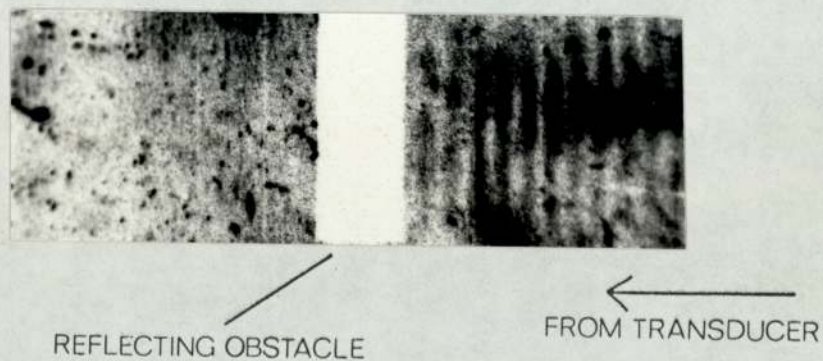

REFLECTING OBSTACLE

FROM TRANSDUCER

FIGURE 5.4   Standing waves in polyurethane rubber

equilibrium has been established between waves in the
liquid and layer media, as predicted by theory.

The above observations have led to several preliminary
conclusions.

(a)   various theoretical considerations of Section
      4.3 have been confirmed in practice;

(b)   it is preferable to use a thin index layer, whose
      acoustic properties are not too different from
      those of the liquid medium;

(c)   the photoelastic display produced by such an
      index layer will have a wavelength characteristic
      of the field being visualised;

(d)   these conclusions will not hold if the index
      layer material differs too widely in its acoustic
      properties from those of the surrounding liquid.

The displays of standing waves, produced under steady illumination,
were found to have a periodicity half that of progressive waves,
produced by stroboscopy; this is illustrated in Fig 5.4.
Displays of standing waves thus contain two bright bands
per ultrasonic wavelength, which agrees with the theoretical
predictions, illustrated in Fig 2.6(b).

It has been seen that the photoelastic display of progressive
waves, produced within the apparatus described, contained

only one bright band per ultrasonic wavelength; this is in disagreement with Fig 2.6(a), which predicts two. This apparent contradiction will be examined in Section 5.4.4.
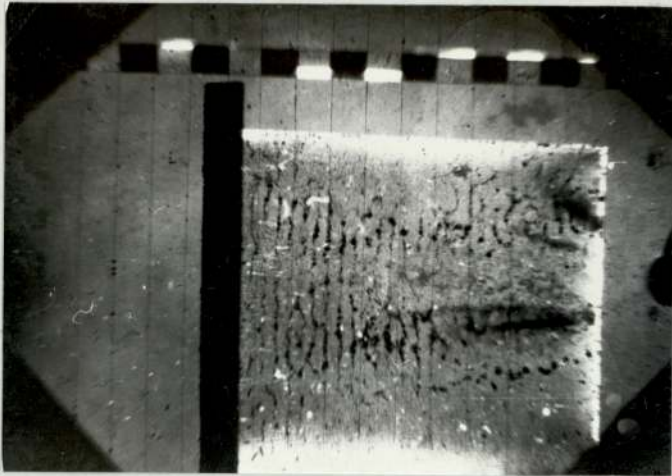
5.4.3 Interpretation of the display of a standing wave

The theoretical variations in light intensity, produced by both progressive and standing ultrasonic waves within a photoelastic material, have been presented in Fig 2.6. These predictions were found to agree with practice in the case of a standing wave, which was established by normal reflection from an aluminium plate. This plate was clamped vertically in the water tank, with one face in contact with one edge of an epoxy resin index layer, horizontally supported on the wire grid.

Fig 5.5(a) shows how a formation of bubbles appeared on the surface of the index layer with time, caused by dissolved gases coming out of solution under ultrasonic irradiation. The bubbles form along lines at which both the particle velocity q and the particle displacement ξ are zero within the standing wave.

The photoelastic display, produced by this standing wave, consisted of parallel light and dark bands, and it was found

(a)
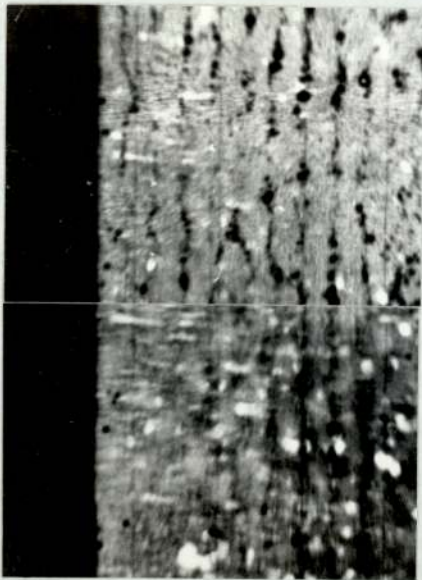
BUBBLES

(b)

PHOTOELASTIC
DISPLAY

FIGURE 5.5   Linking of the display of a standing wave with bubble
formation on an index layer

(a) a general view of the bubble formation

(b) bubbles and photoelastic display compared

that the positions of the dark bands coincided with the

lines along which the bubbles collected. This is shown

in Fig 5.5(b); a section of the display produced, and the

bubble formation, are compared. Although the photoelastic

display is not very clear, and did not appear right up

to the reflecting face, it will be seen that at the right

hand side of the photographs a match is obtained.

It is thus concluded that the theoretical predictions,

illustrated in Fig 2.6(b) are confirmed, a dark band of

the photoelastic display of a standing wave occurring at

positions at which ξ and q are both zero.

5.4.4 Interpretation of the displays of progressive waves

The photoelastic display wavelengths of the progressive ultrasonic

waves described (Section 5.4.1) have been seen to disagree

with theoretical predictions, one bright band appearing

per ultrasonic wavelength whereas theory predicts two. This

contradiction may be explained by a combination of

      (a)   a tendency for elliptical polarization of the

             incident illumination;

      (b)   a relatively weak photoelastic effect, produced

             by ultrasonics within index layers.

To understand this, consider the static experiment shown
in Fig 5.6. Plane-polarized light from the polarizer
passes through plate 1, containing a tensile strain of
such magnitude that elliptically polarized light results
on its far side; this light passes through another such
plate, plate 2, the strain in which may be either tensile
or compressional, but at roughly the same angle to the
polarizer, as its predecessor. The observer then views
the resultant transmitted light through an analyzer, crossed
with the polarizer.

With plate 2 absent, a nett transmission of light through
the system will occur; on plate 2's introduction, however,
the nett transmission will depend on whether the strain
within it is tensile or compressional. A steady increase
in tensile strain i.e. of the same type as that in plate 1,
will increase the transmitted intensity; a compressional
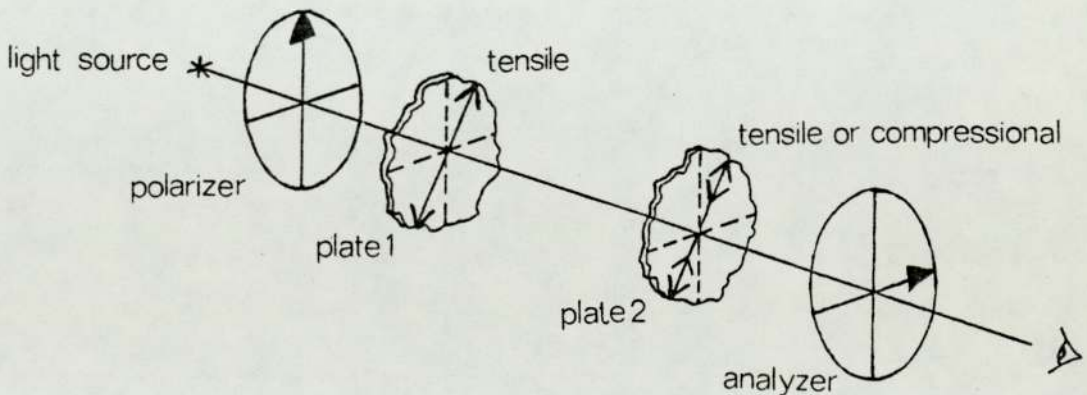strain, however, will cause it to decrease.

FIGURE 5.6   A static photoelastic experiment

These observations are explained by the fact that the sense
of rotation of the generally elliptically polarized light,
produced by a plane polarizer and strained plate, differs
with a tensile strain compared to a compressional one.

Analogy may now be made with the visualisation system,
involving the viewing of weak photoelastic effects within
index layers. The strain distribution within such a layer
will consist of alternating tensile and compressional
strains as an ultrasonic wave passes through it. By analogy
with the static experiment, one might expect the nett
photoelastic effect of a compressional or tensile strain to
differ, if the incident illumination contains a trace of
ellipticity and if the photoelastic effect within the index
layer is weak.

A slight ellipticity in the incident illumination will mean
that polarizer and analyzer, when crossed, will not produce
complete extinction; darkening or brightening of the display
could then occur at regions of either compression or
extension. The photoelastic display of an ultrasonic wave,
originally containing two bright bands per wavelength,
may now only contain one due to this imposed selectivity. It
should be noted that this process, if occurring may increase
the visibility of a display, by enhancing the contrast between
each band.

Ellipticity within the incident illumination may arise from

    (a)   non-perfect production of plane polarization by the polarizer and analyzer, either side of the layer;

    (b)   strains within the perspex laminations of these optical elements;

    (c)   static strain within the layer material,

all of which have been observed.

5.5   Anomalies within index layer displays

It has been indicated, in both Chapters 1 and 4, that various phenomena may reduce the validity of displays within index layers; these will include

    (a)   internal reflection;

    (b)   insufficient ultrasonic intensity within the layer;

    (c)   mode conversion;

    (d)   static strain within the layer.

It will be shown that the affect of the above may be minimised by attention to various layer properties.

5.5.1 <u>The effect of characteristic impedence</u>

The occurance of undesirable effects, arising from an
impedence mismatch between an index layer and water,
was highlighted by the use of glass as the layer material.
The characteristic impedence of glass is approximately
ten times that of water, its low attenuation of ultrasonics
assisting the formation of self-resonance.

Fig 5.7 shows the photoelastic pattern, produced by resonant
mode formation, within a 1.5mm thick glass sheet used
as an index layer. Modulation of the incident illumination
was not needed, as the effect was due to a standing
ultrasonic distribution. This pattern obviously bore no
relation to the ultrasonic field in the surrounding water,
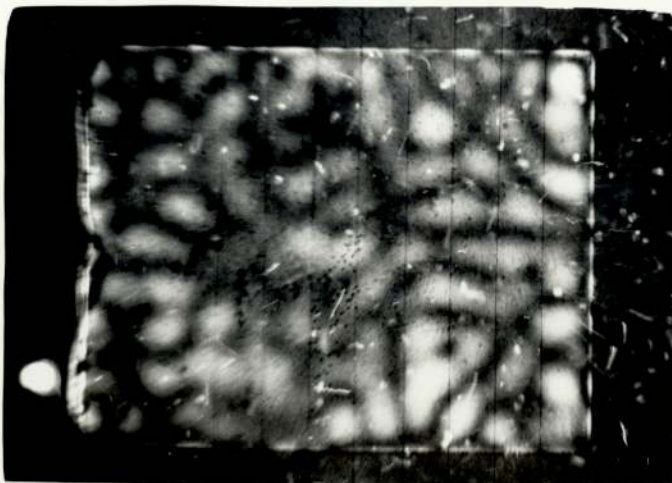and hence was anomolous.

FIGURE 5.7

Stroboscopic illumination enabled internal reflection within a similar glass sheet to be observed. Fig 5.8 shows a resultant photoelastic pattern. Parallel bands, extending across the sheet, were seen to reflect from its shorter edges, and return along their original path.

Both internal reflection and resonant mode formation will be minimised by ensuring that the characteristic impedence of the layer material is as close as possible to that of water.

The level of ultrasonic intensity within an index layer will also depend on characteristic impedence effects, a mismatch potentially causing an insufficient display visibility. Chapter 4 indicated that this effect might be highlighted around a given layer's edge, although at the frequencies used, it was shown that spreading of the ultrasonic field into the layer would cause this effect to occur over only a very limited region.

In practice, no regions of insufficient display visibility were observed around the edge of index layers, although as will be seen later, they may be masked by other effects.

5.5.2 <u>Mode conversion</u>

Mode conversion, as explained in Section 4.2, will be enhanced within index layers whose Poisson's ratio σ differs substantially

FIGURE 5.8   Internally reflected progressive waves in glass
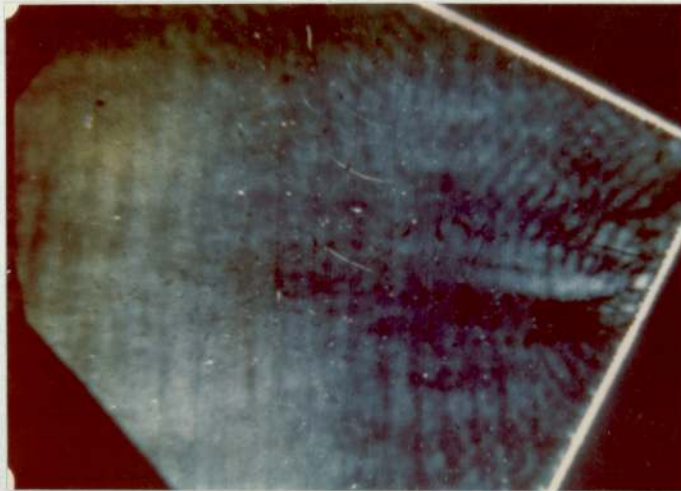

FIGURE 5.9   Shear and longitudinal waves in a polyester sheet

from 0.5, and which can readily support transverse waves.

Epoxy resins and polyesters are such materials, and mode
conversion within each was indeed seen. Fig 5.9 shows
both shear and longitudinal waves, displayed within a
polyester sheet; the former may be distinguished by their
shorter wavelength. The distinction is more clearly
seen in Fig 5.10, which shows the display produced within
an epoxy resin index layer, Fig 5.10(a), interpreted
with the aid of Fig 5.10(b). Shear waves, as explained
previously, are preferentially displayed in directions
parallel to the axes of light polarization; longitudinal
waves, conversely, are more visible in directions at 45° .
to these.

It has thus been shown that mode conversion, self-resonance
and internal reflection may all contribute towards an
anomolous display within index layers; use of materials whose
characteristic impedence is close to that of water, with
a Poisson's ratio close to 0.5, will minimize these effects.
Such a material, polyurethane rubber, has been described;
furthermore, the above effects have never been observed
within index layers fabricated from this material.
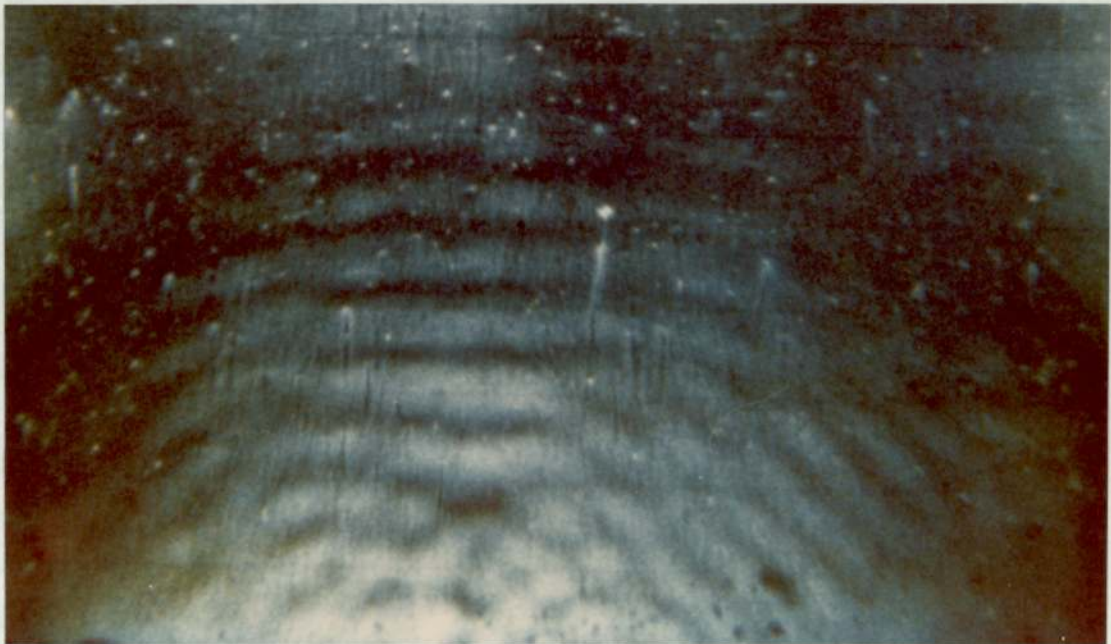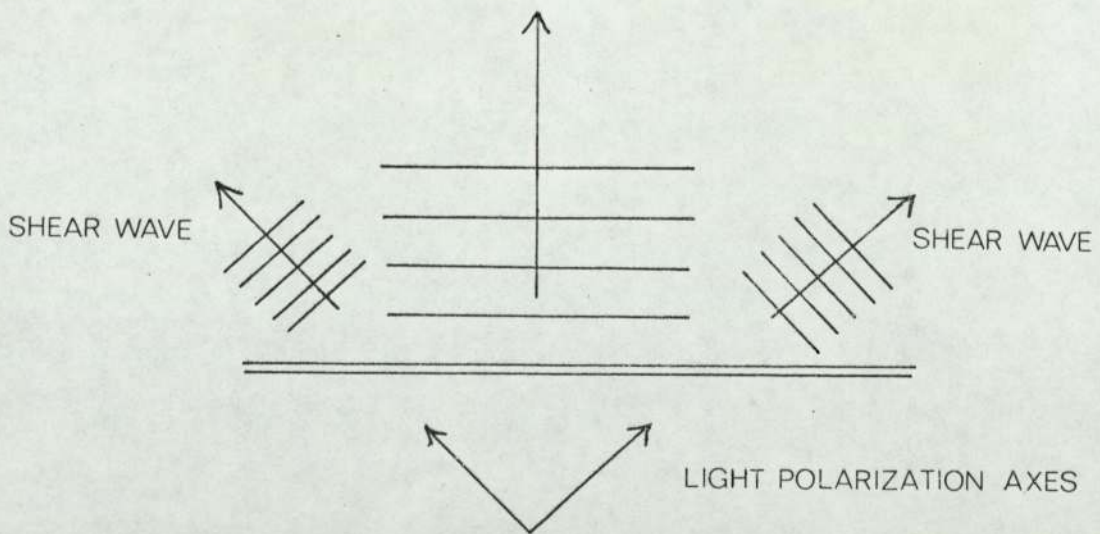
FIGURE 5.10   (a) The display produced within an epoxy sheet

(b) The preferential display directions of longitudinal and shear waves

5.5.3 <u>Additional artefacts within displays</u>

Static strains within index layers will cause bright patches
in the field of view which may even be enough to swamp
the display produced by the ultrasonic field.

Strain due to creep within index layers was minimised by the
use of the wire support grid described; annealing was used
in some cases where excessive initial strain existed.
Additional strains, arising from water absorption by index
layers to give so-called "time-edge" effects, were readily seen
in epoxy resins. Polyesters and polyurethane rubbers are,
however, virtually free of time edge effects.

An additional phenomenon, causing static strains within index
layers, was the absorption of heat from the ultrasonic field,
particularly in regions of high intensity. Fig 5.11
illustrates how a static photoelastic effect is gradually built
up within an index layer of columbia resin by such a process,
the layer's edge being against the face of the 200kHz transducer
previously described. In general, this effect takes a few
seconds to become established, but after this time any display
centred around such a display will be anomolous. It is thus
essential, in regions of high ultrasonic intensity, to make
any observations within the first few seconds of the establishment
of the ultrasonic field.

FIGURE 5.11   Heat-induced strain within a columbia resin index layer:
    (a) 5 seconds
    (b) 10 seconds
    (c) 30 seconds
    (d) 1 minute

Finally, it will be noticed that in some of the displays presented, small bright specks are evident, due to scattering, and hence depolarization, of the incident illumination by dust particles and gas bubbles in water. In the extended volumes of water used, these will be extremely difficult to remove, although the occurrence of bubble formation may be reduced by the use of de-gased water.

5.5.4 <u>Variation of displays with propagation direction</u>

The use of plane-polarized illumination, in the displays presented, means that longitudinal waves travelling in various directions will not be displayed to the same level of visibility; those travelling at 45° to the polarizer will be most visible, whereas those travelling parallel to it will not be displayed at all (Section 2.2.4).

This problem might be dealt with by any of the methods outlined in Section 2.2.2; the rotation of crossed polaroids in unison would, however, be inconvenient. The use of quarter-wave plates i.e. the illumination of index layers with circularly-polarized light was investigated, and found to be unsuitable. The main problem here was a decrease in the contrast of the displays produced; the quarter-wave plates used needed to be at least 20cm in diameter to cover the required field of view, and the only types obtainable which met this criterion were of fairly poor quality.

The use of a double-exposure technique was capable of producing the required results, but was time consuming and tedious; it was finally decided that sufficient information could be obtained by taking two independent photographs, with the polarizer and analyzer rotated in unison by 45° between each, effectively displaying all ultrasonic waves of interest. It should be mentioned that this inherent selectivity was found useful in some situations, e.g. it could effectively filter out angular reflections, from the side walls of the water tank, from the displays.

5.6 An application of the visualisation technique

The proposed visualisation technique will have the greatest application to the study of situations not easily dealt with theoretically; such a situation might arise, say, from the reflection of an irregular wave-front from an object of complicated shape.

To judge the usefulness of the technique in investigating such cases, it was applied to a well-known situation, reflection of a plane wave from a plane face, and the optimum approach determined.

Use of an index layer in investigating reflection from an obstacle can be made in one of two approaches; either the reflecting obstacle under investigation, such as a reflecting

(a)

layer

upper cylinder

lower cylinder

(b)

layer

single cylinder
through layer
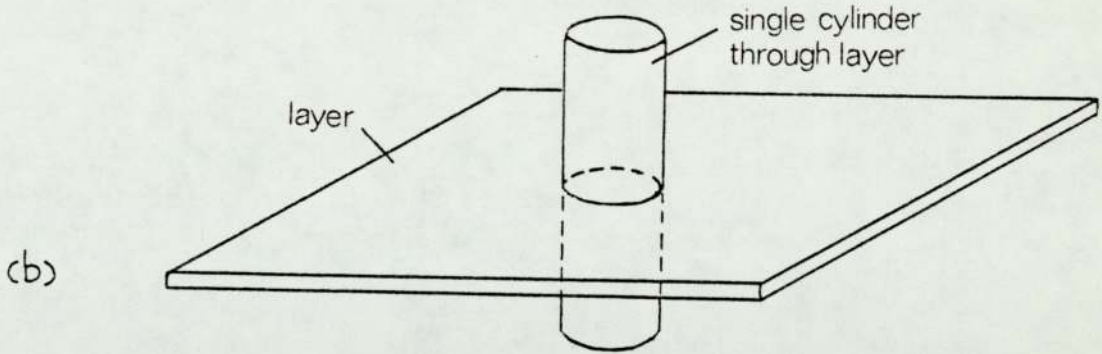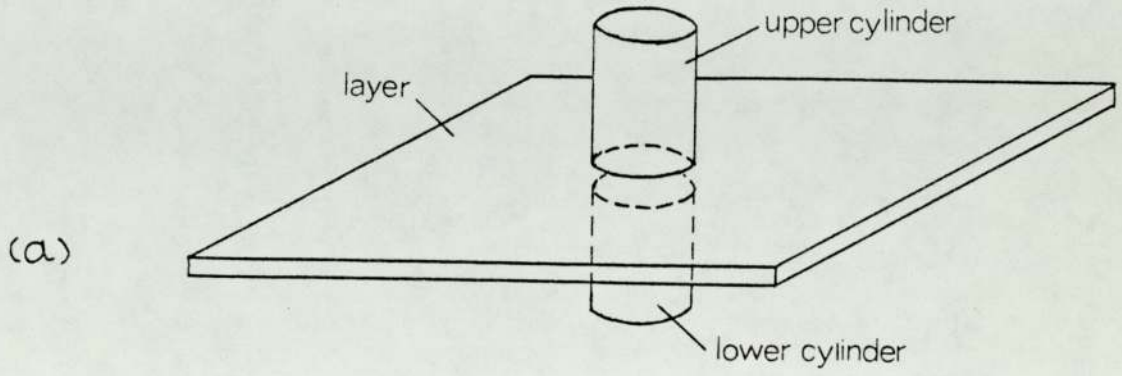
FIGURE 5.12 Use of an index layer in studying the effect of an obstacle;
(a) obstacle either side of layer
(b) single obstacle through layer

cylinder, is placed either side of the layer, as shown in Fig 5.12(a), or a single obstacle is placed through the layer, Fig 5.12(b). The latter implies that a suitable hole be made through the index layer to accommodate the obstacle, and this will be inconvenient for complicated obstacles; additionally, this process may introduce static strain into the material, especially round the cut edges.

No such drawbacks will occur with configuration(a); however, here there is a chance that ultrasonic intensity may continue within the index layer, through the reflecting obstacle, whereas in the real situation this will not occur.

Configuration(a) was examined by placing a plane aluminium plate either side of a polyurethane rubber index layer. The plates were at 45° to the incident wavefronts, and each was fitted with a rubber backing to minimize ultrasonic transmission.

The display produced under stroboscopic illumination is shown in Fig 5.13(b), and is compared to the display prior to the introduction of the obstacle, Fig 5.13(a). The polarizer and analyzer of the optical system had their axes in the directions shown, optimizing each display. It can be seen in Fig 5.13(b) that the incident ultrasonic wave is reflected by the plane obstacle with a suggestion of standing waves in front of the reflecting face. Also visible is a shadow region, behind the obstacle, in which no display can be seen. Thus
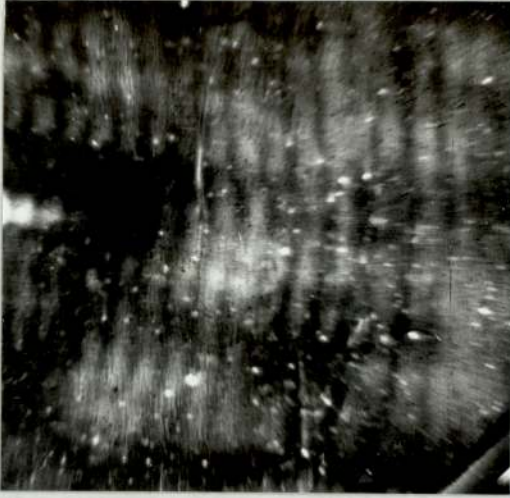
(a)
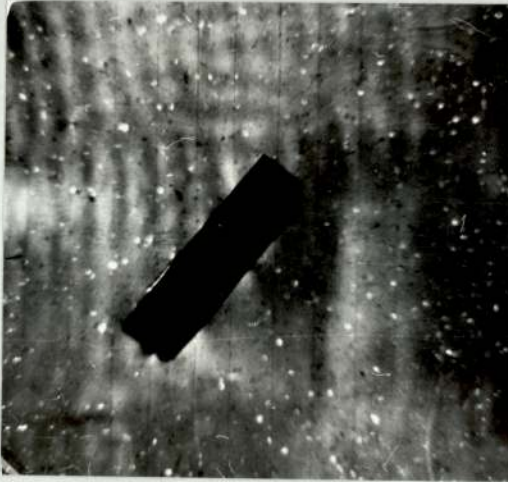
(b)
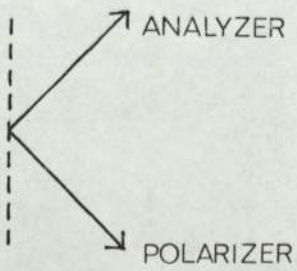
(c)

FIGURE 5.13   (a) display of initial distribution
(b) display after the insertion of the reflecting plate
(c) orientation of polarizer and analyzer in each case

(a)   the acoustic variations, within the index layer,
      are following those within the water either side
      of it;

(b)   despite the fact that the index layer continues
      through the obstacle, no display is produced
      immediately adjacent to the latter's back face.

Both these phenomena will be aided by attenuation within the
layer material.

It has thus been shown that the technique may be simply applied
to the investigation of the effect of an obstacle on a
progressive ultrasonic distribution; by simply moving the index
layer in a direction perpendicular to its face, the three-
dimensional resultant distribution may be determined.

5.7   Cinematography of moving displays

It has been described previously how the apparatus constructed
was able to provide static or moving photoelastic displays;
the former required equal light modulation and ultrasonic
frequencies, the latter a slight difference between the two.

Moving displays were successfully photographed by means
of Bolex 16mm cine camera, fitted with a wide angle lens.
This allowed the progress of a given distribution to be studied,
and diffraction, reflection and other phenomena to be permanently
recorded.

Various phenomena have been photographed in this way, and
an edited cine film of the more interesting cases has been
prepared and is available for presentation.

The contents of this film are now listed:

(a)   the effect of stroboscopy

A moving display of a 200kHz progressive ultrasonic wave is
shown, use being made of slightly different ultrasonic and
light modulation frequencies; the latter was achieved by use
of the circuit, incorporating a rotary potentiometer, which
was described in Section 3.7. Equal frequencies are then
produced, by stopping the rotation of the potentiometer, and
the display is seen to become stationary. Production of a
modulation frequency slightly greater than that of the
ultrasonics causes the display to move in the opposite direction
i.e. backwards.

In contrast, a standing wave is next displayed, under conditions
of steady illumination.

(b)   undesirable phenomena in index layer materials

Internal reflection within a glass sheet is demonstrated; this
phenomena is also seen in a polyester sheet, in which mode
conversion, with the production of both longitudinal and shear
waves, is clearly visible.

Mode conversion within an epoxy sheet is also presented.

Static strain within index layers is demonstrated by
two mechanisms. The time-edge effect, commonly observed
within epoxy sheets, is seen to swamp the display of
progressive waves at the layer's edge. In addition, the
production of heat within a columbia resin sheet is seen
to result in a gradual build-up of static strain with time;
this was produced by placing the sheet's edge up to the
face of a 200kHz transducer.

(c)   The use of polyurethane rubbers

Several shots of this material, in use as an index layer,
demonstrate how it has almost ideal acoustic properties; no
reflection at the edge of a sheet is seen, the photoelastic
display fills the whole area of the sheet, and there is no
time-edge. The extreme sensitivity of this material to stress
is also demonstrated.

(d)   propagating ultrasonic distributions

The use of the technique in displaying the effect of various
discontinuities, placed in the path of progressive ultrasonic
waves, is demonstrated; those presented are

(i)   the effect of a cylindar, 5λ in diameter, where λ

         is the ultrasonic wavelength;

(ii)   the effect of a cylindar 1λ in diameter

(iii)   reflection from a plane obstacle.

In addition, the radiated field of a 200kHz transducer, of

radius 3.5λ is shown; polyurethane rubber is used as the

layer material.

5.8   Preliminary conclusions

Photoelastic displays of progressive and standing ultrasonic

waves in liquids, at a frequency of 200kHz, have been presented;

this was achieved by illuminating a thin index layer of

photoelastic material with polarized light, either amplitude-

modulated for the study of progressive waves, or continuous

for the study of standing waves.

The displays of both types of wave were examined in various

layer materials, and it was judged desirable to use an

index layer

(a)   whose acoustic properties are close to those of water;

(b)   which is as thin as possible;

(c)   which has a Poisson's ratio close to 0.5,

        minimising mode conversion effects;

(d)   which exhibits attenuation to ultrasonics at the

        frequency concerned.

Polyurethane rubber was presented as a photoelastic material

with these properties, readily available in sheet form.

The photoelastic display wavelengths of progressive waves, produced within various polymer index layers, were found to be the same; additionally, the displays were seen not to fade with distance, as might be expected from attenuation within the layer material, and were seen to follow the acoustic variations within the surrounding liquid. These observations were seen to agree with previous theoretical considerations, which predicted an equilibrium wavenumber within the liquid and layer-media, with associated properties close to those normally expected within the liquid.

The photoelastic displays, produced within index layers, were successfully linked to variations in an acoustic parameter in the case of a standing wave. Discrepencies between photoelasticity and the displays of progressive waves were explained by a degree of elliptical polarization within the incident illumination.

CHAPTER SIX

A NEW APPROACH FOR THE THEORETICAL DETERMINATION OF TRANSDUCER
NEAR-FIELD RADIATION PATTERNS

6.1   Introduction

Chapter One has indicated that transducer radiation patterns

have been examined by a variety of theoretical techniques.

The detailed, three-dimensional nearfield pressure distributions

of such transducers have only been described in the case of

disc transducer in an infinite baffle (55, 62), the treatment

of other configurations being limited to descriptions in

the form of e.g. directivity functions (106).

The theory to be presented is designed so that it may be applied

to the evaluation of the nearfield pressure variations of

transducer configurations exhibiting axisymmetric cylindrical

symmetry. Variations in baffle size, ultrasonic frequency

and transducer dimensions may also be studied. The approach

is designed to be inherently simple in form, allowing the

convenient application of boundary conditions and its rapid

evaluation by computer techniques.

The above is achieved by expressing the solution to the

appropriate wave equation as a series with a finite number of

terms. This should not be confused with some other techniques,

which have approximated previously-derived expressions into such

a form; the theory to be presented deliberately uses a series

form from the outset.

6.2   Statement of the proposed approach

The approach to be described, as outlined above, involves
expressing the solution of the appropriate wave equation in
the form of a series. As all problems that will be dealt
with involve axisymmetric cylindrical symmetry, the equation
to which a solution is sought is:

$$\frac{1}{r} \cdot \frac{\partial}{\partial r} (r \frac{\partial \emptyset}{\partial r}) + \frac{\partial^2 \emptyset}{\partial z^2} + k^2 \emptyset = 0 \qquad (6.1)$$

which is the Helmholtz equation expressed in cylindrical polar
coordinates (r, z, θ). Here, ∅ is the scalar velocity
potential within the irradiated medium, z is an axial coordinate,
r is a radial coordinate and variation with the angle θ is zero.
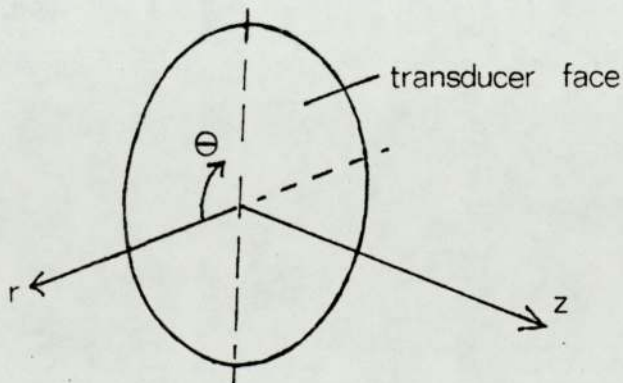The coordinate system used is shown in Fig 6.1.

FIGURE 6.1   The coordinate system

It was outlined in the Introduction that a solution to
equation (6.1) is

$$\emptyset = \frac{A\,J_o(C.r)}{j\sqrt{k^2-c^2}} \ e^{\,j\sqrt{k^2-c^2}\,.\,z} \qquad (6.2)$$

where $J_o(x)$ is a Bessel function of the first kind and zero
order, k is a circular wavenumber, A and C are coefficients
and harmonic time dependence has been assumed. It should be
noted that solutions in Y_o, i.e. containing Bessel functions
of the second kind, are not applicable as $Y_o(0)$ is infinite. .
Solutions such as that shown in (6.2) are well known, and
have been used previously in integral transform approaches(64).

Equation (6.2) represents a wave, travelling in the z
direction, of the form

$$\emptyset = Be^{\,j(bz-\omega t)}$$

where $\qquad B = \dfrac{A\,J_o(C.r)}{jb} \quad$ and $\quad b = \sqrt{k^2-c^2}$

Suppose now that expressions of the type shown in (6.2) are
used as the separate terms in a new equation for $\emptyset$, which is
in the form of an infinite series; we may write this new
expression as

$$\phi = \sum_{n=1}^{n=\infty} \frac{A_n J_o (C_n r)}{j\sqrt{k^2 - C_n^2}} e^{j\sqrt{k^2 - C_n^2} \cdot Z} \qquad (6.3)$$

Each term of (6.3) will be a solution of the wave equation

of interest, (6.1), and will be characterised by its own value

of A_n and C_n. Equation (6.3) is thus a solution of (6.1).

Provided it can be shown that this series is sufficiently rapidly

convergent, a finite number of terms m may be used, which will

lead to an expression for P of the form

$$P = k \rho c \sum_{n=1}^{n=m} \frac{A_n J_o (C_n r)}{\sqrt{k^2 - C_n^2}} e^{j\sqrt{k^2 - C_n^2} \cdot Z} \qquad (6.4)$$

where $P = - \rho \cdot \dfrac{\partial \phi}{\partial t}$

In principle, equation (6.4) may be used to obtain the value of

P at various values of r and z within the irradiated medium,

provided the values of A_n and C_n are known for each value of n, i.e.

for each term. In practice, these values will be dictated by

the boundary conditions existing over the plane containing the

transducer face i.e. $Z = 0$, and these conditions will vary between

various transducer configurations.

6.3 Preliminary discussion

Equation (6.4) is in the form of a series of Bessel functions,

which will have different properties depending on the value of

C_n initially chosen for each term. These types of series have been well investigated; if the C_n's are chosen so that $J_o(C_n) = 0$, equation (6.4) is known as a Fourier-Bessel series. This form was rejected, as the expression for $\emptyset$ will always go to zero at $r = 1$, which is not realistic physically.

If, however, the C_n's are taken as integers, (6.4) is known as a Schlölmilch series, on which no such restrictions exist. This type of series, however, is only normally valid and convergent within the range $r = 0$ to π (107).

It is obviously preferable that equation (6.4) be valid and convergent over more than this range; in fact is is required to be so between $r = 0$ and infinity. It will be shown in Section 6.5 that, by consideration of an additional technique, the boundary conditions existing in each case may be applied over the whole plane $Z = 0$, leading to an expression for $\emptyset$ which can be considered adequately valid and convergent to infinity in r.

An additional point of concern is that the expression normally used to derive a value of A_n for a particular C_n in a Schlölmilch series, does not allow the application of mixed (Cauchy) boundary conditions over the plane $Z = 0$; this would be needed in the case of finite baffle and unbaffled configurations.

The additional technique just mentioned is capable of

applying this type of boundary condition to a series type

of solution. It involves fitting either the pressure P or

any other derivative of $\emptyset$ to a specific value in r over the

plane Z = 0, and hence finding the corresponding values

of A_n and C_n for each term from a simultaneous equation thus

formed; (6.4) may then be used to plot the radiated pressure

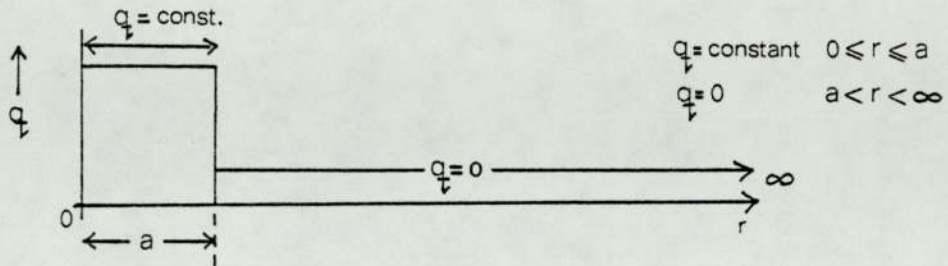distributions of various transducer configurations.

6.4   The boundary conditions

The theory is to be used to study the radiated field of various

ultrasonic transducers, and the boundary conditions to be

applied will exist over the plane containing the transducer

face, the Z = 0 plane.

Fig 6.2 shows the boundary conditions, existing over this plane,

for various transducer configurations, and it is seen that they

involve the definition of either the pressure P or the normal

particle velocity q_t. In all cases, r = 0 represents the centre

of the disc, the distribution over the plane Z = 0 being obtained

by rotating the sections shown through 360° about the r = 0

axis.
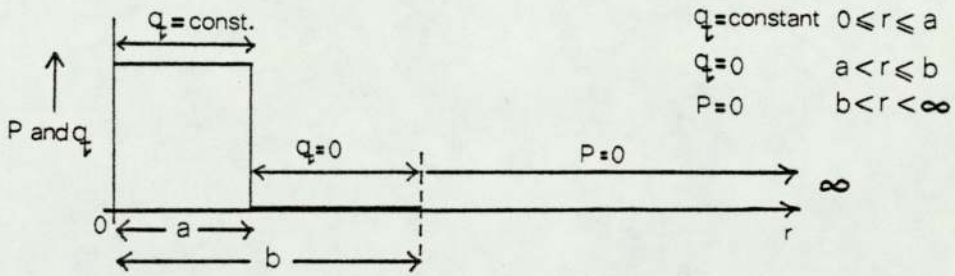

The transducer is assumed to be a disc, the whole front plane

of which is vibrating cophasially, and thus q_t will be constant

(a) <u>INFINITE BAFFLE</u>

q = const.

q = constant $0 \leqslant r \leqslant a$
$q = 0$ $a < r < \infty$

$q = 0$

∞

r

$\leftarrow a \rightarrow$

(b) <u>FINITE BAFFLE</u>

disc radius = a
baffle radius = b

q = const.

q = constant $0 \leqslant r \leqslant a$
$q = 0$ $a < r \leqslant b$
$P = 0$ $b < r < \infty$

P and q

$q = 0$ $P = 0$

∞

r

$\leftarrow a \rightarrow$
$\leftarrow b \rightarrow$

(c) <u>ZERO BAFFLE</u>

q = const.

q = constant $0 \leqslant r \leqslant a$
$P = 0$ $a < r < \infty$

P and q

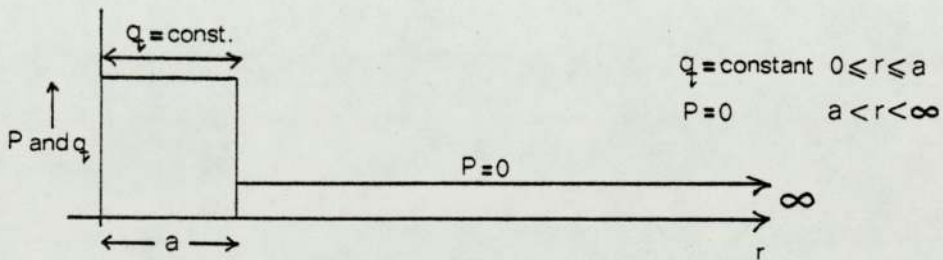$P = 0$

∞

r

$\leftarrow a \rightarrow$

<u>FIGURE 6.2</u>   The boundary conditions, at z=0, for various transducer
configurations

over the transducer face. The baffle is treated as being

a perfectly reflecting boundary; thus over the regions

at which a baffle exists, $q_t = \dfrac{\partial \emptyset}{\partial Z} = 0$

The region not containing the transducer or any baffle,

on the $Z = 0$ plane, will be characterised by the boundary

condition $P = 0$. This arises from the antisymmetric

pressure distribution either side of the $Z = 0$ plane, and

assumes that the rear transducer face vibrates 180° out of

phase with respect to the front face. It should be noted

that a thickness vibration of the transducer is equivalent

to the existence of an infinite baffle at the $Z = 0$ plane.

6.5   The application of boundary conditions over the plane Z = 0

The use of equation (6.4) to plot the radiated field of various

transducer configurations will depend on the successful

application of boundary conditions, outlined in Fig 6.2, over

the plane $Z = 0$.

From the equation (6.3),

$$q_t = \frac{\partial \emptyset}{\partial z} = \sum_{n=1}^{n=m} A_n J_o (C_n r) e^{j\sqrt{k^2 - C_n^2} \cdot Z} \qquad (6.5)$$

whereas the expression for P was

$$P = k \rho c \sum_{n=1}^{n=m} \frac{A_n J_o (C_n r)}{\sqrt{k^2 - C_n^2}} e^{j \sqrt{k^2 - C_n^2} \cdot Z} \qquad (6.4)$$

At the plane $Z = 0$, these expressions reduce to

$$q = \sum_{n=1}^{n=m} A_n J_o (c_n r) \qquad (6.6)$$

$$P = k \rho c \sum_{n=1}^{n=m} \frac{A_n J_o (C_n r)}{\sqrt{k^2 - C_n^2}} \qquad (6.7)$$

Both (6.6) and (6.7) may be treated as a Schlölmilch series
if the C_n's are integers i.e. if $C_1 = 1$, $C_2 = 2$ etc.

Consider now the case of the infinitely baffled disc. Here,
q is the only parameter defined over the plane $Z = 0$, and thus
equation (6.6) is the only one to be applied. The values of A_n
required could be found from the well-established expression
(107) for the coefficients of a Schlölmilch series, dictated
by the distribution of q; the expression is, however, in the
form of a double integral, and is complicated in itself.

Additionally, use of this expression for finite baffled or
un-baffled configurations is not possible, as this would require
the simultaneous solution of two double-integrals, obtained by
applying the expression to both (6.6) and (6.7) respectively.

Bearing the above difficulties in mind, an alternative approach
to the application of the relevant boundary conditions, existing
in each case, is desirable; such an approach will now be
described.

6.5.1 The simultaneous equation method

This approach involves fitting equations (6.6) and (6.7)
to a given magnitude at a given value of r on the plane Z = 0,
the fitting being repeated at regular intervals within the
range

$$0 \leqslant |r| < \pi$$

i.e. within the range of validity normally ascribed to a
Schlölmilch series. The effectively sets up m simultaneous
equations with m terms, m being the number of points fitted;
the A_n's and C_n's may then be obtained by solving this set
of simultaneous equations, conveniently achieved by a computer.

It might at first be thought that, by this process, the
boundary conditions are only met within the stated defined range;
it will be shown in the next section, however, that by a
suitable scaling process, they can be effectively applied to

infinity in the r direction.

The beauty of this method is that it is not restricted to fitting either P or q_t only to a required distribution at $Z = 0$; equation (6.6) or (6.7), or both, may be fitted to a specific magnitude at a given value of r within the defined range, thus allowing the A_n's and C_n's to be obtained under either Neumann (q_t only defined), Dirichlet (P only) or Cauchy (P and q_t) boundary conditions.

The proposed method of applying the boundary conditions is thus a very powerful technique, allowing all three types of boundary conditions to be applied quickly and simply; the result is that problems involving a wide range of baffle dimensions can be conveniently studied.

Let us now examine the simultaneous equation technique in greater detail by considering an example to be met in practice i.e. that of a vibrating unbaffled disc, of radius a. The boundary conditions that exist over the plane $Z = 0$, containing the transducer face, will be, as in Fig 6.2,

$$q_t = \text{constant (unity say)} \qquad 0 \leqslant r \leqslant a$$
$$P = 0 \qquad a < r < \infty$$

Suppose now 32 terms are chosen for the series representing P (equation (6.4)) and q_t (equation (6.5)) i.e. m = 32 in each,

and let the distribution be appropriately scaled so that

all regions of immediate interest around the disc are within

the range

$$0 \leqslant |r| < \pi$$

as shown in Fig 6.3. Equally spaced values of r within this

range are then chosen; these will be the values at which

P and q_t will be fitted to the required distribution, and in

the case shown they have been chosen to be 0.1 units apart

i.e. at the positions r = 0, 0.1, 0.2 .... 3.1. 10 points have

been distributed over the disc radius a; the remaining 22

points will be evenly distributed over the region at which P

is to be zero.

The expressions for q_t and P are now fixed at these chosen points

in accordance with stated boundary conditions i.e. equation

(6.6) is equated to unity at r = 0, 0.1, 0.2 ...0.9,

and equation (6.7) to zero at r = 1.0, 1.1, 1.2 .... 3.1. The

result is the set of simultaneous equations shown in Fig 6.4.

These are then solved by computer techniques to obtain the

coefficients A_1-A_{32}, corresponding to the values for C_1-C_{32},

normally the integers 1-32. The values for A_1-A_{32}, arising

from such a procedure, are presented in Table 6.1.

These values for the A_n's may then be substituted into equation

(6.4), the series for P, to allow the predicted pressure

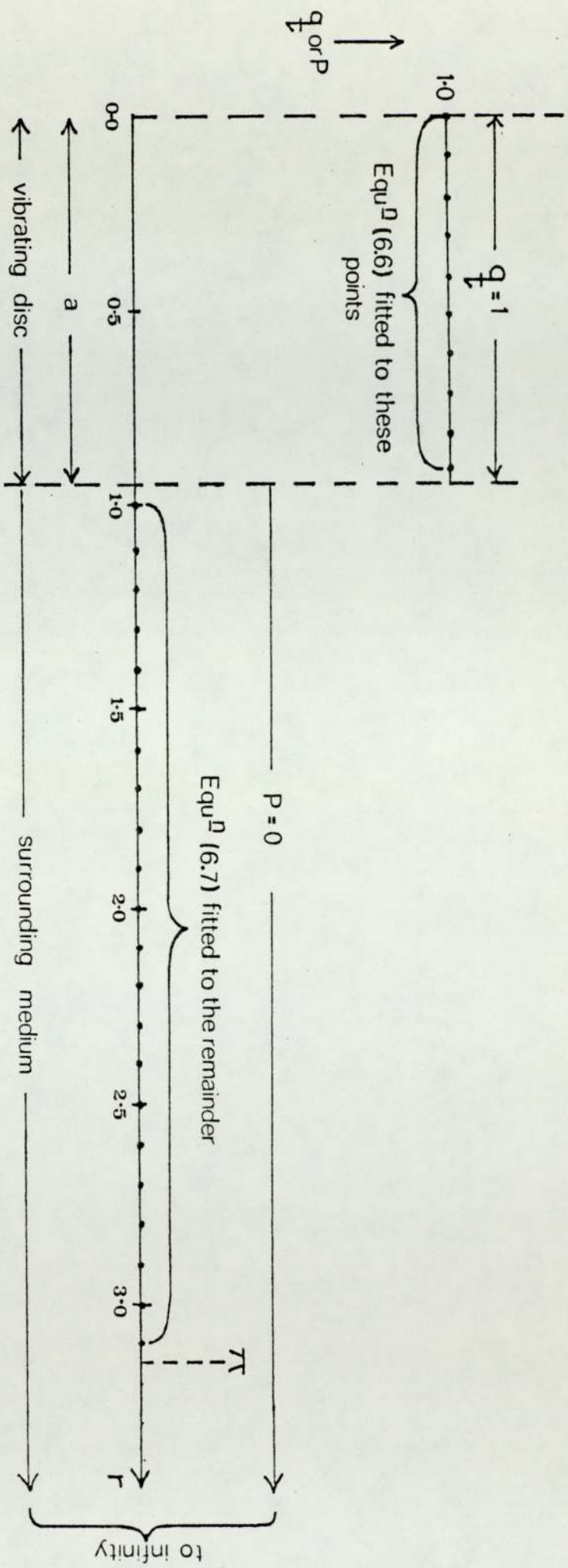variations of the radiated field to be studied with both r and z.

q or P →

q = 1

1·0

Equⁿ (6.6) fitted to these points

0·0   0·5   1·0
         a
← vibrating disc →

P = 0

Equⁿ (6.7) fitted to the remainder

1·0   1·5   2·0   2·5   3·0

π

r

← surrounding medium →

to infinity

FIGURE 6.3   The fitting of equations (6.5) and (6.4) to the required distribution

$$A_1 J_0(C_1.0) + A_2 J_0(C_2.0) + \text{\textemdash\textemdash} A_{32} J_0(C_{32}.0) = 1$$

$$A_1 J_0(C_1.0\cdot1) + A_2 J_0(C_2.0\cdot1) + \text{\textemdash\textemdash} A_{32} J_0(C_{32}.0\cdot1) = 1$$

$$\vdots$$

$$A_1 J_0(C_1.0\cdot9) + A_2 J_0(C_2.0\cdot9) + \text{\textemdash\textemdash} A_{32} J_0(C_{32}.0\cdot9) = 1$$

$$\left.\right\} q=1 , r = 0-0\cdot9$$

and

$$\frac{A_1 J_0(C_1.1\cdot0)}{\sqrt{k^2-C_1^2}} + \frac{A_2 J_0(C_2.1\cdot0)}{\sqrt{k^2-C_2^2}} + \text{\textemdash\textemdash} \frac{A_{32} J_0(C_{32}.1\cdot0)}{\sqrt{k^2-C_{32}^2}} = 0$$

$$\frac{A_1 J_0(C_1.1\cdot1)}{\sqrt{k^2-C_1^2}} + \frac{A_2 J_0(C_2.1\cdot1)}{\sqrt{k^2-C_2^2}} + \text{\textemdash\textemdash} \frac{A_{32} J_0(C_{32}.1\cdot1)}{\sqrt{k^2-C_{32}^2}} = 0$$

$$\vdots$$

$$\frac{A_1 J_0(C_1.3\cdot1)}{\sqrt{k^2-C_1^2}} + \frac{A_2 J_0(C_2.3\cdot1)}{\sqrt{k^2-C_2^2}} + \text{\textemdash\textemdash} \frac{A_{32} J_0(C_{32}.3\cdot1)}{\sqrt{k^2-C_{32}^2}} = 0$$

$$\left.\right\} P=0 . r = 1\cdot0-3\cdot1$$

FIGURE 6.4   The set of simultaneous equations resulting from the fitting shown in Fig.6.3

C_n	A_n	C_n	A_n	C_n	A_n
1	0·4759	12	−0·2860	23	0·2032
2	0·4602	13	−0·1179	24	−0·0118
3	0·4680	14	−0·1084	25	−0·0737
4	−0·0633	15	0·2206	26	−0·1950
5	−0·1756	16	0·1282	27	−0·0516
6	−0·4010	17	0·1586	28	0·0361
7	−0·0349	18	−0·1511	29	0·1559
8	0·0486	19	−0·1226	30	0·0977
9	0·3454	20	−0·1909	31	−0·0334
10	0·0886	21	0·0798	32	−0·0928
11	0·0403	22	0·1029		

TABLE 6.1

The resulting coefficients

6.5.2 <u>Optimisation of the application of boundary conditions</u>

The simultaneous equation method applies boundary conditions
within the defined range

$$0 \leqslant |r| < \pi$$

The degree of correlation obtained between the required
distribution and that predicted by equations (6.6) and (6.7),
after the application of boundary conditions, will now be
examined, bearing in mind that the required distribution
extends to infinity in r.

The correlation obtained is seen to depend on various factors,
namely

(a)   the number of terms used in each series, which
       is the same as the number of points fitted to the
       required distribution at $Z = 0$;

(b)   the scaling factor used in the fitting process.

Consider an infinitely baffled disc; the boundary conditions,
shown in Fig 6.2, define q only at the plane $Z = 0$. Suppose
now that the transducer face, of radius a, is suitably scaled
so that it occupies a quarter of the defined range i.e.
approximately $\pi/4$; a region of infinite baffle will then extend
from approximately $\pi/4$ to π , within the defined range.

Fig 6.5 (a) shows the computed distribution in q over the plane Z = 0, predicted by equation (6.6), as a result of fitting the required distribution to 20 and 105 points respectively within the defined range. Several phenomena are evident:

> (i)   the computed distribution becomes closer to
>   that required with a greater number of terms
>   i.e. with more points fitted, within the defined
>   range;
>
> (ii)   an effect, analogous to the Gibb's Phemonenon
>   in Fourier Series(108), is occuring;
>
> (iii)   a discontiniuty exists at $r = \pi$, beyond which
>   the computed distribution does not obey the
>   prescribed boundary conditions.

The phenomenon in (ii) above affects the representation of the discontinuity at the edge of the piston, and will not be removed completely even with the use of an infinite number of terms; the boundary conditions will thus not be applied rigorously over this limited region, although they will be applied to a greater accuracy over the remainder of the plane Z = 0. The maximum deviation from the prescribed boundary conditions, due to this effect, has been estimated at 10%.

(iii) may be minimised by the use of a suitable scaling process i.e. the section of boundary conditions, required to extend

to infinity in r, is caused to occupy as great a part of
the defined range, up to $r = \pi$, as possible; the dis-
continuity is then caused to become less prominent. Fig 6.5(b)
shows the distribution computed from equation (6.6) when
the transducer radius a occupies approximately a tenth
of the defined range only; it will be seen that the dis-
continuity has been reduced to an acceptable level, and that
the distribution beyond $r = \pi$ shown remains a good
approximation to $q = 0$.

Plots in the r direction have confirmed that q remains close
to zero as r increases beyond π ; this is expected, as $J_o(C_n r)$
tends to zero as r becomes large. This latter tendency also
agrees with the physical situation, P and q tending to zero
at large values of r.

The application of mixed boundary conditions, as in the case of
finite baffled or unbaffled pistons, follows the same trends,
a better representation resulting from a greater number of
terms and a suitable scaling process e.g. Fig 6.6 shows the
computed distribution of q and P over the plane $Z = 0$ for an
unbaffled disc. The boundary conditions, shown in Fig 6.2,
are seen to be met, within the limitations of the previous
case.

Thus, by increasing the number of fitted points and suitably
scaling the required distribution, the boundary conditions in
each case may be applied to obtain the values of A_n for each
value of n, which may then be used in equation (6.4) to plot
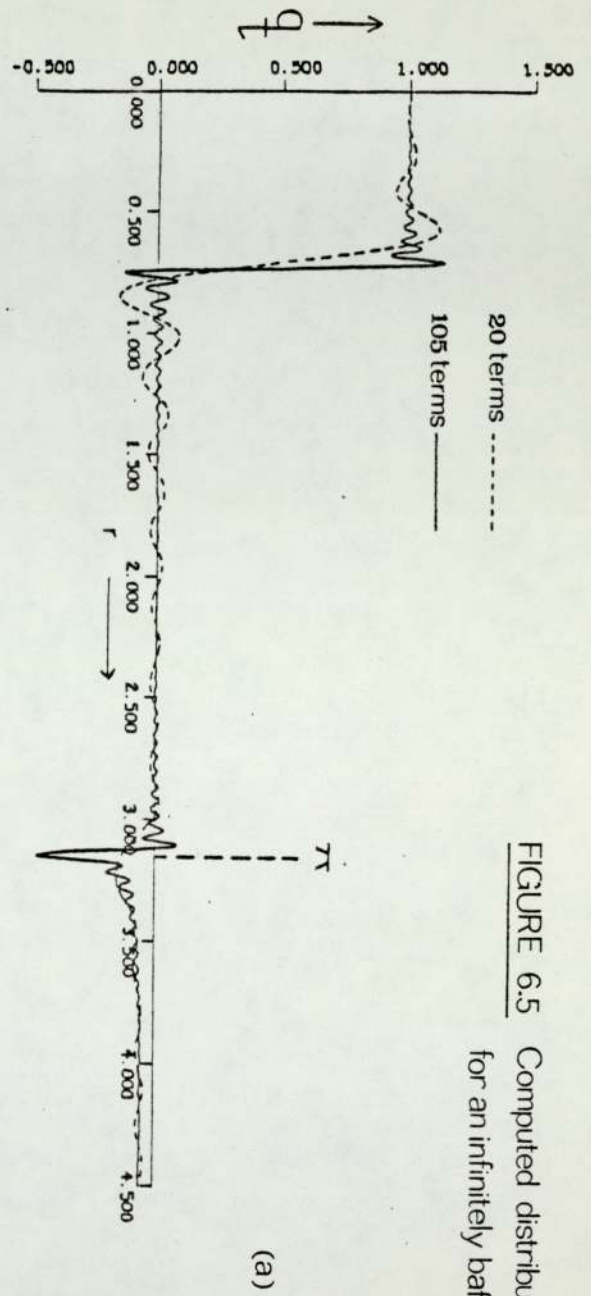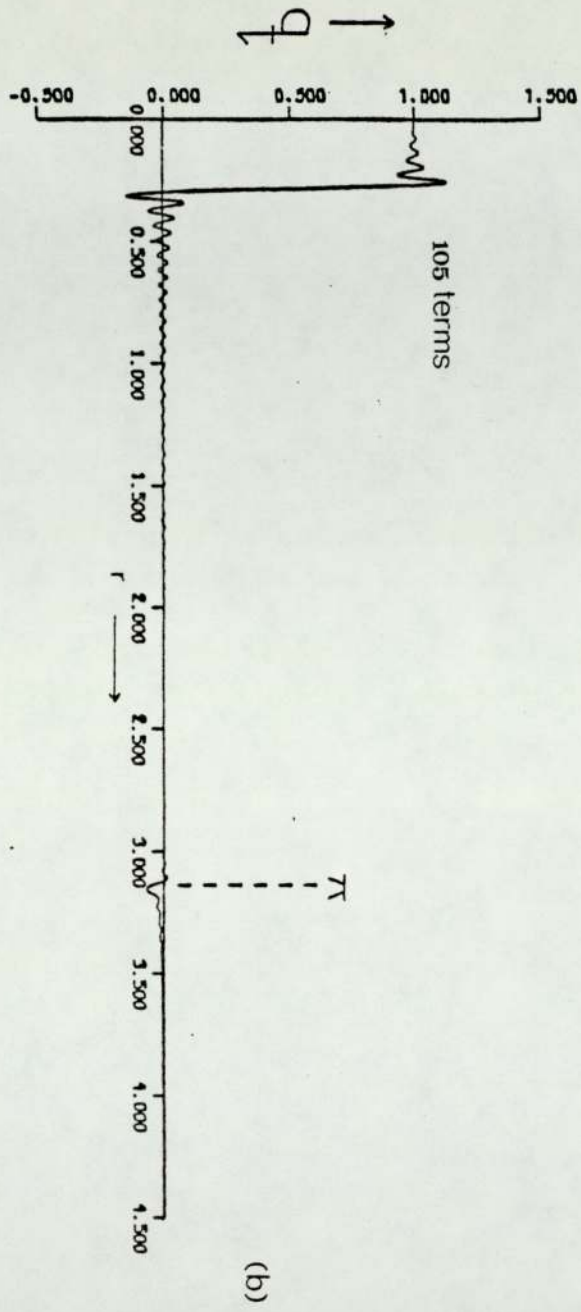
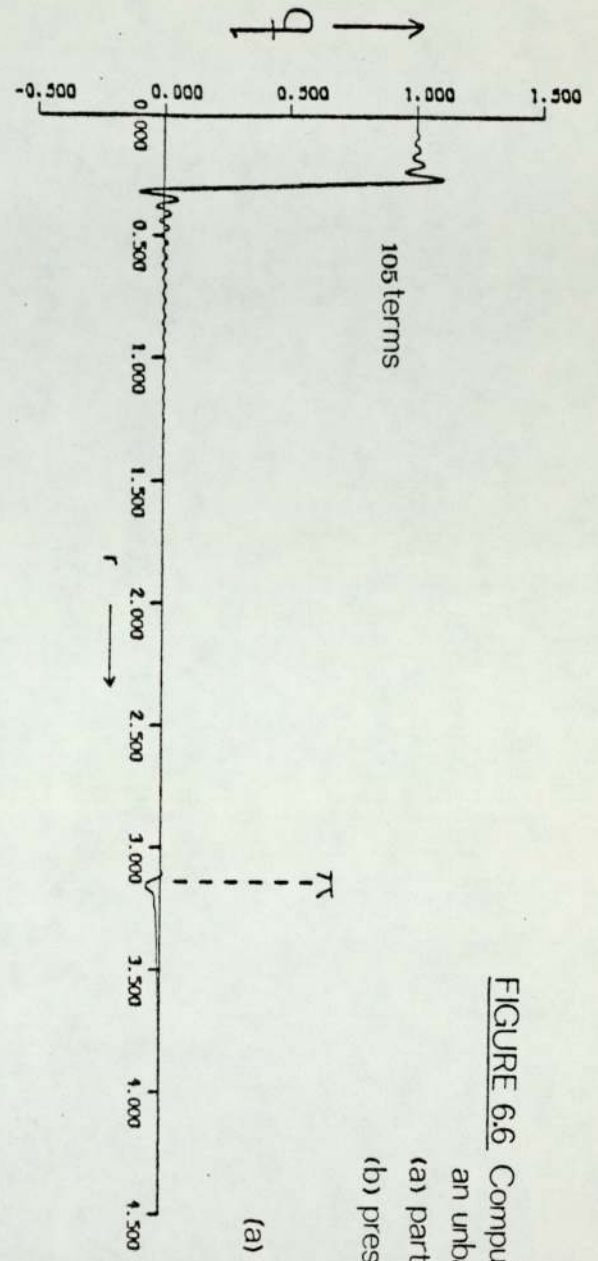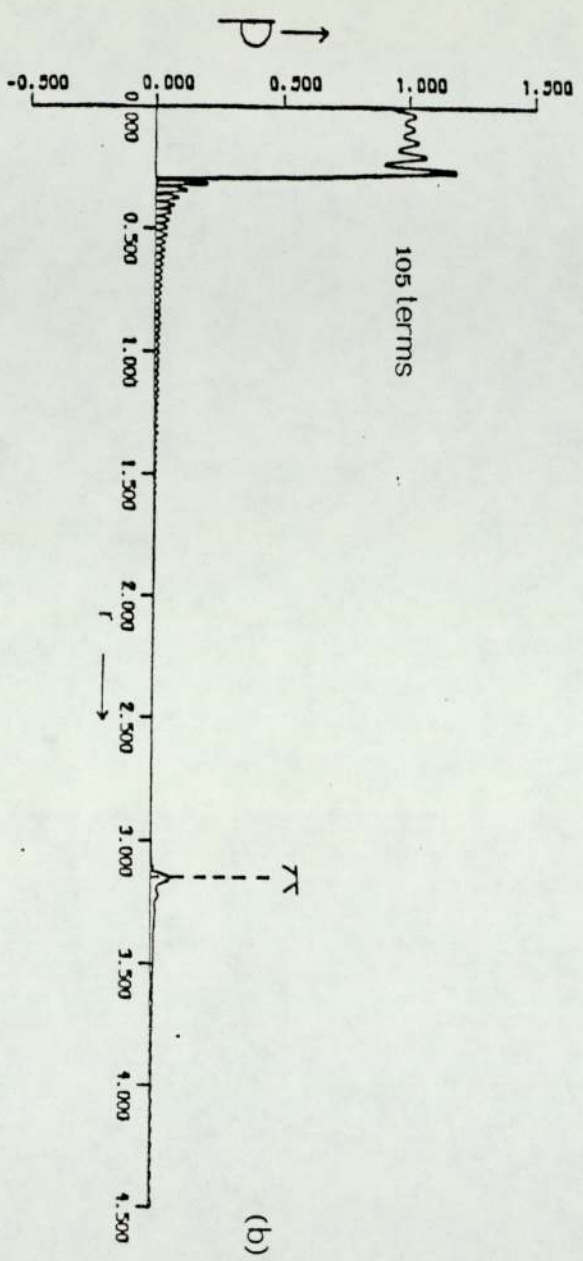FIGURE 6.5 Computed distributions in particle velocity at z=0 for an infinitely baffled disc

FIGURE 6.6 Computed distributions at z=0 for
an unbaffled disc
(a) particle velocity
(b) pressure

the predicted pressure variations within the irradiated
medium.

6.6   Further considerations

6.6.1 The respective values of k and C_n

The expression for P in the acoustic field, equation (6.4),
contains the circular wavenumber k, allowing the effect of a
change in ultrasonic frequency to be studied; the higher the
ultrasonic frequency, the larger k becomes.

Inspection of equation (6.4) shows that for any terms at
which $k^2 = C_n^2$ i.e. if k is any integer up to an including
the number of terms in the series, a discontinuity will
result; the $(k^2-C_n^2)^{\frac{1}{2}}$ term will go to infinity, and the
exponential term will become unity. Further, if at any stage
k is less than any value of C_n, $(k^2-C_n^2)^{\frac{1}{2}}$ becomes imaginary,
and the exponential term becomes simply

$$e^{-\sqrt{C_n^2-k^2} \cdot z} ;$$

the resultant expression is no longer a wave, but is solely
an attenuating term.

These occurrences may be avoided by ensuring that in all cases the
value of k exceeds the integer representing the number of terms
in the series. It is found that this latter requirement is met
by scaling the disc area to be as small as possible within the

defined range $0 - \pi$, and this is compatible with the

optimum application of boundary conditions, as described

in the previous section. It must be stated, however, that

this process cannot continue indefinitely, and a practical

limit is reached at which, with the number of terms

available, the radius of the disc can be reduced no further.

It is found that this limit occurs around the $a = \lambda$ region, i.e.

when the radius of the disc is comparable to the ultrasonic

wavelength in the irradiated medium.

Thus, the technique in its present state is unable to study

ultrasonic frequencies which are lower than this latter limit;

frequencies higher than this present no problem. This

lower limit is not thought to be too serious, as transducers

of radii less than one ultrasonic wavelength are not commonly

used.

6.6.2 Application to computation

In Section 6.5.2, the distribution predicted by equations

(6.6) and (6.7) were compared to the prescribed boundary

conditions by computer evaluation and graphical techniques.

These equations are not particularly complicated, and their

evaluation is not too difficult. The use of equations (6.5)

and (6.4), to plot the variations in P and q respectively

away from the plane $Z = 0$ requires a further adaptation to

computer techniques, because of the additional exponential terms.

Equations (6.4) and (6.5) have been written previously in
complex notation for compactness, but these must be expressed
in terms of separate real and imaginary terms before they
can be dealt with by a computer. Consider, as an example,
equation (6.4), which may be written as

$$p = k \; \rho \; c \sum_{n=1}^{n=m} A_n J_o(C_n r) \left[\cos \; (k^2 - C_n^2)^{\frac{1}{2}} Z + j \sin (k^2 - C_n^2)^{\frac{1}{2}} Z \right] \quad (6.8)$$

Equation (6.8) may, in turn, be split up into its real and
imaginary parts P_r and P_i respectively; the magnitude of
P will then be given by

$$|P| = (P_r^2 + P_i^2)^{\frac{1}{2}}$$

A similar process may be applied to the computer evaluation of
q_t for any value of r and z.

The above assumes that in all cases, k is greater than the value
of C_n in each term of the series, following the considerations

of the previous section. In practice, if the wavenumber

k is chosen so that at any time a value of C_n becomes

greater than k, it is found that inconsistent results are

obtained.

6.6.3 The convergence of the series used

It is necessary to show that equation (6.4) is a convergent

series, before it is used to plot the radiated pressure

distribution of various transducers.

One requirement for convergence may be stated as:

For a series $\displaystyle\sum_{n=1}^{\infty} U_n$ to be convergent,

$$\lim_{n \to \infty} U_n = 0$$

Equation (6.4) is seen to meet this requirement. As $n \to \infty$

$C_n \to \infty$; thus, $J_o(C_n r) \to 0$ for a given value of r.

In addition, $(k^2 - C_n^2)^{\frac{1}{2}} = j(C_n^2 - k^2)^{\frac{1}{2}}$ if $C_n > k$; thus as $n \to \infty$,

$$e^{j\sqrt{k^2 - C_n^2}} \to e^{-\infty} \quad \text{and} \quad \frac{1}{\sqrt{k^2 - C_n^2}} \to \frac{1}{j.\infty}$$

and the expression for P tends to zero as required.

This convergence is confirmed in Fig 6.5(a), a better
representation of the required distribution arising from
an increased number of terms in the series.

It must now be shown that a sufficient number of terms are
taken in the series, so that the predicted distribution is
a close approximation to that resulting from an infinite
number of terms. This may be achieved by steadily increasing
the number of terms in the series, and finding the stage at
which a further increase produces little change in the
predicted value of P at a point.

Consider first the case of an infinitely-baffled disc, of
radius 5 λ , λ being the ultrasonic wavelength, and let us
examine the predicted nearfield axial distribution. Fig 6.7 shows
the computed axial distributions, predicted by equation (6.4)
for 80, 105 and 175 terms in its series. It can be seen that
increasing the number of terms from 105 to 175 makes little
difference, whereas using less than 105 causes the predicted
distribution to be markedly different; it may thus be concluded
that, over the region presented, the series is sufficiently
convergent that 105 terms will predict a distribution which
is a good approximation to that predicted by an infinite series.

The convergence of equation (6.4) for the nearfield axial
pressure distributions of other transducer configurations,
with a = 5 λ , is seen to follow this trend, 105 terms in the
series being found adequate in each case. Convergence of the
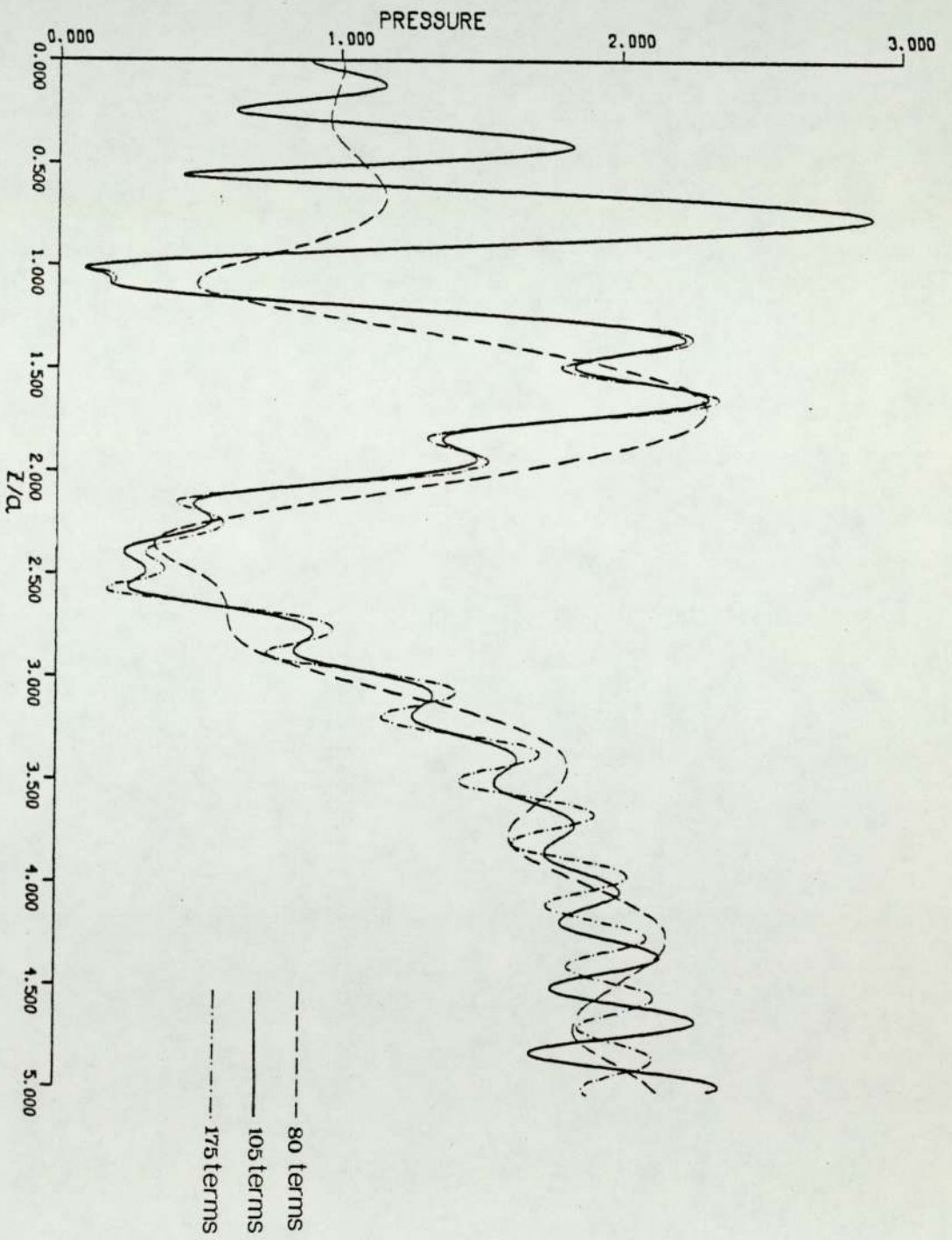series at points in the farfield, however, is not so good, as shown

FIGURE 6.7 Predicted axial distribution of an infinitely baffled disc; a=5γ

PRESSURE
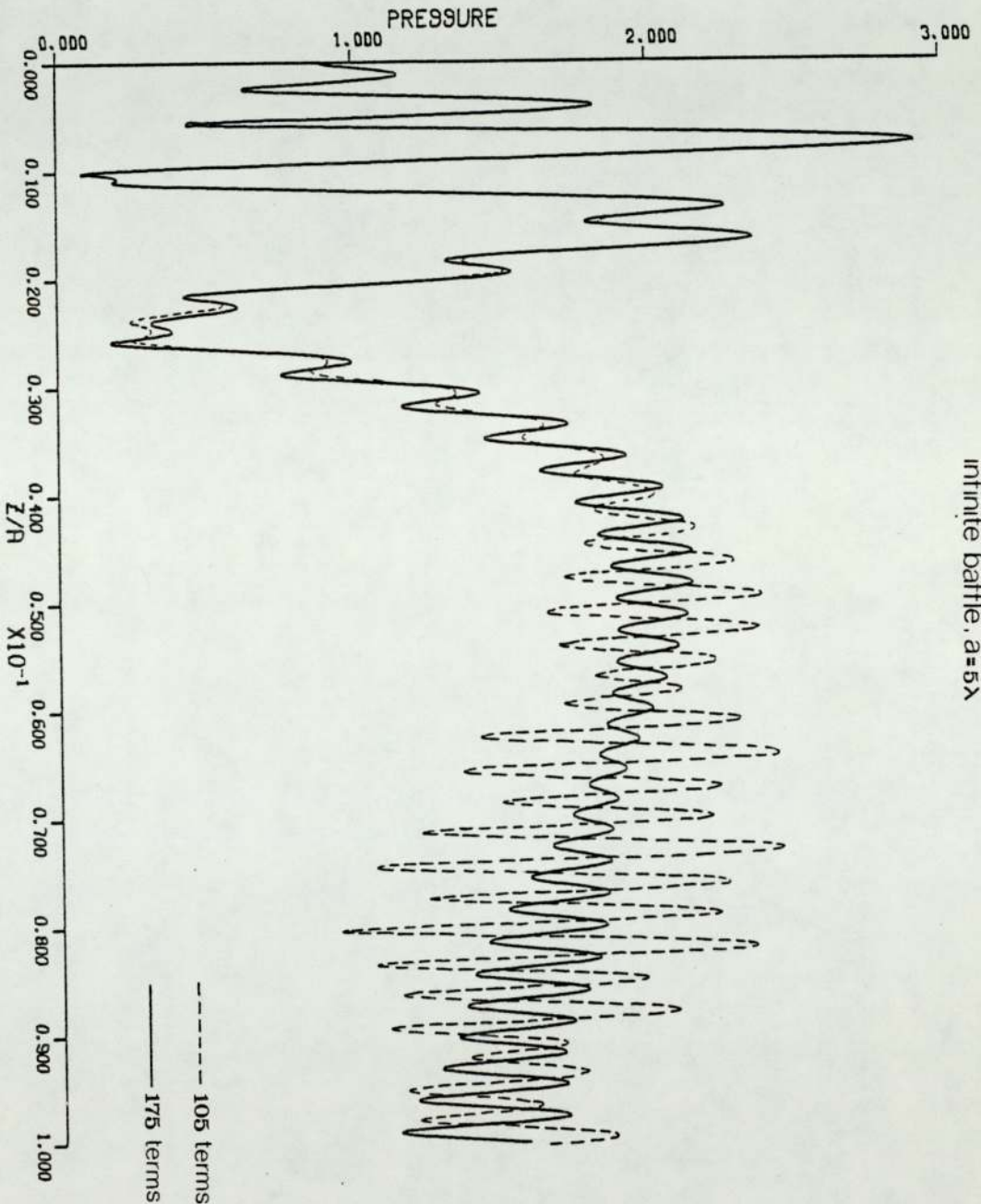
z/a

---- 80 terms
—— 105 terms
—·—·— 175 terms

FIGURE 6.8 Nearfield and farfield axial distribution;
infinite baffle. a=5λ

in Fig 6.8; increasing the number of terms from 105 to 175 makes
little difference to the computed nearfield, but the farfield
region has still not converged to a steady distribution even
with 175 terms in the series.

It is not immediately evident why such a series should become
less convergent at greater values of Z, the axial coordinate,
but this has been found generally to be the case. It may
thus be stated that the approach is of greatest application
to the nearfield regions of various radiating transducers,
which, it seems, are the areas least explored previously.

It is found that the above phenomena occur for a wide range
of conditions. Fig 6.8 explored the case where the
transducer radius a was 5λ. When, for a given transducer,
the ultrasonic frequency is lowered so that a becomes less
than 5λ , the farfield still suffers from an increasing
lack of convergence with Z, the nearfield remaining adequately
convergent.For higher frequencies,it has been found that the
validity of the computational technique is only acceptable if the
magnitude of k becomes comparable to the upper value of C_n in the
series;this requires a greater number of terms, if a larger wavenumber
is employed.

6.6.4 The estimated accuracy of the technique in evaluating
transducer nearfields

It has been demonstrated that the use of an acceptable number

of terms in the series used produces a good approximation

to that predicted by an infinite series, within the nearfield

region. The accuracy of such a series in evaluating

nearfield pressure distributions must now be estimated.

It has been shown (Section 6.5.2) that the boundary conditions

may only be applied to a certain accuracy; over certain regions

of the plane Z = 0, the computed distribution, predicted

after the application of these boundary conditions, deviates from

these prescribed conditions by as much as 10%.

It must thus be stated that the accuracy of the proposed

approach may only be guaranteed to within 10% of the true

value, in regions at which the adequate convergence of the

series has been demonstrated.

6.7   Predicted nearfield distributions - comparison with surface integral techniques

It has been shown that the proposed series approach is capable

of predicting the value of P at any point (r, z), within the

nearfield region of various transducers, to an acceptable accuracy.

The resulting distributions will now be compared to those

predicted by surface integral techniques.

The case of the infinitely baffled disc has been investigated

by Zemanek (55) and Bashter (109), both using a surface integral;

Zemanek numerically evaluated the resulting double integral, whereas Bashter used specialist geometry, reducing the expression to a single integral.

Fig 6.10 shows the axial pressure distribution of an infinitely baffled disc of radius a = 5λ , as predicted by Bashter, with which the distribution predicted by the series approach has been compared. It is seen that a degree of correlation exists in the nearfield region, whereas the farfield region predicted by the series approach is non-convergent as described. The surface integral predicts zeroes in the positions shown within the nearfield, with maxima occuring at a constant magnitude. The series approach predicts maxima and minima in the same general positions, but the minima are not zeroes, and the maxima vary in magnitude as indicated.

Nearfield plots in the radial (r) direction are also possible with the same series approach, and these are compared, in the case of an infinite baffle, with those predicted by surface integral techniques Fig 6.11; a degree of agreement is again seen.

A comparison with surface integral techniques may also be made in the case of an unbaffled disc. The surface integral approach assumes the disc to be comprised of an infinite number of
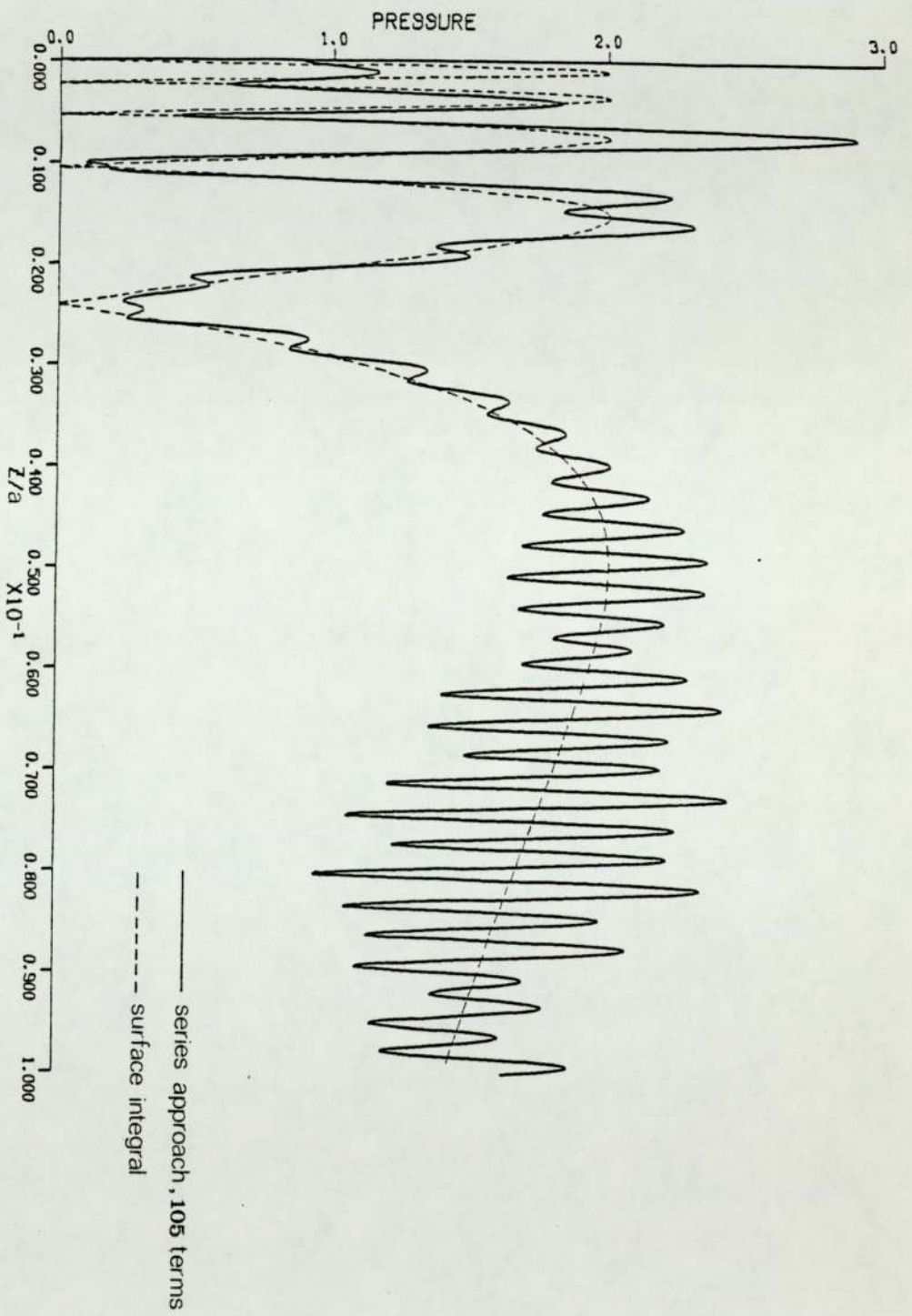
FIGURE 6.10 Axial pressure distribution of an infinitely baffled disc;

a=5λ
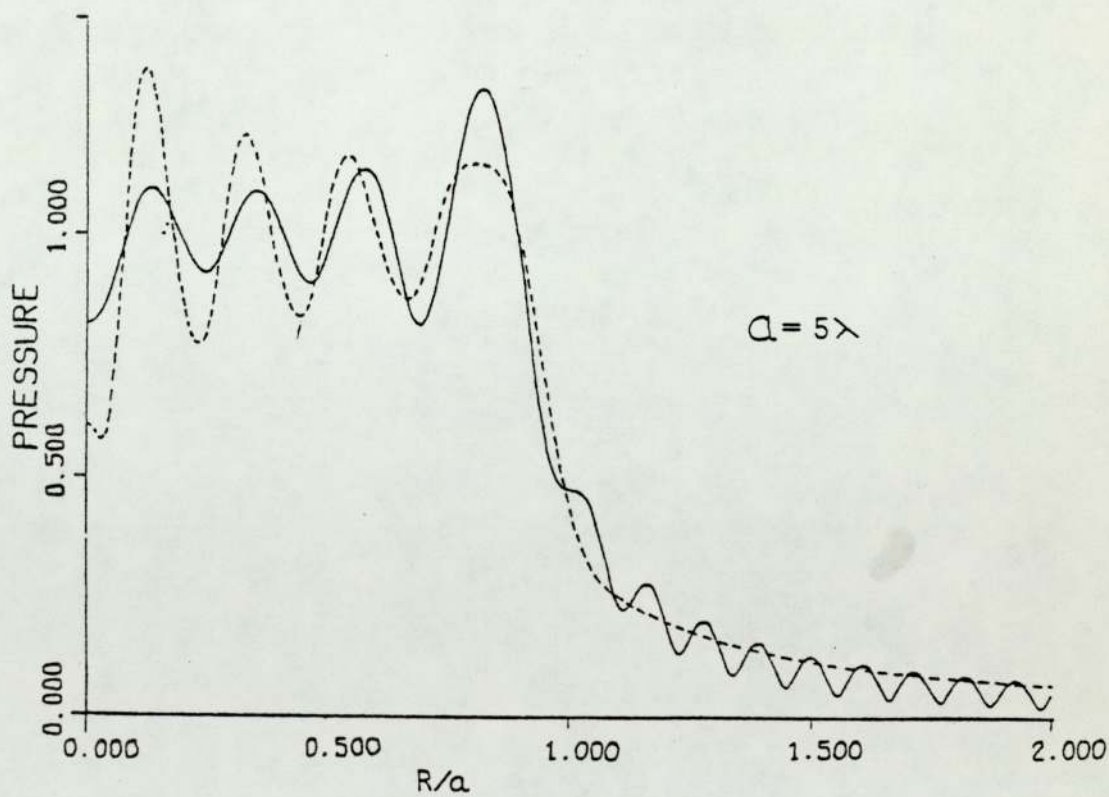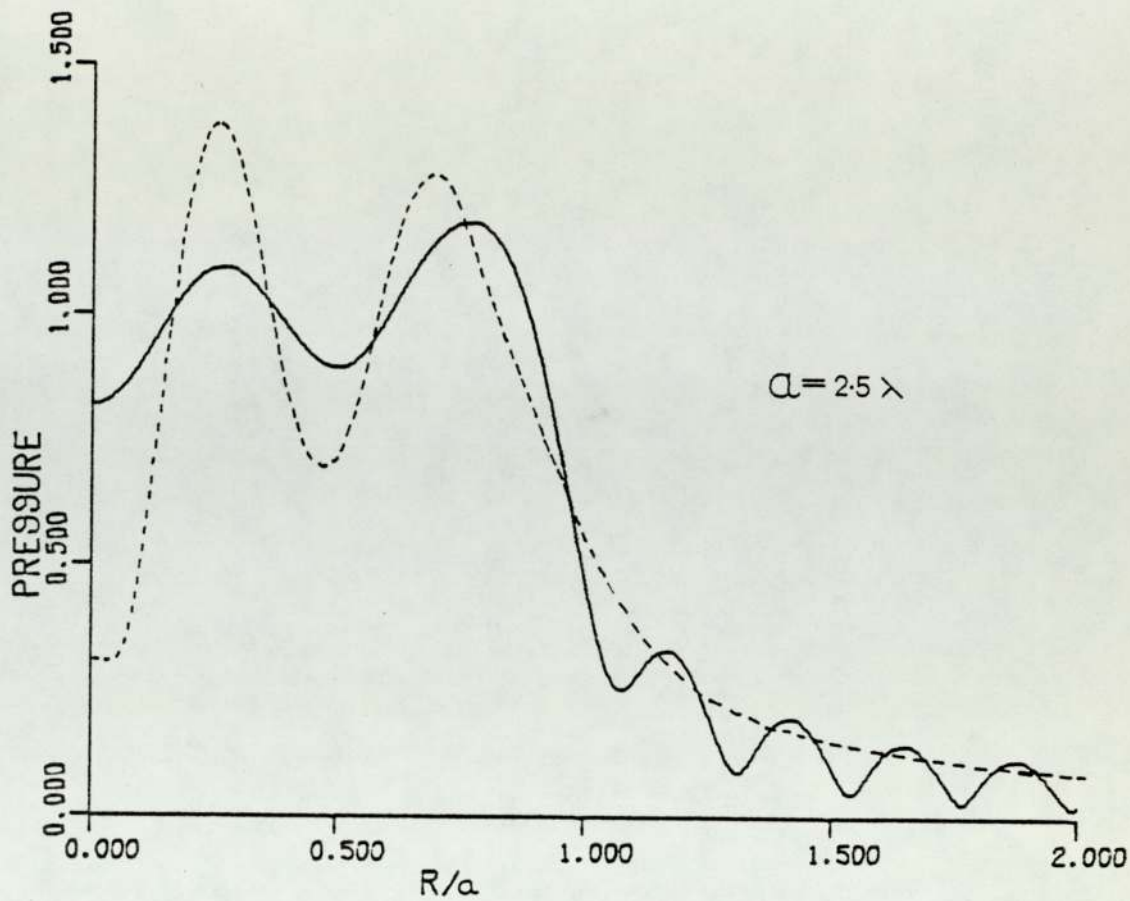
FIGURE 6.11   Radial plots, at the plane z = a/5, for infinitely baffled discs

——————— series approach
– – – – – surface integral

FIGURE 6.12 Axial pressure distributions of unbaffled discs
(a) a = 5λ
(b) a = 2·5λ
——— series approach
– – – – surface integral

radiating dipoles, vibrating in phase. Appendix 1 shows how
an expression for the axial distribution of an unbaffled
disc may be obtained by this approach.

The nearfield axial distributions of such a disc, as predicted
by the surface integral and series approaches, are compared
in Fig 6.12. It is seen that again the maxima and minima
predicted by the two approaches, are in the same general
positions, but that their relative magnitudes differ.
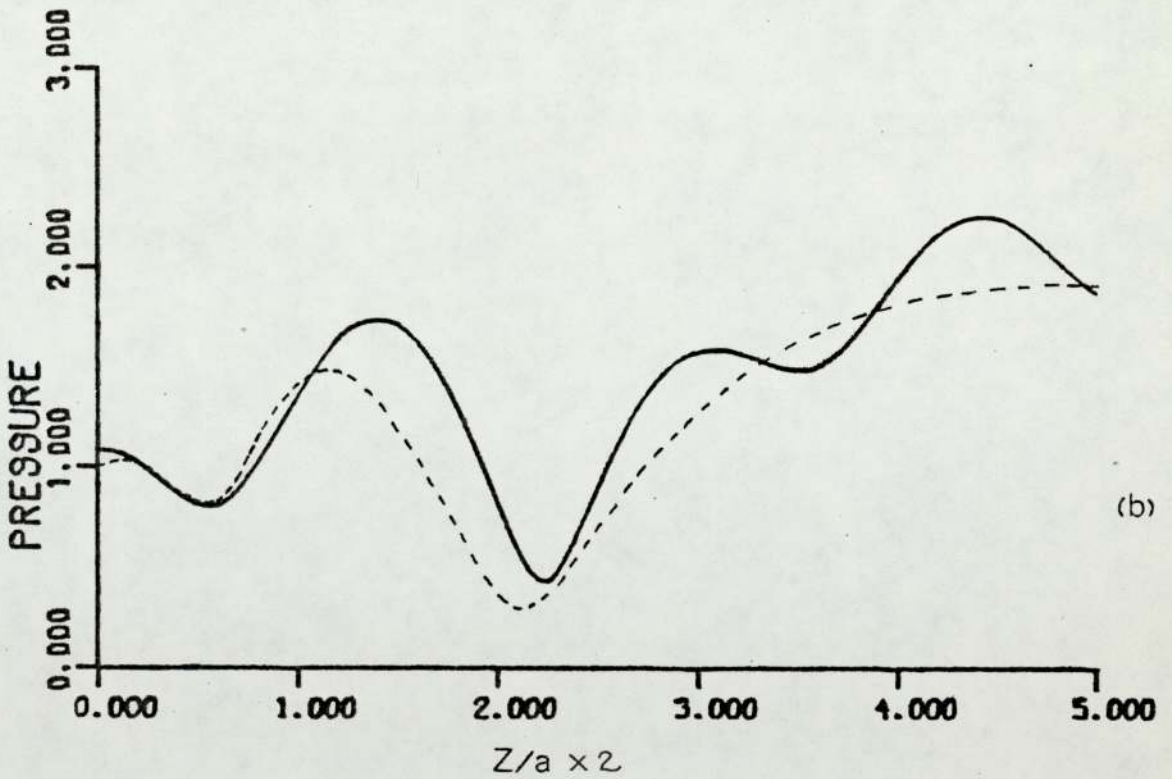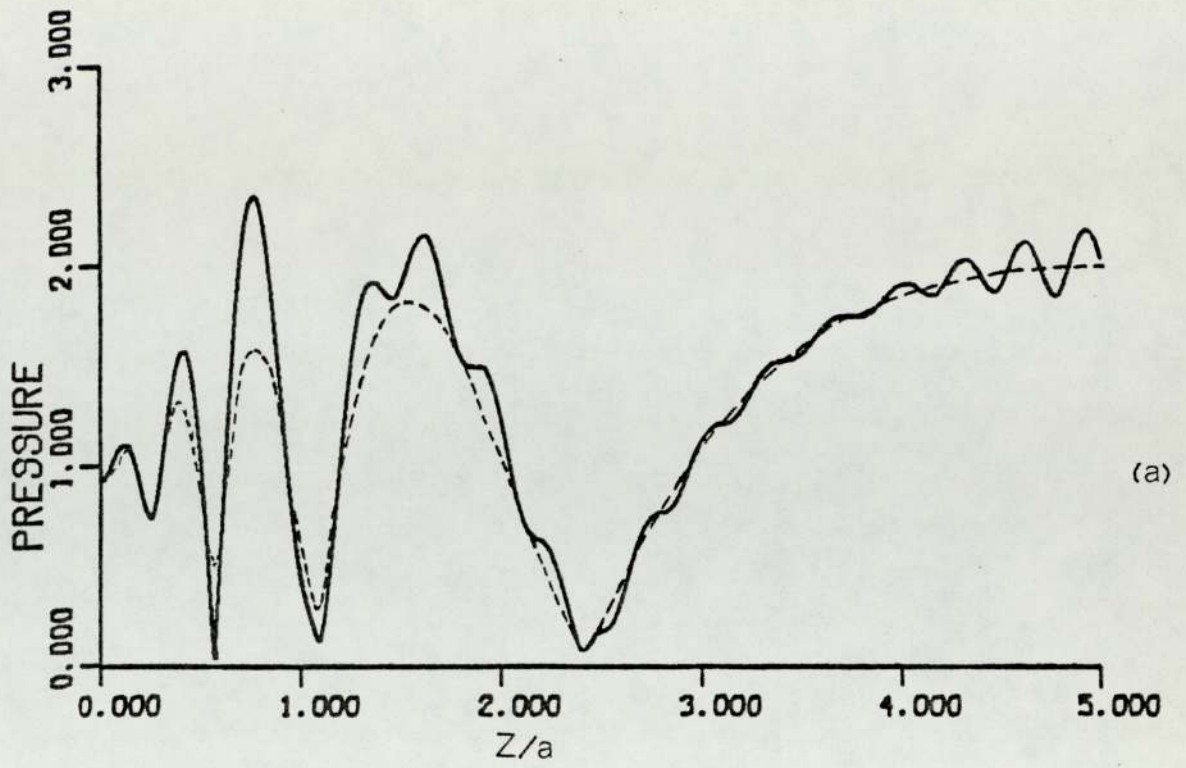
From Figs 6.10 - 6.12, it is clear that a degree of correlation
exists between the proposed series approach and existing surface
integral techniques, when the predicted nearfield distributions
are compared.

Some of the apparent differences may be explained by the estimated
error in the application of the boundary conditions in the
series approach, some 10%. However, it will be seen that
some differences lie outside this range of error; this is
especially the case with the zero, predicted by the surface
integral, at the centre of a disc with an infinite baffle. It
is suggested that further analysis of this discrepency be
undertaken in future study.

6.8   Use of the series approach in studying three-dimensional
       nearfield variations

An advantage of the series approach is its convenient evaluation
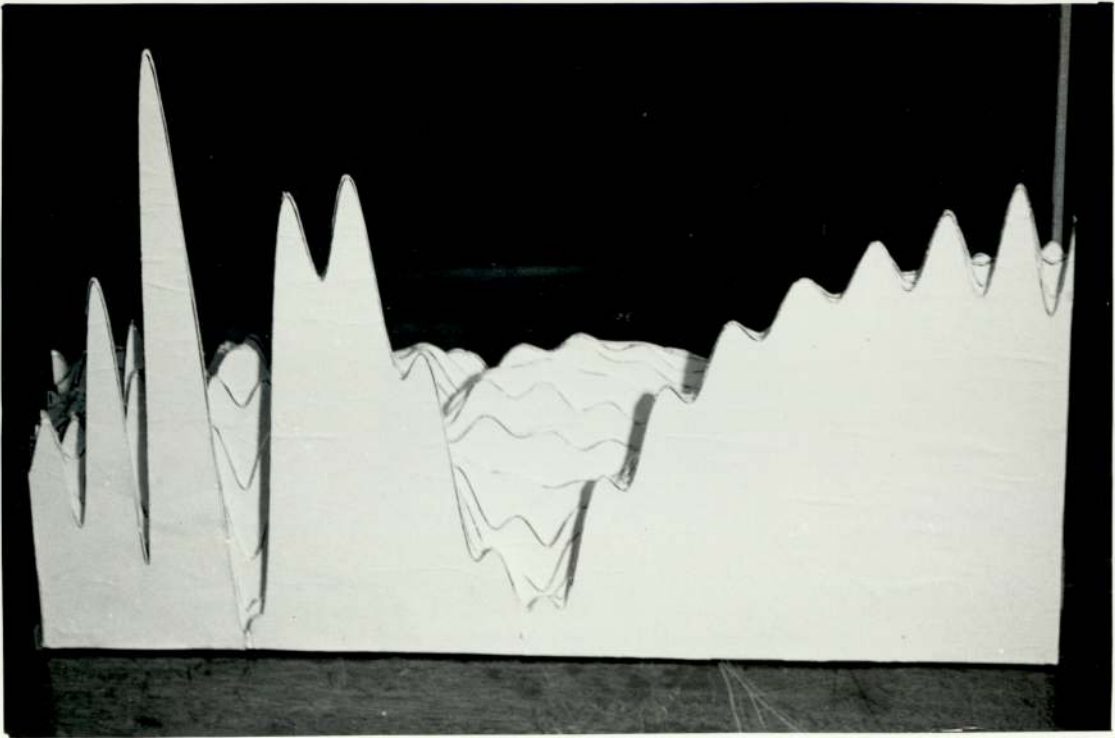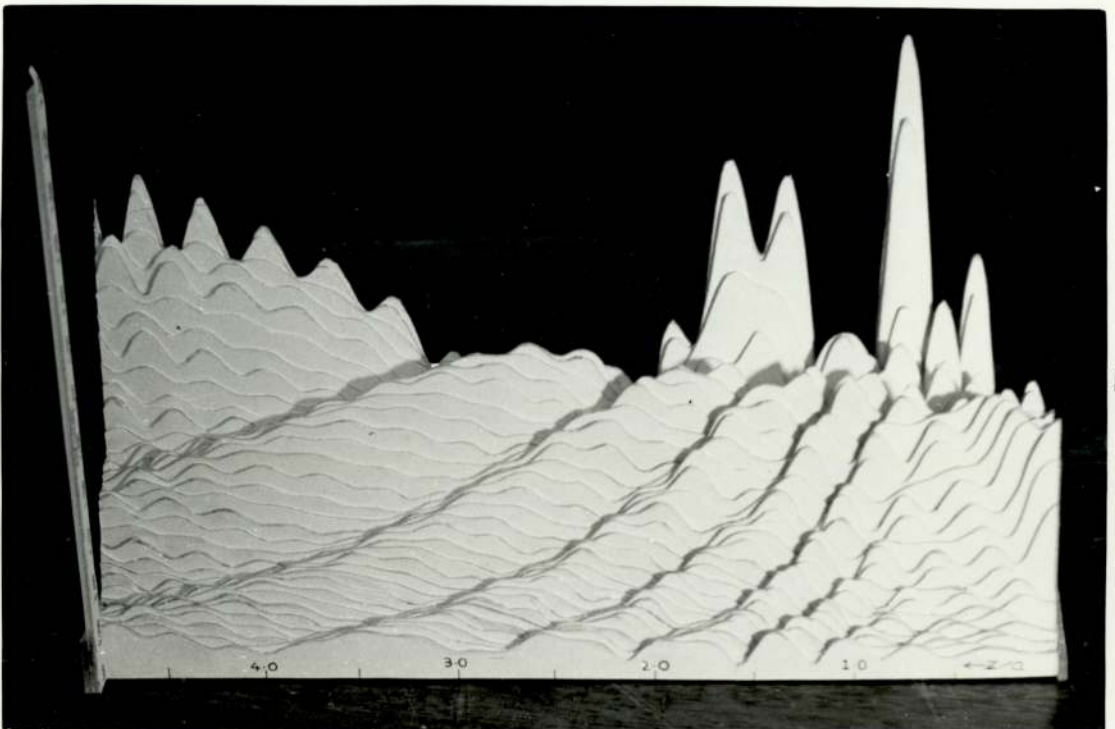
FIGURE 6.13   3D nearfield distribution of an infinitely baffled disc, radius = 5λ.

(A) looking from the axis; (B) looking from outside the disc.

by computer techniques, enabling whole sections of complicated

sound fields to be plotted in a single operation; in this

way, three-dimensional distributions may be swiftly determined.

This has been achieved in the case of an infinitely-baffled

piston, of radius a = 5λ , the resulting nearfield pressure

variations being presented in Fig 6.13. Fig 6.13(a) is a view

of the axial distribution and the field immediately adjacent

to the axis i.e. at small values of r; Fig 6.13(b) shows how

the field spreads outwards as the distribution progresses in

the z direction.

6.9   The study of variations in baffle size and ultrasonic frequency

A further advantage of the proposed technique is its ability

to study variations in baffle size i.e. to see how the radius

of a circular baffle, surrounding a disc transducer, affects

the radiated field.

Consider again the case of a disc transducer, of radius a = 5λ .

The nearfield axial pressure distribution for infinite baffle,

two radii of finite baffle and unbaffled conditions of

such a transducer are presented in Fig 6.14. It is seen that

(i)   the axial distributions of infinite and finite baffled

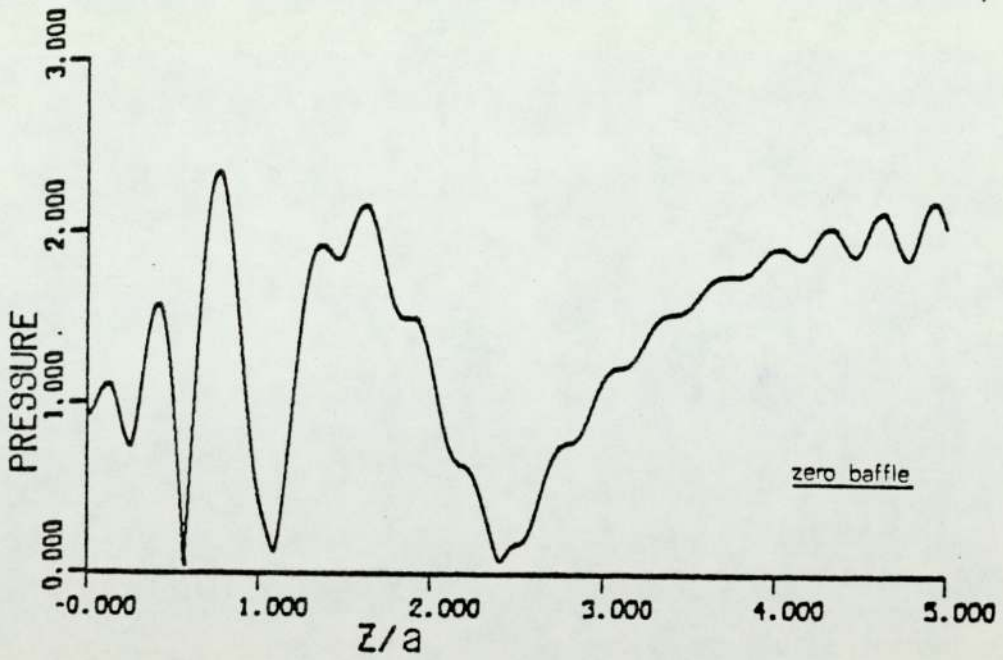discs are almost the same, being virtually
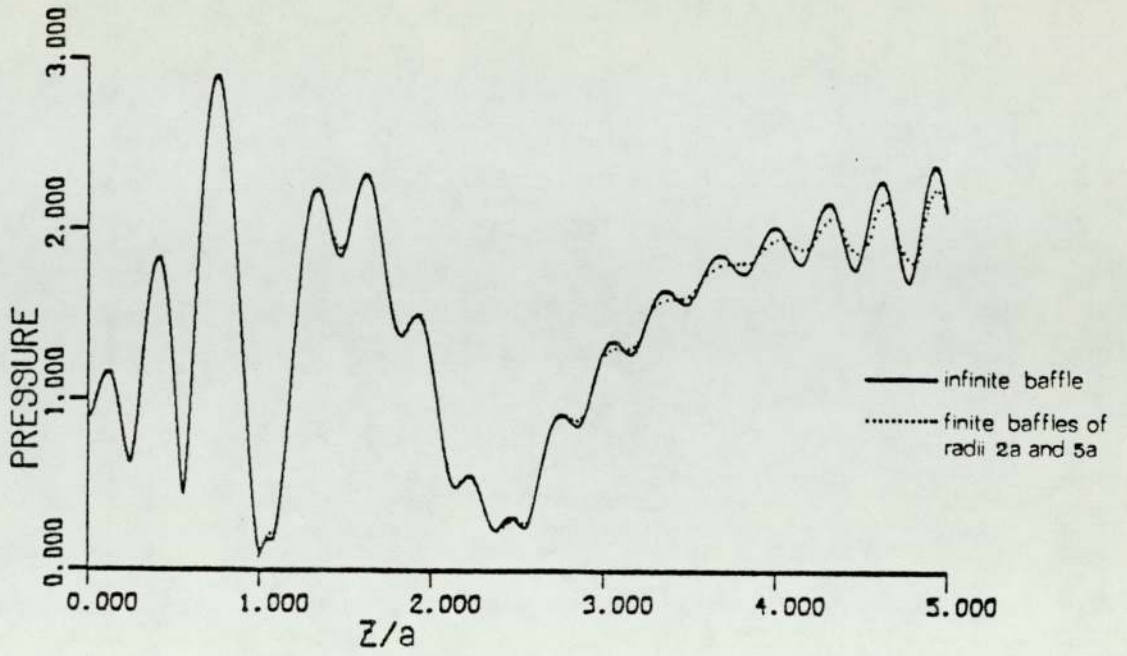
FIGURE 6.14 Nearfield axial distributions for discs under various conditions of baffle.
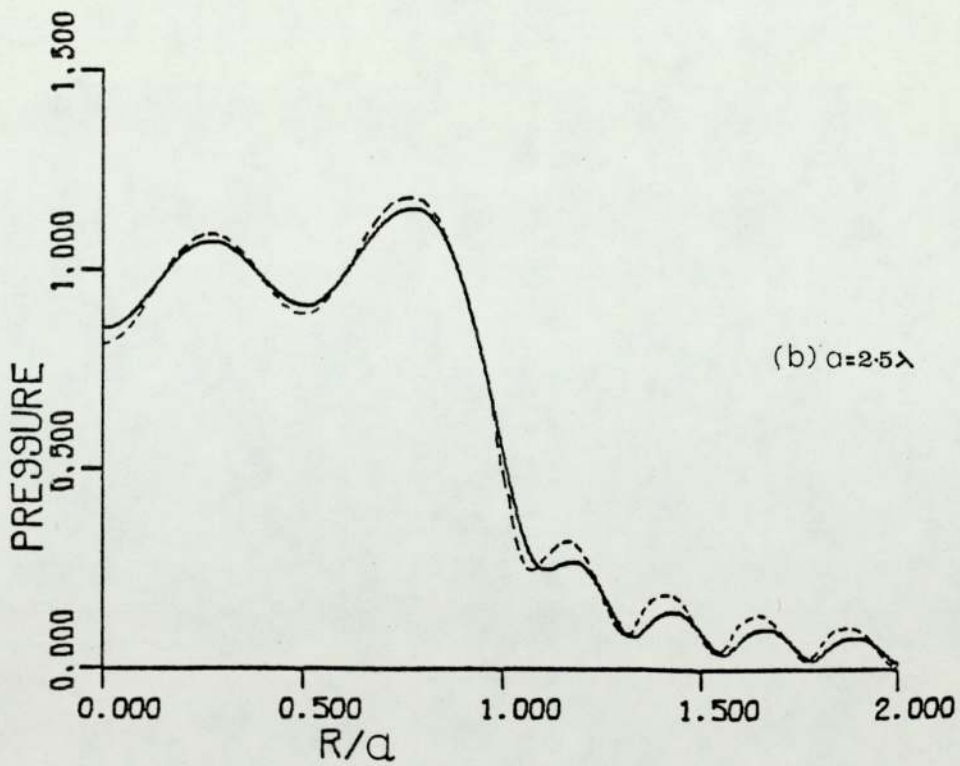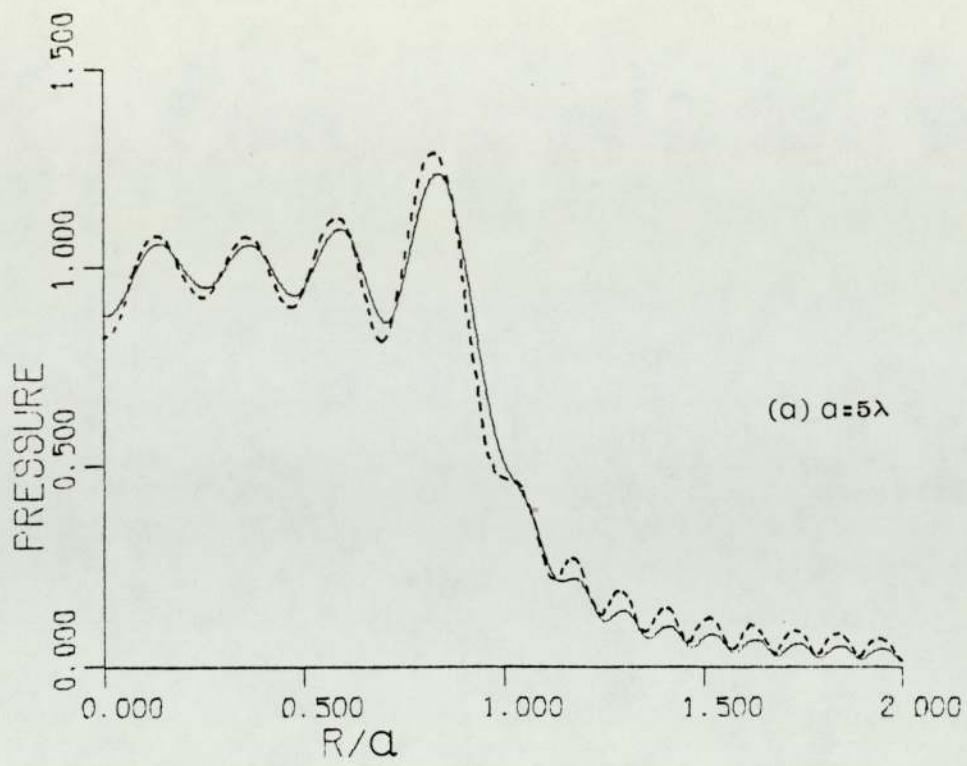
FIGURE 6.15 Radial plots at the plane z=a/5

----- infinite baffle

———— unbaffled
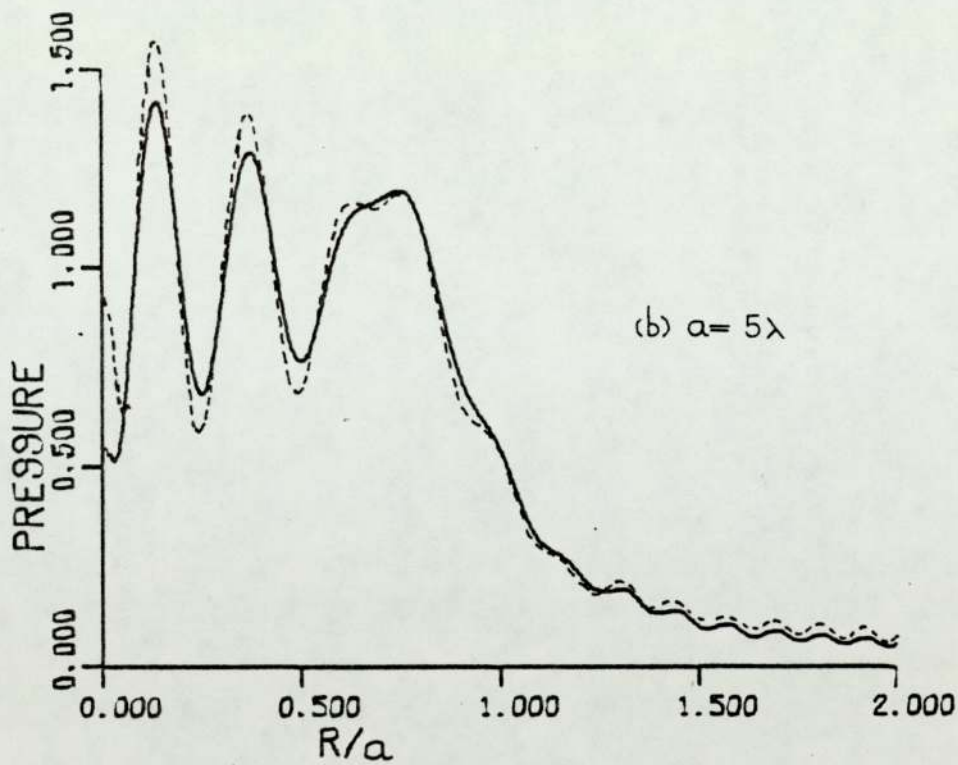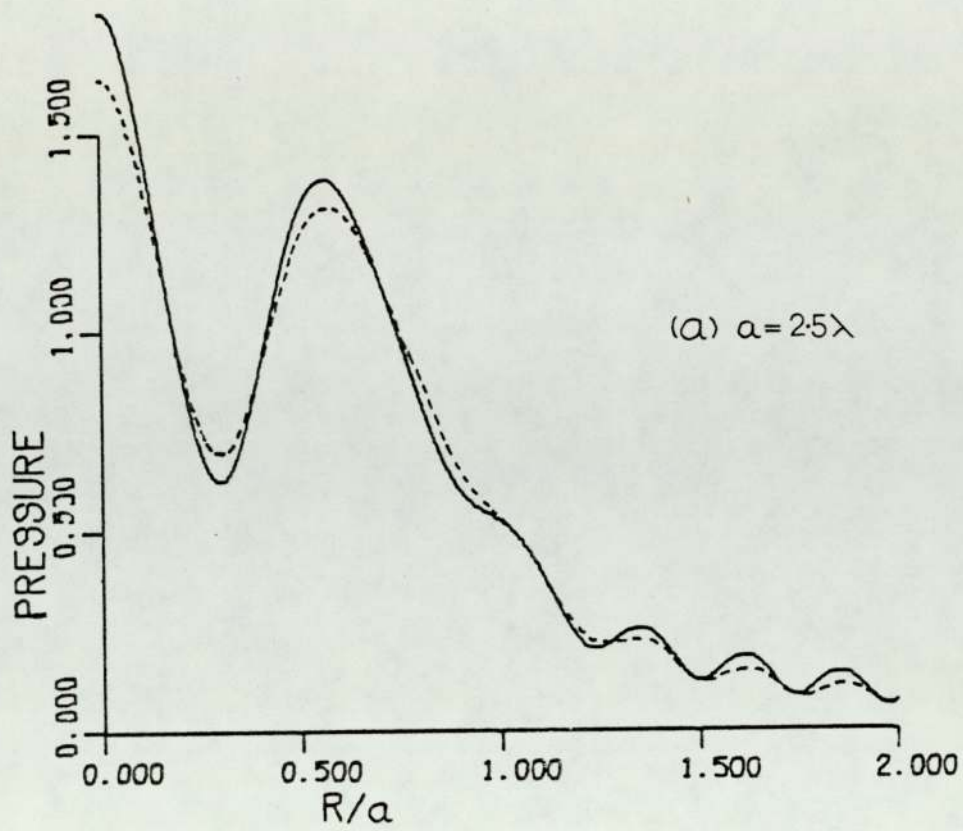
FIGURE 6.16   Radial plots at the plane z=0·6a

——————— unbaffed

— — — — — infinite baffle

independent of variations in baffle size; thus

a circular baffle of only twice the radius of

the disc causes the radiated distribution to

be close to that of an infinite baffle.

Variations in baffle size greater than 2a seem

to produce little difference in the radiated

field.

(ii) the radiated nearfield axial distribution from

an unbaffled disc differs from those of finite

and infinitely baffled configurations in

several minor respects, although the curves

assume the same general shape. The values of

various maxima and minima are seen to differ,

but their positions remain essentially similar.

Radial plots i.e. in the r direction are also possible. Fig 6.15

shows a comparison in the field produced by unbaffled and

infinitely baffled discs, at two ultrasonic frequencies

at the plane z = a/5 i.e. just off the transducer face; little

difference between the two configurations is evident. Further

from the disc's face, however, greater differences exist

e.g. Fig 6.16 shows plots in the r direction, at the plane

z = 0.6a, for both unbaffled and infinitely baffled discs at

the same two frequencies.

6.10 <u>A further application of the series approach - the study</u>

<u>of the radiated field of ring transducers.</u>

The proposed series technique is capable of examining any
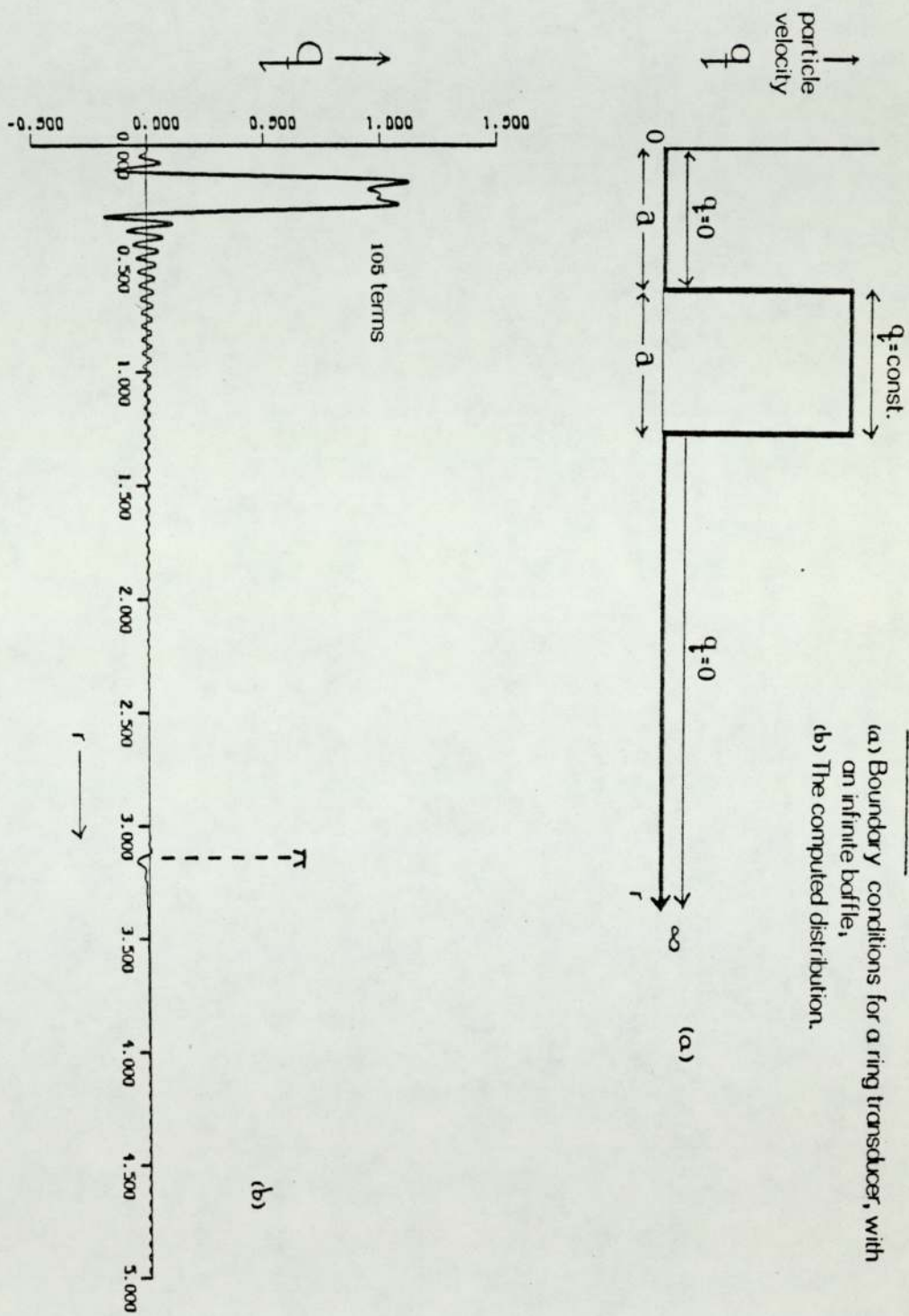
FIGURE 6.17

(a) Boundary conditions for a ring transducer, with an infinite baffle,

(b) The computed distribution.

transducer configuration which exhibits axisymmetric
cylindrical symmetry; ring transducers are such a case.

Fig 6.17(a) shows the boundary conditions, existing over
the plane z = 0, for a ring transducer exhibiting an
infinite baffle over the regions not containing the
radiating face. Fig 6.17(b) shows the computed distribution
in particle velocity, predicted by equation (6.6) after
the application of boundary conditions in the manner
described (Section 6.5), and it is seen that good agreement,
as before, is obtained between the required and computed
distributions over the plane Z = 0.

Having applied the boundary conditions, the radiated field
may be studied as before, for the case of an infinite baffle
Fig 6.18 shows the pressure distribution, across the Z = 0
plane, for a ring transducer whose outside radius is twice
that of its inside radius, at a frequency given by a = 5λ .
A zero is seen at the centre of the ring, which is, in fact,
predicted by surface integral techniques. The nearfield axial
distribution of this configuration is presented in Fig 6.19.

FIGURE 6.18 Pressure distribution at the z=0 plane
for a ring transducer with an infinite baffle.
a=5λ, 105 terms used.
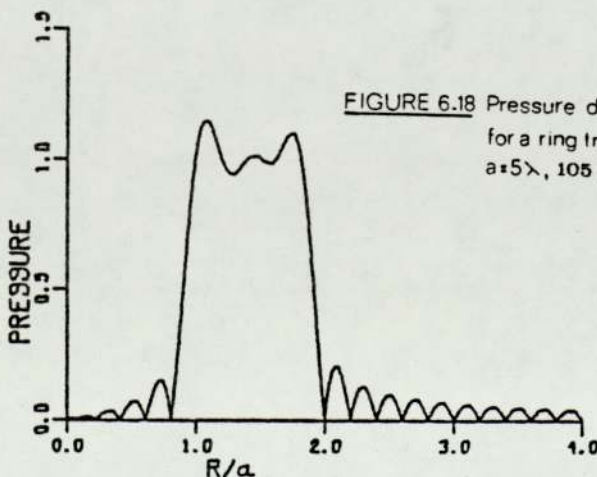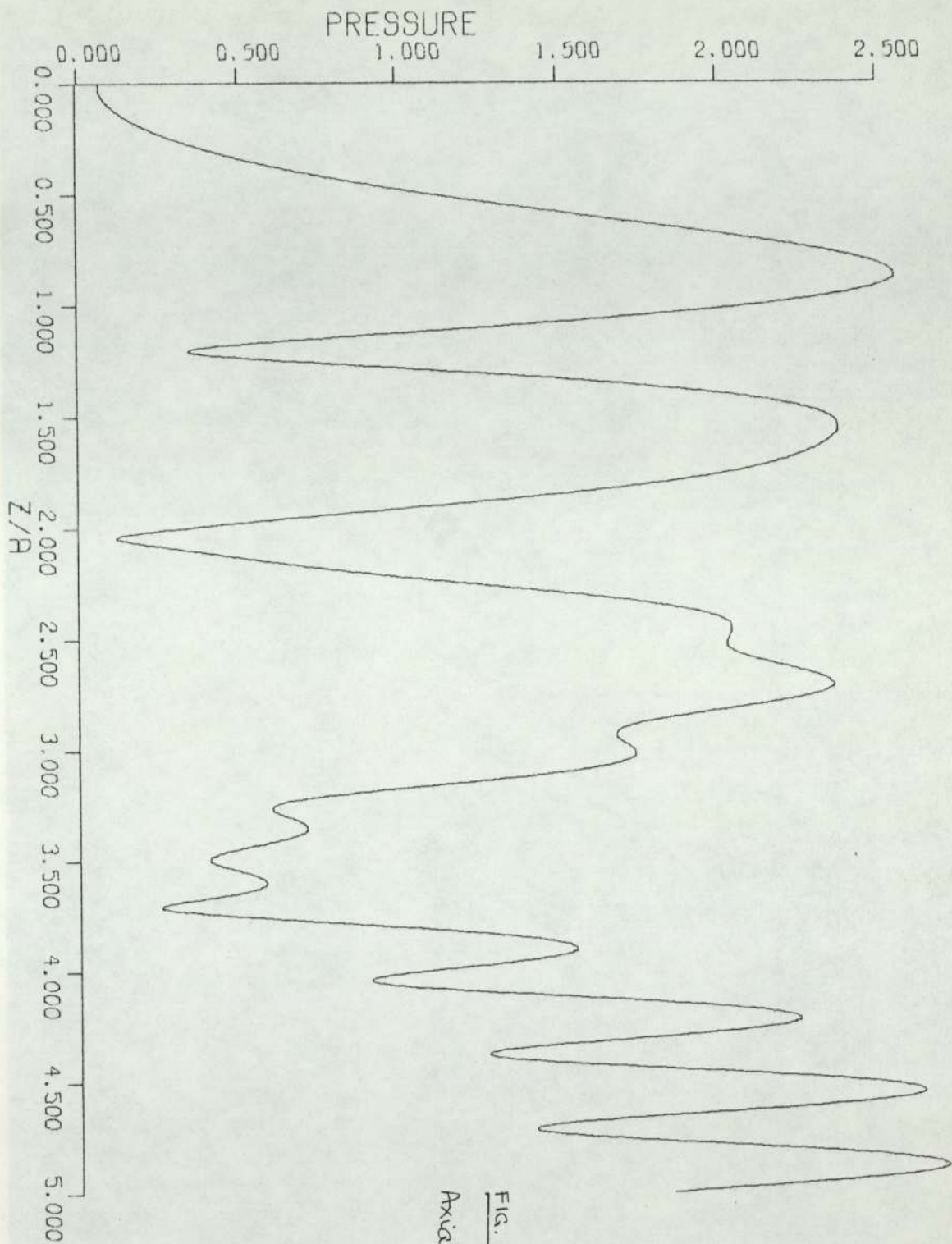
FIG. 6.19 Ring transducer
Axial distribution, $a = 5\lambda$.
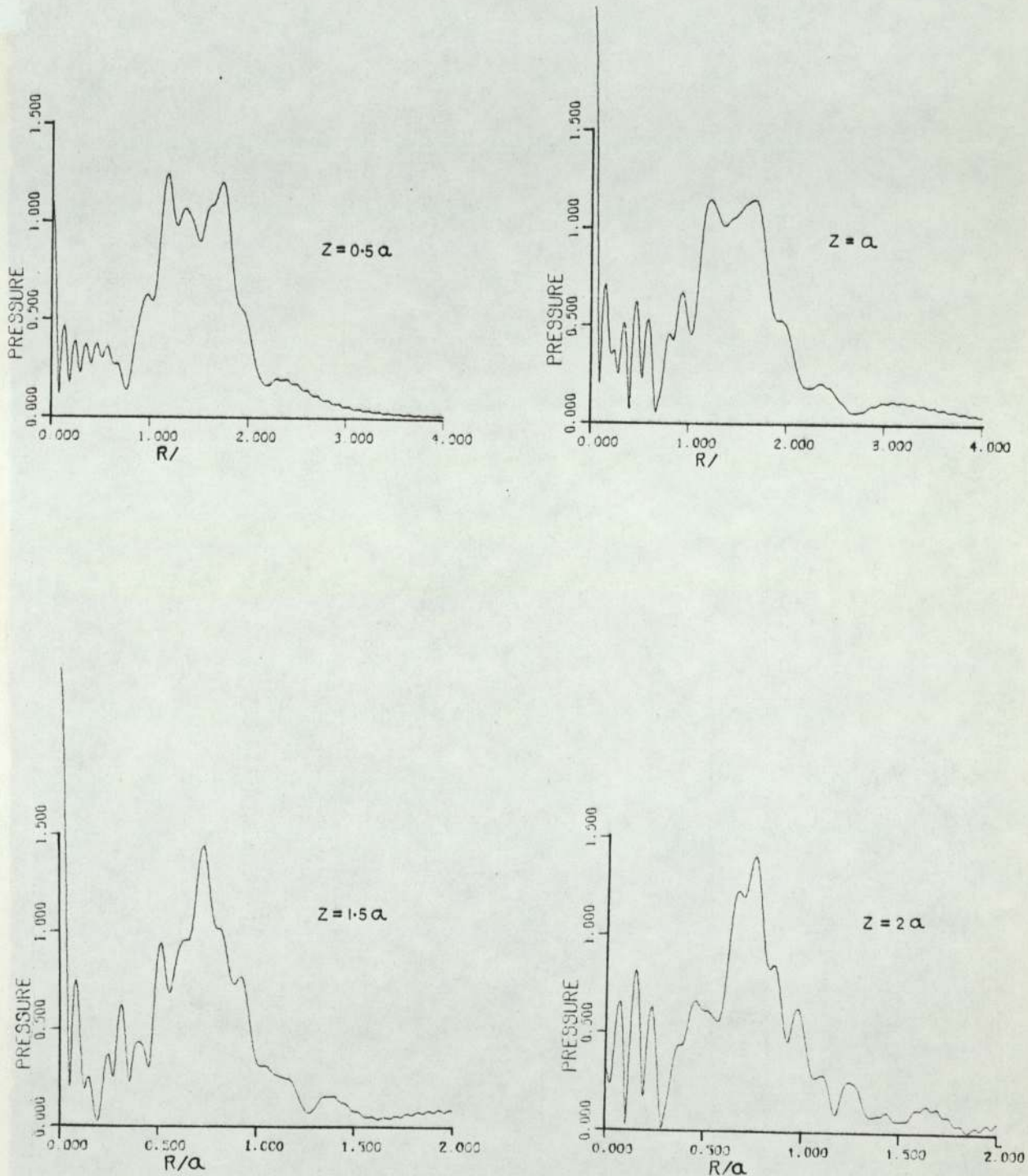
FIGURE 6.20 Radial plots at various values of z
for the same ring transducer as Fig. 6.19

Finally, to show again the ability of the technique in
swiftly sampling two dimensional sections, radial plots at
various distances (z) from the face of the same transducer
are presented in Fig 6.20.

6.11 Preliminary conclusions

A technique has been presented whereby the nearfield distributions
of various axisymmetric transducer configurations may be
determined; the theory allows variations in baffle size and
ultrasonic frequency to be studied.

The basis of the approach is the expression of the solution .
to the relevant wave equation in the form of a series with
a finite number of terms. Such a series usually have a limited
range of validity, and investigations have shown how this
range may be extended, so that boundary conditions may be
applied to infinity in the radial direction, over the plane
containing the transducer face.

The boundary conditions are applied by the simultaneous equation
method, and it has been shown that the predicted distribution
over the plane $Z = 0$ meets these conditions to within 10%,
provided a sufficient number of terms are used in the series,
and that suitable scaling is undertaken.

The resulting predictions of the theory have been compared
in a number of cases to those predicted by surface integral
techniques and general agreement has been demonstrated.
Significant differences, however, have been observed
in the case of the infinitely baffled disc, which cannot
be explained in terms of lack of convergence or insufficient
accuracy in the series approach; the two approaches are at
variance in this respect and further study into this disagreement
is needed.

Several limitations of the technique have been described.
Its inability to determine farfield distributions, due to a
decreasing tendency for absolute convergence of the series with
distance from the transducer face, is not considered too
serious a limitation; nearfield regions are normally those
of greatest interest. Additionally, it has been shown that
the approach may only be used at frequencies above that
resulting from an ultrasonic wavelength equal to the transducer
radius; this results from a limitation of the mathematical
expression in dealing with wavenumbers whose value is less
than the integer representing the number of terms in the series.
This again is not considered too serious, as transducers
in common use invariably have radii which are multiples of
the ultrasonic wavelength in the irradiated medium.

Despite the above limitations, the approach remains a powerful
technique for the quick and simple determination of radiated

nearfield distributions, variations in baffle size being

conveniently studied.   It would appear that no other

unified theory, capable of studying such variations with

the use of a single expression, exists in the literature.

CHAPTER SEVEN

CONCLUSIONS AND FURTHER WORK

The work presented in this thesis has been concerned with the
determination of ultrasonic distributions by independent
experimental and theoretical approaches.

The experimental work involves the optical display of both
progressive and standing ultrasonic waves by a technique
combining strain anisotropy and stroboscopic illumination.   The
theoretical work has investigated the radiated field of various
ultrasonic transducers.

7.1   The visualisation technique

The essence of the technique lies in its ability to sample
two-dimensional sections of ultrasonic fields; this it does by the
use of an index layer, a thin sheet of material in which direct
visualisation takes place.

Two optical effects have been considered, whereby an ultrasonic
wave, travelling within an index layer, might be converted into a
light pattern.

The first involves the use of molecules, with an inherent mass
asymmetry, which exhibit a substantial optical activity and/or
circular dichroism in the random state.   It is proposed that such
molecules may exhibit a varying degree of alignment, capable of

following the acoustic variations of an ultrasonic cycle, as
the result of a kinematic equilibrium between orientational
forces, supplied by the ultrasonic waves, and random thermal
motion. Investigations into the expected times of orientation
and randomisation have been seen to place a realistic limit on
the size and mass asymmetry of the molecules involved.

Alignment of such molecules is expected to produce an enhancement
of their optical activity and circular dichroism, resulting in
a display system if this alignment varies with an ultrasonic
cycle. Accordingly, molecules with the appropriate properties
have been presented. Time factors, however, have not allowed the
proposed effects to be investigated experimentally, but reasonable
grounds for the expectance of an observable effect have been
presented.

Photoelasticity, the production of strain-induced double refraction,
has been examined theoretically and practically, and found to be
of use as a display mechanism within index layers. Experimental
verification was performed in pilot experiments, before a full-
scale apparatus, utilising this effect, was constructed.

7.1.1 Apparatus

The design of the apparatus incorporates

(a)   the production of a high intensity ultrasonic
        field;

(b)   the adequate illumination of an extended area

of index layer, held horizontally within the field;

(c)   amplitude modulation of the incident illumination,

        adjustable in frequency but centred about that of

        the ultrasonics, to give the required stroboscopic

        effect;

(d)   control over the relative ultrasonic and light

        modulation frequencies.

(a)   the presence of hissing and streams of bubbles has

indicated that the ultrasonic generating system is capable of

causing the onset of cavitation within the irradiated water; it

is thus considered suitable for the investigation of insensitive

optical effects within index layers.

(b)   an optical system has been constructed which results in the

adequate illumination of an index layer over a circular area of

20 cm diameter. Careful design has allowed the system to be

relatively free from aberrations, and a good image of effects

within index layers, over an extended field of view, is observed.

Suitable wavelength bands in the visible region may be selected

by filters, or by dyes dissolved in the cooling water of the

lens closest to the arc-lamp.

(c)   modulation of the incident illumination has been achieved

via a photoelastic light modulator, incorporating several novel

features giving an advantage over previous designs. The non-

resonant nature of the construction allows an extended frequency

of operation, and is also thought to contribute to the production

of a pulse-like modulation waveform by increasing the ultrasonic

harmonic content within the optical element.

80% amplitude modulation is achieved at the frequency of the
driving signal, which is judged to be sufficient in its present
application.

(d)   control over the rate of stroboscopy is achieved by
controlling in turn the difference between the light modulation
and ultrasonic frequencies. This involves a coupling between
the two signal generators used to feed the respective supply
circuits. Simple interlocking produces equal frequencies and a
static photoelastic display, whereas an added frequency difference
provides a simple means of producing a moving display.

The combination of the above separate components results in an
apparatus capable of permanently recording photoelastic displays
of ultrasonic fields in liquids, the display representing a two-
dimensional section through the field. This cheap and simply-
constructed apparatus thus achieves its desired aims.

Improvements to the apparatus

It is thought that attention to several details of the design of
the apparatus might lead to improvements in the quality of the
displays produced:

(i)   displays within the apparatus are found to contain
reflections from the walls of the water tank, although this is
reduced by their polyurethane foam covering. Improvements in this

area would arise from the use of a bigger tank, with its sides covered in a more absorbing material. The use of a transducer with a greater ratio of its radius to the ultrasonic wavelength in water would also reduce the rate of spread of the ultrasonic beam with distance, in turn reducing side reflections.

(ii) stroboscopic illumination has been achieved by the photoelastic light modulator, pulse-like modulation at a frequency close to that of the ultrasonics being available. It has been indicated that the on-time of these pulses is not negligible in comparison to the period of the ultrasonics, and some blurring of the displays must be occuring.

Improvements might arise from the use of a light source, capable of producing short-duration light flashes of high intensity, at a repetition rate of a few hundred Hz. Such light sources have been described and used by several authors (95 , 96) for the photoelastic investigation of ultrasonic pulses in solid media; they are based on a spark light source, and incorporate a thyratron. These light sources would be particularly applicable to the study of pulsed fields, but some difficulty might arise in effectively controlling the rate of stroboscopy in the investigation of continuous-wave fields.

(iii) It has been indicated, Section 5.5.4, that adequate visualization of longitudinal waves, travelling in all directions, may be achieved by taking two photographs with the mutually crossed polarizer and analyzer rotated by 45° between each. A more useful result, allowing the complete display to be presented as a single

photograph, will arise from a double exposure technique,
described in Section 2.2.2, in which the polarizer and analyzer
are rotated by 45° between each exposure.

In the present state of the apparatus, this rotation is not
easily achieved without a disturbance to the alignment of various
optical elements, and is in any case tedious. A properly
designed system, in which the polarizer and analyzer are mechanically
coupled and may be rotated in unison, will allow photography
under the required conditions.

7.1.2 The displays produced and their agreement with theory

A fundamental requirement of the proposed visualization technique
is that the displays produced should be an accurate representation
of the ultrasonic field that would have existed at the sampled
plane, in the layer's absence.

Assuming that the layer is thin enough, so that ultrasonic variations
across its thickness are minimal, it might intuitively be thought
that the above requirement would be met; the ultrasonic distribution
within the layer will be expected to be forced to be close to that
existing in the surrounding ultrasonic field. This concept is, in
fact, predicted theoretically in Chapter Four. Initially different
wavenumbers are assumed in the liquid and layer media, and it is
predicted that ultrasonic waves in each will interact to produce
a new, common wavenumber, whose value is close to that normally
associated with the liquid medium.

This theoretical prediction has been found to be met in practice, provided the liquid and layer media do not differ too widely in their acoustic properties. The display over a particular area is the same for considerable variation in the acoustic properties of the layer material; additionally, the area covered by the display seems to be unaffected by the attenuation characteristics of the layer material. These observations agree with the concept that the induced wave within such index layers is a forced one.

The above only holds if the acoustic properties of the layer and surrounding water are initially similar, an anomolous display wavelength arising within e.g. a glass sheet; it may thus be concluded that it is essential to use an index layer whose acoustic properties are close to those of the liquid medium.

Various anomalies have been seen to result within index layers exhibiting a characteristic impedence mismatch with water; these include mode conversion and internal reflection. These effects are minimised by the use of polyurethane rubber as the index layer material; its impedence matches that of water, and its Poisson's Ratio is close to 0.5 so that shear waves are not readily supported.

The photoelastic displays of standing waves have been linked successfully to the expected acoustic variations, in complete agreement with photoelastic theory.

The displays of progressive waves, produced under stroboscopic illumination, seem at first, however, to disagree with photoelastic theory, only one bright band per ultrasonic wavelength being

observed, whereas two are predicted. This discrepency is probably due to the existence of static strains, within the effective optical path, combined with a relatively weak optical effect within the index layer material.

7.1.3 The disturbance to the ultrasonic field

This has been shown theoretically to occur from

   (i)   reflection and diffraction of the field by the
         index layer;

   (ii) a change in the field's wavenumber.

Both of these will be minimised by the choice of a layer material whose acoustic properties are close to those of water. In addition, Chapter Four indicated theoretically that the field's wavenumber will only be slightly affected, and to be affected even less by the use of thinner layers.

7.1.4 Extension of the technique to other ultrasonic fields

The proposed technique has been applied to the display of 200 kHz continuous-wave ultrasonics, and the resultant displays analysed. Application of the technique to pulsed fields, and higher frequencies will now be discussed.

The visualization of pulsed fields will benefit from a different stroboscopic technique to that used in this investigation; high intensity, short-duration light flashes, at a repetition rate

equal to that of the ultrasonic pulses, will be suitable, as described in Section 7.1.2.

As the ultrasonic frequency is increased, the ultrasonic wavelength will be smaller, and attenuation within layer materials will be greater.

Effective sampling of two-dimensional sections of ultrasonic fields will only occur if the thickness of an index layer is less than half an ultrasonic wavelength. In the work described, this criterion has been met by the use of 1-3mm thick layers for ultrasonic wavelengths of approximately 0.74cm. At higher frequencies of say 1MHz, where the ultrasonic wavelength in water is approximately 1.5mm, the thinnest photoelastic layers found to produce an acceptable effect (approximately 1mm thick) will barely meet this criterion. It may thus be concluded that the use of the photoelastic layer materials described will limit the technique to frequencies of 1MHz or less. The sensitivity of the technique, in this application, has been put at $0.5Wcm^{-2}$ with the use of 1-3mm index layers.

A more sensitive optical effect would, however, allow the study of higher frequency distributions by the presence of a thinner index layer; it is unlikely that photoelastic layers will be found with the required sensitivity, and thus other optical mechanisms require investigation. Such a mechanism, involving the enhancement of optical activity, has been described.

Attenuation within an index layer material will increase with frequency; the attenuation to the ultrasonic field will thus

become greater for a given layer thickness. As, however, thinner
layers must in any case be required, this effect is not considered
important.

7.1.5 Final conclusions on the visualization technique

The technique has been shown to produce acceptable displays of
progressive and standing ultrasonic waves, the information being
obtained across a two-dimensional section of the field. This has
been achieved by a photoelastic index layer, although other optical
mechanisms have been investigated. The photoelastic phenomenon
has been seen to be insensitive, and to be adversely affected by
static strains within the layer material. An alternative
mechanism, mentioned in the previous section, is expected to produce
a greater sensitivity.

It is finally concluded that the technique has accomplished its main
aims in sampling two-dimensional sections of ultrasonic fields in a
single operation, the displays being characteristic of the field
being visualized. This has been achieved simply, and at a low cost.

7.2   The theoretical determination of transducer radiation

       patterns

The technique described in Chapter Six is based on a solution to

the wave equation which is in the form of a series. This approach

has been seen to have several advantages over other techniques,

which may be listed as:

       (i)   the method is inherently simple and easily adapted

              to computer evaluation;

       (ii)   it may be applied to a wide range of axisymmetric

              transducer configurations, including various

              conditions of baffle;

       (iii) it is capable of determining the three-dimensional

              nearfield distributions of these configurations

whereas limitations are

       (iv)   its accuracy in the farfield cannot be guaranteed;

       (v)   it is only useful for frequencies above which

              the radius of the transducer is greater than the

              ultrasonic wavelength.

7.2.1 The application of boundary conditions

This has been achieved by the simultaneous equation method, whose

main advantage is that mixed boundary conditions may be applied to

the series solution over the plane containing the transducer face,

the $Z = 0$ plane. It has been stated, however (Section 6.6.4.), that

in some cases the error in this application may be as much as 10%, but over the majority of the plane Z=O the accuracy is better than this. The error is greatest over the discontinuity at the edge of the disc, and will not be reduced significantly even by an infinite number of terms in the series.

The type of series used, a Schlölmilch series, will only normally be valid and convergent between O and π in the radial (r) direction, but it has been shown that by an appropriate scaling process, the series is continuous over the $r = \pi$ boundary, and that the boundary conditions are effectively applied to infinity in r. This is aided by the fact that $J_o(x) \rightarrow O$ as $x \rightarrow \infty$.

7.2.2 The range of validity of the approach

Two limitations to the approach have been stated. The first concerns the accuracy of the predicted farfield distributions, arising from a lack of convergence of the series used. As stated previously, Section 6.6.3., it is not immediately evident why such a series should become less readily convergent at greater values of Z, but this is invariably observed.

The second concerns the range of frequencies to which the approach is applicable. The lower limit mentioned in (v) arises from the inability of the expression to deal with a wavenumber k whose value is less than the highest value of C_n in the expression

$$e^{j \sqrt{k^2 - c_n^2} \cdot z}$$

Both these limitations, however, are not considered too serious.
Farfield distributions are simple in form and have been well
investigated, whereas nearfields are complicated and less-well
understood. Additionally, most transducers in practical use are
operated at frequencies above the imposed lower limit.

7.2.3 Comparison with surface integral techniques

The predicted nearfield distributions have been compared, in
Section 6.7 , with those evaluated from surface integral techniques,
infinitely baffled and unbaffled discs being treated. In most cases,
general agreement is seen, but in some, notably the axial minima
of infinitely baffled discs, the differences between the two approaches
are marked. Thus, the two approaches differ in this respect, and
further work is needed to establish the cause of this discrepancy.

7.2.4 Final conclusions concerning the series approach

The technique outlined is capable of predicting the three-dimensional
nearfield pressure distributions of a wide range of transducer
configurations, with an acceptable accuracy and in a quick and simple
fashion. The use of 105 terms in the series for the pressure has been
found to be adequate for this purpose. The main use of the theory,
in studying detailed differences resulting from changes in the size
of a surrounding baffle, is seen as a major advantage over other
techniques.

APPENDIX I

THE AXIAL PRESSURE DISTRIBUTION OF AN UNBAFFLED DISC

A.1.1 The system under consideration

The approach involves finding the scalar velocity potential,
produced at a point P in the irradiated medium, by treating
the disc as a series of acoustic dipoles; this is mathematically
identifiable with the case of a freely-suspended unbaffled
disc in an infinite medium.

Consider such a disc, vibrating in the direction as shown in
Fig. A.1.1. The treatment assumes that the disc is a thin
membrane, vibrating in such a fashion that the effect on the
medium on either side of it is antisymmetric; each point on
such a membrane could thus be considered as an acoustic
dipole radiator, represented by two point sources S_1 and S_2, a
distance $2 \delta y$ apart. The effect at P, due to each of these
sources, may be represented as

$$\phi_1 = e^{-jkr_1} \frac{}{r_1} \qquad \text{for source } S_1$$

$$\phi_2 = -e^{-jkr_2} \frac{}{r_2} \qquad \text{for source } S_2$$

Where ϕ is a scalar velocity potential, r_1 and r_2 are the distances
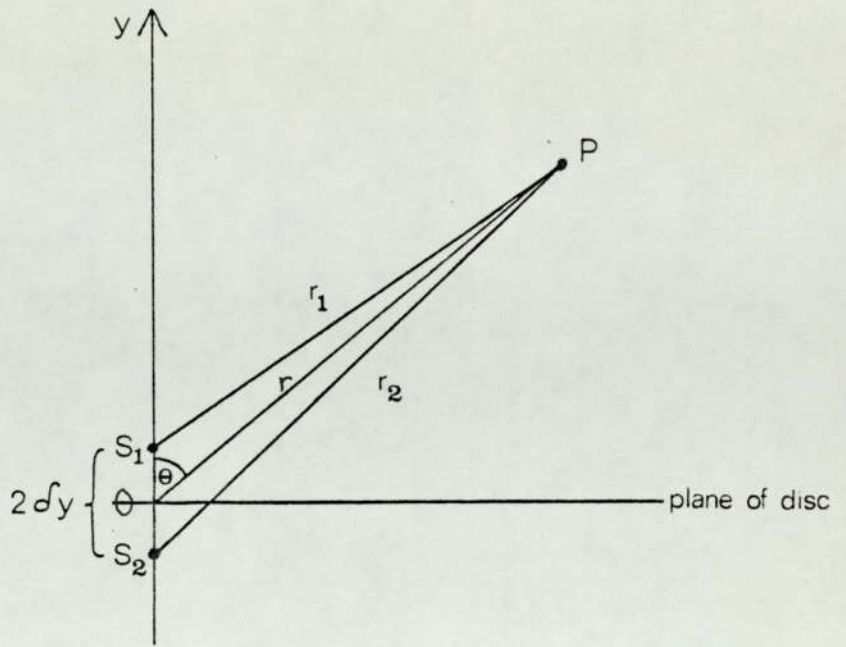of each source from the point P, and k is a circular wavenumber.

FIGURE A.1.1 THE RADIATING DIPOLE.
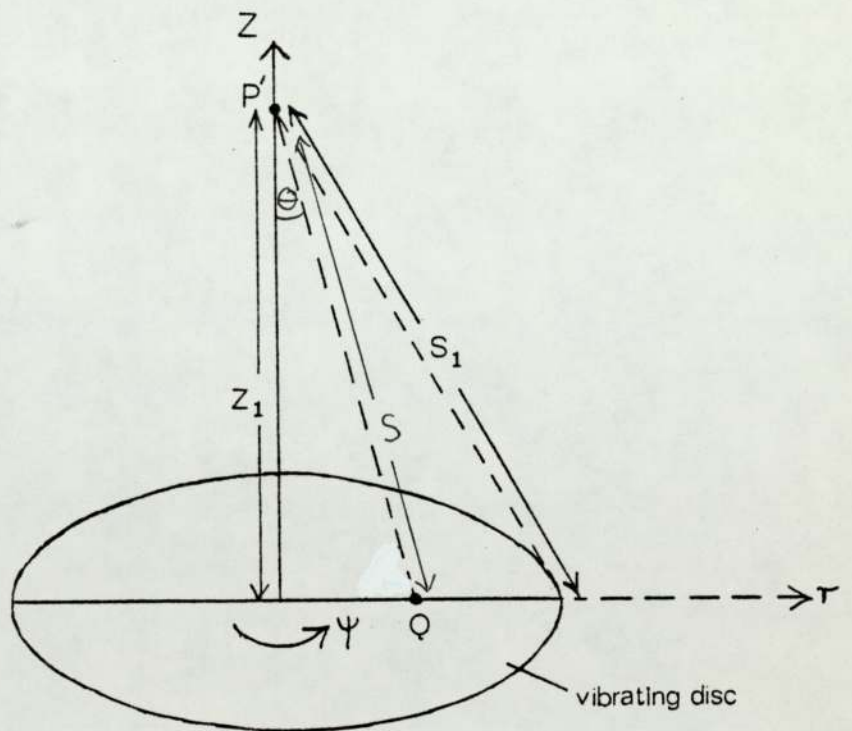
FIGURE A.1.2 THE COORDINATE SYSTEM.

Each source has been assumed to be a radiator of spherical waves, the functions of r shown being the Green's function for a point source.

The treatment that follows predicts the scalar velocity potential at a point due to a radiating dipole, and then applies this expression, with the use of a surface integral, to the axial pressure distribution of an unbaffled disc. The reasons for believing that the expressions derived are valid will be outlined.

A.1.2 The scalar velocity potential at a point due to an acoustic dipole

Consider Fig. A.1.1; as $\delta y \rightarrow o$,

$$r_1 = r + \frac{\partial r}{\partial y} \cdot \delta y \qquad\qquad (A.1.1)$$

Operation of the cosine rule on triangle OSP gives

$$\left(r + \frac{\partial r}{\partial y} \cdot \delta y\right)^2 = r^2 + \delta y^2 - 2r \cdot \delta y \cos \Theta$$

$$\therefore \ r^2 + \left(\frac{\partial r}{\partial y} \cdot \delta y\right)^2 + 2 \cdot \frac{\partial r}{\partial y} \cdot r \cdot \delta y = r^2 + \delta y^2 - 2 \cos \Theta \cdot r \cdot \delta y$$

$$\therefore \ \frac{\partial r}{\partial y} = - \cos \Theta \qquad\qquad (A.1.2)$$

and this result will be used later.

Consider now the resultant scalar velocity potential at P, ϕ_p, due to the dipole radiator at O; this will be given by

$$\phi_p = \phi_1 + \phi_2$$

$$= \frac{e^{-jkr_1}}{r_1} - \frac{e^{-jkr_2}}{r_2} \, ,$$

assuming unit magnitude for each.

From (A.1.1), as $\delta y \to 0$,

$$\frac{e^{-jkr_1}}{r_1} = \frac{e^{-jk(r+\delta r)}}{(r + \delta r)} = \frac{e^{-jkr}}{r} + \frac{\partial}{\partial y} \left(\frac{e^{-jkr}}{r} \right) \delta y$$

$$\therefore \; \underset{\delta y \to 0}{\mathsf{L}_t} \; \phi_p = \mathsf{L}_t \; \frac{\partial}{\partial y} \left(\frac{e^{-jkr}}{r} \right) \cdot 2 \; \delta y$$

$\therefore$ Assigning an arbitrary amplitude A to each source,

$$\phi_p = 2A \, \delta y \, (-jk - \frac{1}{r}) \; \frac{e^{-jkr}}{r} \cdot \frac{\partial r}{\partial y}$$

where $2A\delta y$ may now be regarded as the dipole strength, B say; thus, we may write, by use of equation (A.1.2),

$$\phi_p = B \, (jk + \frac{1}{r}) \; \frac{e^{-jkr}}{r} \cdot \cos \theta \qquad \text{(A.1.3)}$$

and an expression for the scalar velocity potential at P, due
to a radiating dipole, has been derived. This will be a solution
to the Helmholtz wave equation, having been derived from the
combination of the expressions for $\emptyset_1$ and $\emptyset_2$, which are themselves
solutions.

A.1.3 The distribution of $\emptyset$ on the axis of an unbaffled disc

The coordinate system that will be applied to an unbaffled disc
is shown in Fig A.1.2; R is a radial coordinate, Z an axial one,
and S is the distance from a point on the disc's surface, Q say,
to a point P$'$ on its axis. The angle θ in equation (A.1.3) is
now the angle shown for that particular point Q; in addition, S_1
is the distance from the disc's circumference to the point P$'$.

It is clear from Fig A.1.2 that

$$\text{Cos } \theta = \frac{Z}{S}$$

Thus, the expression for the scalar velocity potential at the
point P$'$ on the axis of the disc, due to a point Q on its
vibrating surface, is, from equation (A.1.3),

$$\emptyset_p = (jk + \frac{1}{S}) \frac{e^{-jks}}{S^2} . Z \qquad\qquad (A.1.4)$$

The resultant scalar velocity potential at P$'$ due to the
whole vibrating disc may now be considered to be caused by an
assembly of points, such as Q, acting as dipole radiators; this

resultant may thus be written, in surface integral form, as

$$\emptyset_p = \int_0^{2\pi} d\psi \int_0^a (jk + \frac{1}{S}) \frac{e^{-jks}}{S^2} Z_1 . r \ dr$$

$$= 2\pi \int_{Z_1}^{S_1} (jk + \frac{1}{S}) \frac{e^{-jks}}{S} . Z_1 . ds$$

where $S^2 = r^2 + Z^2$, and hence $sds = r \ dr$

From the above, it follows that

$$\emptyset_p = -2\pi \left| \frac{e^{-jks}}{S} . Z_1 \right|_{Z_1}^{S_1}$$

$$\therefore \quad \emptyset_p = 2\pi (e^{-jkz_1} - \frac{e^{-jks_1}}{S_1} . Z_1) \qquad (A.1.5)$$

and equation (A.1.5) is an expression for the scalar velocity potential along the disc's axis.

From equation (A.1.5), the particle velocity q_p at the point P will be given by

$$q_p = \frac{\partial \emptyset}{\partial z} = 2\pi \left[-jk \ e^{-jkz_1} + (jk + \frac{1}{S_1}) \frac{e^{jkS_1}}{S_1} . \frac{Z_1}{S_1} \right]$$

Thus, at the centre of the disc's face,

$$q_p = -2\pi jk$$

and further analysis of equation (A.1.5) shows that this will
be the particle velocity across the disc's face. The condition
that P must be zero, at the plane Z = O and outside the area of
the disc, will intuitively be met from equal values of $\emptyset$, but
of opposite sign, on either side of this plane.

A final expression for the axial scalar velocity potential
distribution, as obtained from equation (A.1.5), will thus be

$$\emptyset_p = \frac{2\pi.U}{2\pi\ jk} \ (e^{-jkZ}1 - \frac{e^{-jkS}1}{S_1}.Z_1)$$

Where U is the prescribed velocity; hence,

$$\emptyset_p = \frac{U}{jk} \ (e^{-jkZ}1 - \frac{e^{-jkS}1}{S_1}.Z_1) \qquad (A.1.6)$$

and the axial pressure distribution will be given by

$$Pressure = U\omega\rho \ (e^{-jkZ}1 - \frac{e^{-jkS}1}{S_1}.Z_1) \qquad (A.1.7)$$

A.1.4 Application of the theory to computation

Comparison with the previously described theory (Chapter Six) is
facilitated by the assumption that U is unity; expression (A.1.7)
may then be adapted to computational evaluation by its separation
into real and imaginary parts. With U = 1, equation (A.1.7) may
be written as

$$P = \omega \rho (\cos kZ - j.\sin kZ)$$

$$- \left(\frac{\cos k \sqrt{Z^2 + a^2} - j \sin k \sqrt{Z^2 + a^2}}{\sqrt{Z^2 + a^2}} \right) Z$$

from which the real and imaginary parts may be separated; $|P|$ then follows.

APPENDIX 2

THE SOLUTION OF WAVE EQUATIONS BY THE PRINCIPLE OF
SEPARATION OF VARIABLES

Various solutions to the Helmholtz wave equation have been
sought during this investigation, and in all cases the
solutions obtained are a function of more than one variable.
The principle of separation of variables is then applied to
arrange that the chosen expressions are suitable solutions.

As an example, consider the solution of the equation

$$\frac{1}{r} \cdot \frac{\partial}{\partial r} \left(r \frac{\partial \phi}{\partial r} \right) + \frac{\partial \phi}{\partial z^2} + k^2 \phi = 0$$

where the wave equation is expressed in cylindrical polar
coordinates, there being no variation with Θ. ϕ will be a
function of both r and z, and may be written as

$$\phi = R(r) \cdot Z(z)$$

Substitution gives

$$Z \cdot \frac{1}{r} \frac{d}{dr} \left(r \cdot \frac{dR}{dr} \right) + \frac{R d^2 Z}{dz^2} + k^2 RZ = 0$$

i.e. $\underbrace{\frac{1}{R} \cdot \frac{1}{r} \frac{d}{dr} \left(r \cdot \frac{dR}{dr} \right)}_{a} + \underbrace{\frac{1}{Z} \cdot \frac{d^2 Z}{dz^2}}_{b} = -k^2$

Both a and b contain only R or Z only. Let $a = -p^2$;

$\therefore b = -k^2 + p^2$. This will be true for any set of values of R and Z.

$$\therefore \quad \frac{1}{r} \cdot \frac{d}{dr} \left(r \cdot \frac{dR}{dr} \right) = - p^2 R \qquad (A.2.1)$$

and $\quad \dfrac{d^2 Z}{dz^2} = - (k^2 - p^2) Z \qquad\qquad (A.2.2)$

A solution to (A.2.1) is $J_o(pr)$;

A solution to (A.2.2) is

$$e^{\pm j \sqrt{k^2 - p^2}} \cdot Z$$

Thus, an expression of the form quoted in Section 6.1 is a
solution to the relevant wave equation. The expressions quoted
in other Chapters for other situations may be shown to be
solutions by a similar process.

APPENDIX 3

CALCULATION OF THE INDUCTANCE AND CAPACITANCE NEEDED TO
PRODUCE CURRENTS, 120° MUTUALLY OUT OF PHASE, IN THREE
SECTIONS OF A ROTARY POTENTIOMETER

To illustrate the method for calculating values for L and C,
consider the circuit shown in Fig A.3.1, which represents
the three-phase circuit feeding sinusoidal currents to three
equal sections of a rotary potentiometer.

For the purpose of calculation, I_1, I_2 and I_3 are chosen so
that their phases, represented in complex notation, differ
mutually by 120°; suitable values are

$$I_1 = \sqrt{3} + j$$
$$I_2 = -\sqrt{3} + j$$
$$I_3 = -2j$$

These values will dictate the currents through L and C to be

$$I_\ell = I_3 - I_2 = \sqrt{3} - 3j$$
$$I_c = I_1 - I_3 = \sqrt{3} + 3j$$
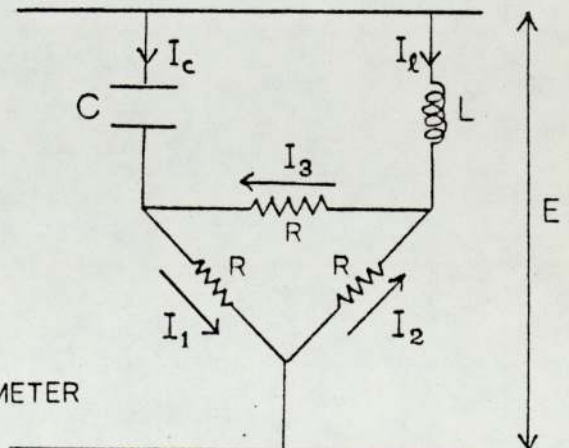
FIGURE A.3.1 THE ROTARY POTENTIOMETER

leading to

$$j\omega L \ (\ \sqrt{3} - 3j) + R \ (-\ \sqrt{3} + j) \ = E$$

$$\frac{1}{j\omega C} \ (\ \sqrt{3} + 3j) + R \ (\ \sqrt{3} + j) \ = E$$

Where $\omega = 2\pi f$, f being the frequency of the sinusoidal

signal used. Thus

$$j\omega L \ (\ \sqrt{3} - 3j) + R \ (-\ \sqrt{3} + j) = \frac{1}{j\omega C} \ (\ \sqrt{3} + 3j) + R \ (\ \sqrt{3} + j)$$

$$(A.3.1)$$

Equating the real parts of (A.3.1)

$$(\ \omega L + \frac{1}{\omega C})\ .\ \frac{\sqrt{3}}{2} = R \qquad\qquad (A.3.2)$$

Equating the imaginary parts

$$\omega L = \frac{1}{\omega C} \qquad\qquad (A.3.3)$$

Use of equations (A.3.2) and (A.3.3) gives

$$L = \frac{R}{\sqrt{3}\,\omega} \qquad \text{and C} \ = \frac{\sqrt{3}}{\omega R}$$

and the required values of L and C may be established

REFERENCES

1.   Romanenko, E.V., Sov. Phys. Acoust. 3, 364 (1957)

2.   Saneyoshi, J., Okujima, M. and Ide, M., Ultrasonics 4, 64 (1966)

3.   Schmitt, H.J., Rev. Sci. Instrum. 32, 215 (1961)

4.   Aveyard, S., B.J.N.D.T. 4, 120 (1962)

5.   Christie, D.G., Materials Research 1, 86 (1962)

6.   Filipczynski, L., Acustica 21, 173 (1969)

7.   Smith, A.W., Weimer, D.K., Rev. Sci. Instrum. 18, 188 (1947)

8.   Yeager, E., Dietrich, H., Bugosch, J., Hovarka, F., J Acoust.
     Soc. Amer. 23, 627 (1951)

9.   Fox, F.E., Herzfeld, K.F., Rock, G.D., Phys. Rev.(2) 70, 329 (1946)

10. Wells, P.N.T., Bullen, M.A., Follett, D.H., Freundlich, H.F.,
     James, J.A., Ultrasonics 2, 129 (1964)

11. Fox, F.E. and Griffing, V., J Acoust. Soc. Amer. 58, 581 (1975)

12. Fry, W.J. and Fry, R.B., J. Acoust. Soc. Amer. 26, 294 (1954)

13. Murayama, N., Nakamura, K., Obara, H., Segawa, M., Ultrasonics
     14, 15 (1976)

14. Jacobs, J.E. and Peterson, D.A. in 'Acoustical Holography'
     5, 633 (Plenum, New York, 1974)

15. Gunton, J.H. and Marsh, D.M., The Radio and Electronic
     Engineer 40, 316 (1970)

16. Smirnov, E.P., Kheifets, E.I., Shenderov, E.L., Sov. Phys.
     Acoust. 19, 159 (1973)

17. Hubbard, J.C., Fitzpatrick, J.A., Kankovsky, B.T., Thaler, W.T.,
     Phys. Rev. 74, 107 (1948)

18. Newman, D.R., Sonics and Ultrasonics SU-20, 282 (1973)

19. Barnes, R.B., and Burton, C.J., J. Appl. Phys. 20, 286 (1949)

20. Neubauer, W.G., J. Acoust. Soc. Amer. 55, 407 (1974)

21. Fitch, C.E., Mater. Eval. 22, 124 (1964)

22. Dragonette, L.R. and Neubauer, W.G., Mater. Eval. 32, 218 (1974)

23. Stanic, S.,Applied Optics 17, 837 (1978)

24. Bucaro, J.A.,Flax, L.,Dardy, H.D.,Moore, W.E.,J Acoust. Soc. Amer. 60, 1079 (1976)

25. Sato, T. and Ueda, M.,Ultrasonics 12, 16 (1974)

26. Defebvre, A.,Ultrasonics 13, 73 (1975)

27. Cook, B.D.,J. Opt. Soc. Amer. 65, 682 (1975)

28. Korpel, A.,Appl. Phys. Lett. 9, 425 (1966)

29. Mueller, R.K.and Sheridon, N.K.,Appl. Phys. Lett 9, 328 (1966)

30. Reibold, R.,Acustica 38, 253 (1977)

31. Mezrich, R.S.,Etzold, K.F.,Vilkomerson, D.H.R.,R.C.A. Rev. 35, 483 (1974)

32. Taylor, K.J.,J. Acoust. Soc. Amer. 59, 691 (1976)

33. Rust, H.,Haul, R.,Studt, H.J.,Naturwissenschaften 36, 374 (1949)

34. Bennet, G.S.,J. Acoust. Soc. Amer. 24, 470 (1952)

35. Rust, H.,Agnew Chemie 64, 308 (1952)

36. Peterman, L.,J. Acoust. Soc. Amer. 24, 416 (1952)

37. Ernst, P.J. and Hoffman, C.W.,J. Acoust. Soc. Amer. 24, 207 (1952)

38. Iizuka, K.,Appl. Phys. Lett. 16, 91 (1970)

39. Cook, B.D. and Werchan, R.E.,Ultrasonics 9, 101 (1971)

40. Pohlman, R.,Z. Agnew. Phys. 1, 181 (1948)

41. Mailer H.,Likins, K.L.,Taylor, T.R.,Fergason, J.L.,Appl. Phys. Lett. 18, 105 (1971)

42. Kapustina, O.A.,Sov. Phys. Acoust. 20, 1 (1974)

43. Kapustina, O.A. and Talashev, A.A.,Sov. Phys. Acoust. 19, 397 (1974)

44. Greggus, P.,Acustica. 29, 52 (1973)

45. Bertolotti, M.,Martellucci, S.,Scudieri, F.,Sette, D., Appl. Phys. Lett. 21, 74 (1972)

46. Elliot G.,G.E.C. J. Science and Techn. 42, 51 (1975)

47. Lowry, T.M. 'Optical Rotary Power', DOVER PUBLICATIONS, NEW YORK (1964), p. 347

48. Ibid, p. 149

49. Blitz, J., 'Fundamentals of Ultrasonics', BUTTERWORTHS,
     London (1967), p. 25.

50. Ibid, p. 29

51. Morse, P.M. and Feshbach, H., 'Methods of Theoretical Physics
     pt. 1', McGRAW-HILL, NEW YORK (1953) p. 828.

52. Lord Rayleigh, 'Theory of Sound' $\underline{2}$, MACMILLAN AND CO.,
     NEW YORK, p. 107.

53. Stenzel, H., Acustica $\underline{2}$, 263 (1952)

54. McLachlan, N.W., Phil. Mag. Series 7, $\underline{14}$, 1012 (1932)

55. Zemanek, J., J. Acoust. Soc. Amer $\underline{49}$, 181 (1971)

56. Schoch, A., Akust. Z. $\underline{6}$, 318 (1941)

57. Dehn, J.T., J. Acoust. Soc. Amer. $\underline{32}$, 1692 (1960)

58. Carter, A.H. and Williams, A.O., J. Acoust. Soc. Amer.
     $\underline{23}$, 179 (1951)

59. Archer-Hall, J.A., Bashter, A.I., Hazlewood, L., To be published.

60. Stepanishen, P.R., J. Acoust. Soc. Amer. $\underline{59}$, 749 (1976)

61. Robinson, D.E., Lees, S., Bess, L., IEEE Trans. Acoust.
     Speech and Sig. Proc., $\underline{A.S.S.P.-22}$, 395 (1974)

62. Lockwood, J.C. and Willette, J.G., J. Acoust. Soc. Amer.
     $\underline{53}$, 735 (1973)

63. Junger, M.C. and Feit, D., 'Sound, Structure and their
     Interaction', M.I.T. PRESS (1972)

64. King, L.V., Can. J. Res. Phys. Sci (Section A) $\underline{11}$, 135 (1934)

65. A.O Williams Jnr., J. Acoust. Soc. Amer. $\underline{36}$, 2408 (1964)

66. A.O Williams Jnr., J. Acoust. Soc. Amer. $\underline{39}$, 1142 (1966)

67. Rogers, P.H. and A.O. Williams, Jnr., J. Acoust. Soc. Amer.
     $\underline{52}$, 865 (1972)

68. Tranter, C.J., 'Integral Transforms in Mathematical Physics'
     METHUEN, London (1960) ch. 8.

69. Todamota Nimura and Yoshiyuki Watanabe, J. Acoust. Soc. Amer.
     $\underline{25}$, 76 (1953)

70. Devore, R.D., Hodge, D.B., Kouyoumjian, R.G., J. Acoust. Soc. Amer.
     $\underline{48}$, 1128 (1970)

71. Lauchle, G.C., J. Acoust. Soc. Amer. $\underline{57}$, 543 (1975)

72. Watson, G.N.,'A Treatise on the Theory of Bessel Functions', CAMBRIDGE UNIVERSITY PRESS (1966), p. 579

73. Lucas, R.,Comptes Rendus Acad. Sci. $\underline{206}$, 827 (1938)

74. Lucas, R.,Revue D'Acoustique $\underline{8}$, 121 (1939)

75. Frenkel, J.,'Kinetic Theory of Liquids', CLARENDON (1946) Ch. 5.

76. Peterlin, A.,J. Phys. et le Radium $\underline{11}$, 45 (1950)

77. Jerrard, H.G.,Ultrasonics $\underline{2}$, 74 (1964)

78. Personal Communication.

79. In 'Optical Rotary Dispersion and Circular Dichroism in Organ Chemistry', Ed. G. Snatzke, HEYDON, London (1965).

80. Beams, J.W.,Rev. Mod. Phys. $\underline{4}$, 133 (1932)

81. Kielech, S.,J. Coll. Inter. Sci. $\underline{33}$, 142 (1970)

82. O'Konski, C.T. and Zimm, B.H.,Science $\underline{111}$, 113 (1950)

83. Krause, S. and O'Konski, C.T.,Biopolymers $\underline{1}$, 503 (1963)

84. Brunnenberg, E. and Djerassi, C.,J. Am. Chem. Soc. $\underline{82}$, 5953 (1960)

85. Koch, W.M. and Sego, P.A.,J. Appl. Mech. $\underline{21}$, 198 (1954)

86. Jenkins, F.A. and White, H.E.,'Fundamentals of Optics', McGRAW-HILL (1957), p. 556.

87. Durelli, A.J. and Riley, W.F.,'Introduction to Photomechanics', PRENTICE-HALL INC/ENGLEWOOD CLIFFS, N.J. (1965), p. 32.

88. Feder, J.C., Gibbons, R.A.,Gilbert, J. T.,Offenbacher, E.L., Proc. S.E.S.A. $\underline{14}$, 109 (1956).

89. Betser, A.A. and Frocht, M.M.,J. Appl. Mech. $\underline{24}$, Trans. A.S.M.E. $\underline{79}$, 509 (1957)

90. Pih, H. and Snyders, L.S.,Proc. S.E.S.A. $\underline{26}$, 186 (1969)

91. Becker, H.,Proc. S.E.S.A. $\underline{18}$, 2, 214 (1961)

92. McNamara, F.L. and Rogers, T.F.,J. Acoust. Soc. Amer. $\underline{25}$, 338 (1953)

93. Wyatt, R.C.,Non-Destr. Test. $\underline{5}$, 354 (1972)

94. Hanstead, P.D.,Brit. J.N.D.T. $\underline{14}$, 162 (1972)

95. Wyatt, R.C.,Brit. J.N.D.T. $\underline{17}$, 133 (1975)

96. Hall, K.G., Ultrasonics 15, 57 (1977)

97. Hall, K.G., Ultrasonics 15, 245 (1977)

98. Hall, K.G., N.D.T. 9, 121 (1976)

99. Clark, A.B.J., Proc. S.E.S.A. 14, 195 (1956)

100. Viktorov, I.A., 'Rayleigh and Lamb waves', PLENUM PRESS, New York (1967)

101. Kemp, J.C., J. Opt. Soc. Amer 59, 950 (1969)

102. Mollenauer, L.F., Dounie, D., Engstrom, H., Grant, B., Appl. Opt. 8, 661 (1969)

103. Jasperson, S.N. and Schnatterly, S.E., Rev. Sci. Instr. 40, 761 (1969)

104. Blitz, J., 'Fundamentals of Ultrasonics', BUTTERWORTHS, London (1967) p. 206.

105. This is caused by the dependence of the refractive indices of ordinary and extraordinary rays on illumination wavelength.

106. Gooberman, G.L., 'Ultrasonics - Theory and Application', ENGLISH UNIVERSITIES PRESS LTD., London (1963), p. 31.

107. Watson, G.N., 'A Treatise on the Theory of Bessel Functions', CAMBRIDGE UNIVERSITY PRESS (1966), p. 579.

108. Davis, H.F., 'Fourier Series and Orthogonal Functions', ALLYN AND BACON INC., Boston (1963) p. 113.

109. Bashter, A.I., PhD Thesis, University of Aston in Birmingham, Department of Physics (1977)